Muscle Mitochondria in Vascular Disease: A Novel Genetic Target for Limb Salvage

By

Emma Joy Goldberg

May 2022

Director of Dissertation: Joseph M. McClung

Major Department: Physiology

Abstract

Peripheral arterial occlusive disease (PAD) is a manifestation of systemic atherosclerosis defined by an occlusion in the peripheral arteries, most commonly those supplying blood to the lower extremities. Chronic limb threatening ischemia (CLTI) is the most severe clinical manifestation of PAD, and is associated with high rates of limb loss, mortality, and reduced quality of life. Despite increasing PAD prevalence, treatments have been largely stalled over the past two decades, and therapeutics aimed at restoring residual blood flow have been largely unsuccessful in improving limb outcomes, especially for patients with CLTI, suggesting that the restoration of blood flow may not be enough to restore muscle functional ability. Exercise rehabilitation has established efficacy in lessening functional impairments observed in PAD patients who can tolerate it, making it only accessible to patients with less severe PAD manifestations. These

findings indicate that targeting and improving ischemic skeletal muscle quality could provide great benefits to patients with PAD. Further supporting this idea, *ex vivo* studies of skeletal muscle myofibers from patients with PAD demonstrate decreased oxygen consumption and enzyme activity indicative of a unique and intrinsic skeletal muscle bioenergetic dysfunction. The overall aim of this dissertation was to establish whether the restoration of blood flow necessarily guarantees recovery of muscle contractile function, and to determine the role of a specific mitochondrial protein, Cox6a2, in skeletal muscle bioenergetic function. This dissertation ties together multiple *in vivo* studies using preclinical animal models of PAD, as well as a novel, inducible mouse model of skeletal muscle Cox6a2 loss (Cox6a2 KO). The overarching hypothesis is that the myopathy observed in preclinical models of PAD and in the clinical PAD population is due to dysfunctional skeletal muscle mitochondrial bioenergetics, not perfusion recovery. Further, we hypothesize that skeletal muscle Cox6a2 is required for normal skeletal muscle mitochondrial function, and that its loss will result in a preclinical phenotype that mimics the bioenergetic phenotype observed in the clinical population. Our results establish that the restoration of tissue perfusion does not guarantee the recovery of muscle contractile function or structure in a preclinical model of PAD, and that the loss of Cox6a2 in mature skeletal muscle results in a mitochondrial bioenergetic phenotype.

Muscle Mitochondria in Vascular Disease: A Novel Genetic Target for Limb Salvage

A Dissertation

Presented to the Faculty of the Department of Physiology

East Carolina University

In Partial Fulfillment of the Requirements for the Degree

Doctor of Philosophy in Physiology

by

Emma Joy Goldberg

May, 2022

Muscle Mitochondria in Vascular Disease: A Novel Genetic Target for Limb Salvage.

by

Emma Joy Goldberg

May, 2022

Approved By:

Director of Dissertation: _____

Joseph M. McClung, Ph.D.

Committee Member: _____

Espen E. Spangenburg, Ph.D.

Committee Member: _____

Kelsey Fisher-Wellman, Ph.D.

Committee Member: _____

Tonya Zeckzyci, Ph.D.

Chair of the Department of Physiology: _____

Robert M. Lust, Ph.D.

Dean of the Graduate School: _____

Paul J. Gemperline, Ph.D.

ACKNOWLEDGEMENTS

I would like to first thank my advisor, Dr. Joseph McClung, for being an incredible mentor to me over the last four and a half years. Through the highs and lows, you've supported me and have always reminded me of just how capable I am. I'm beyond grateful to have had you as my Ph.D. advisor, and I can't imagine a better mentor to have had on this journey. Thank you for believing in me, guiding me, and giving me space to grow as a scientist and as a person.

I'd next like to thank my dissertation committee members, Dr. Espen Spangenburg, Dr. Kelsey Fisher-Wellman, and Dr. Tonya Zeczycki. You've each been an invaluable asset to me, and I couldn't have completed this dissertation without you. I will forever be grateful to you for your support both inside and outside of lab. I'd also like to thank the whole of the Physiology department and ECDOI for all of the support, friendship and laughs.

I would like to thank all of the members of the McClung lab who have truly become a second family to me. To Tom Green and Reema Karnekar: your skills are truly unmatched, and I'm so grateful to have had you both by my side since day one. To Dr. Cameron Schmidt: thank you for teaching me how to make the most of my Ph.D. experience and always being there to talk science with me. Lastly, to my fellow McClung lab trainees, Zoë Terwilliger, Makenzie Kolasa, and Ananya Pentakota: thank you for giving me the privilege of mentoring you and being a part of your journeys – I can't wait to see all of the incredible things you do!

Finally, I would like to extend the biggest thank you to my incredible parents, Arnold Goldberg and Phyllis Rosenzweig, my sister, Marissa Metzger, and my brother, Alex Goldberg, for being my biggest cheerleaders and answering my calls no matter the time of day. Without your unconditional and unwavering love, I wouldn't be who or where I am today.

TABLE OF CONTENTS

LIST OF TABLES

LIST OF FIGURES

LIST OF SYMBOLS/ABBREVIATIONS

CLTI – Chronic limb threatening ischemia

CD31 – Platelet endothelial cell adhesion molecule 1

CcO - Cytochrome C oxidase

Cox6a2 – Cytochrome C oxidase subunit VIa polypeptide 2

Cre – Cre recombinase

EDL – Extensor digitorum longus

HLI – Hindlimb ischemia

IC – intermittent claudication

PAD – Peripheral artery occlusive disease

PBS – Phosphate buffered saline

Sol - soleus

CHAPTER 1: INTRODUCTION AND SPECIFIC AIMS

Peripheral artery occlusive disease (PAD) is a manifestation of systemic atherosclerosis defined by an occlusion in the peripheral arteries, most commonly those supplying blood to the lower extremities[1,2]. PAD is estimated to affect over 230 million individuals worldwide and is the 3rd leading cause of atherosclerotic vascular morbidity[3,4]. Chronic limb threatening ischemia (CLTI) is the most severe clinical manifestation of PAD defined by ischemic pain at rest that persists for more than two weeks[5–7]. Although the CLTI presentation is less common, there are no effective treatments for these patients and it is associated with high rates of amputation, mortality, and significant financial burden[8].

The clinical treatment plan for PAD has focused on restoring blood flow for more than 150 years despite the fact that revascularization procedures have proven largely unsuccessful as a treatment[9–11]. Pharmacotherapeutic options that target the vascular compartment, such as anti-coagulants or statins, have also proven to be minimally effective[12]. Complicating this approach are multiple studies demonstrating a disconnect between limb blood flow and muscle functional capacity[13–19]. Multiple preclinical studies have identified that common inbred strains of mice, namely C57BL/6J and BALB/cJ, have drastically different responses to similar ischemic burden independent of vascular density[20–23]. Additionally, a recent study suggests that regenerating capillary networks only reorganize when injured myofibers are mature[24]. Thus, the myopathy present in the skeletal muscle of PAD patients cannot be attributed solely to altered hemodynamics. Exercise rehabilitation, which does not directly target or alter limb blood flow, has proven effective in lessening PAD-associated muscle functional impairments those who can tolerate it[25–29], though it is not a viable therapeutic option for CLTI patients. The benefits associated with exercise

therapy support the idea that better understanding PAD skeletal muscle pathophysiology could greatly improve our ability to treat the disease and provide novel therapeutic targets.

Skeletal muscle is an incredibly malleable tissue, with the ability to adapt metabolically and morphologically to stressors including exercise and disease[30,31]. Part of this plasticity comes from the ability of the skeletal muscle mitochondria to similarly adapt to physiologic and pathophysiologic stressors[32–34]. The dense mitochondrial networks within the skeletal muscle are responsible for ATP production, maintenance of redox charge and intracellular communication. Compromises in mitochondrial function result in increased oxidative stress, mitochondrial DNA (mtDNA) damage and progressive respiratory chain dysfunction – all of which are implicated across aging and various disease states including PAD[1,35–38]. *Ex vivo* studies of skeletal muscle myofibers from PAD patients in normoxic conditions demonstrate decreased oxygen consumption and enzyme activity[35,39–41], substantiating the notion that PAD patients suffer from an intrinsic skeletal muscle mitochondrial dysfunction.

Our lab recently identified that the mitochondriopathy observed in PAD patients distinguishes CLTI and IC paitents[42] from each other. This differential mitochondriopathy can also be observed in common preclinical inbred mouse models of PAD that segregate with poor tissue perfusion and limb loss following hindlimb ischemia (HLI). A unique component of both the clinical (CLTI patient) and pre-clinical (BALB/c) mitochondriopathy is reduced Cox6a2 – a nuclear-encoded regulatory protein subunit of complex IV that is expressed exclusively in mature, striated muscle (cardiac and skeletal). Cox6a2 is also one of 37 genes identified in quantitative trait locus (QTL) *lsq*-1[43], which was discovered based on inherent differences in tissue loss and perfusion recovery observed between BALB/c and C57BL/6J mice.

We believe that dysfunctional mitochondria are at the heart of the skeletal muscle myopathy observed in CLTI patients and a potential site for therapeutic development for this clinical presentation. To develop effective therapies, a clear understanding of required mitochondrial targets is needed. This dissertation attempts to establish whether restoration of tissue perfusion and muscle contractile function in a preclinical model of CLTI are temporally connected, and whether the skeletal muscle mitochondrial Complex IV component Cox6a2 is necessary for normal mitochondrial function. We will do this by performing the following Specific aims:

Specific Aim 1: Determine the Temporal Relationship Between Capillary Reperfusion and Muscle Contractile Function Recovery Following Ischemic Injury

The overall goal of this aim is to determine whether the restoration of tissue blood flow and contractile function occur on a similar timeline following ischemic injury, and whether muscles with distinct physiologic phenotypes have unique patterns of regeneration or inherent genetic benefits. We will answer the question: Does the re-establishment of tissue perfusion, muscle contractile function and myofiber architecture occur concomitantly? Further, we will investigate whether fast, glycolytic, and slow, oxidative skeletal muscles have distinct timelines or patterns of perfusion and contractile recovery following ischemia. We will compare the capillary perfusion, muscle force production, and muscle structure of extensor digitorum longus (EDL) and soleus (Sol) muscles from BALB/cJ mice 14- and 56-days following hindlimb ischemia.

Specific Aim 2: Develop and Validate a Mouse Model of Skeletal Muscle Cox6a2 Loss (HSA-MCM;Cox6a2$^{f/f}$).

The overall goal of this aim is to determine whether genetic reduction of Cox6a2 in mature skeletal muscle results in altered mitochondrial or contractile function in mice at baseline. We will answer the question: Does the loss of Cox6a2 in mature skeletal muscle alter mitochondrial respiration and skeletal muscle morphology? We will compare the mitochondrial function, muscle force production, and muscle structure of BL6J background HSA-MCM;Cox6a2f/f mice after tamoxifen induction of Cox6a2 deletion to vehicle control mice that are genetically matched. Additionally, we will challenge HSA-MCM;Cox6a2f/f mice after tamoxifen induction or vehicle (control) with chronic high fat diet feeding to determine if genetic reduction of Cox6a2 alters the muscle response to nutritional stress.

CHAPTER 2: REVIEW OF THE LITERATURE

Overview of Peripheral Arterial Disease and Chronic Limb Threatening Ischemia

Peripheral artery disease (PAD) affects 8-12 million individuals in the U.S[44]. The general functional impairments with PAD are substantial and include reduced or absent physical activity, pain, mobility loss, severe myopathy, and reductions in quality of life[4,45]. The two primary symptomatic clinical manifestations of PAD are: (1) intermittent claudication (IC), which is defined as exertional leg pain that is alleviated with rest[46,47]; and (2) chronic limb threatening ischemia (CLTI), defined as atherosclerotic PAD in association with ischemic pain at rest that is persistent for more than two weeks, tissue necrosis or gangrene[6]. PAD patients may also present with ischemic leg pain that is not consistent with the traditional definition of claudication[8]. IC patients have impairments in exercise and higher rates of mobility loss than those without PAD[48,49]. CLTI, meanwhile, is associated with high rates of morbidity, significant mortality rates, limb loss and substantial reductions in quality of life[6].

IC is the most common clinical presentation of PAD and is heavily studied. CLTI is typically resigned to a designation as the end stage of PAD, indicative of the prevalent assumption that claudication is an intermediate stage on a progressive scale. There are inherent issues with this idea, including a relative inefficiency in predicting clinical presentation based on atherosclerosis burden (IC or CLTI; Figure 1) and the presence of additional and underlying biological/genetic risk factors that may influence the severity of clinical presentation[6,47,50,51]. The biological/genetic part of this determination is readily evident in pre-clinical models of PAD, with differing inbred strains of mice presenting with either IC or CLTI phenotypes acutely after surgical onset of limb ischemia[21,23,52–54]. This has further driven the concept that CLTI may not simply be the "final stage"

of PAD, but a clinical manifestation of PAD with unique determinants and myopathic attributes. It has also created a conundrum of relevance for pre-clinical modeling of CLTI and has contributed to a lack of forward momentum in therapeutic development over the last few decades. Twenty years of trials and pre-clinical testing have largely failed to advance PAD therapeutics overall, especially for CLTI patients[55]. As a result of these trials, current medical therapies are not designed to specifically improve lower limb perfusion or repair the myopathy that plagues this population[51,56–60]. This review summarizes the current information on pre-clinical research models and clinical findings related to PAD that will guide therapeutic development across the next several decades, with an emphasis on the CLTI (CLI) presentation.

CLTI

Available data suggests that only a small percentage of claudicating patients ultimately progress to CLTI[61–64]. Historically, clinical Rutherford classifications of III/IV are based on the presence or absence of tissue loss/critical limb ischemia. Patients with claudication (Rutherford I/II) progress to CLTI (Rutherford III/IV+) at a very low rate (1-2%/limb/year) and the major clinical outcomes are vastly different from those with CLTI[59,65,66]. The most recent reported rates of progressively worsening PAD, in any form, come from secondary analysis of the EUCLID (Examining Use of Ticagrelor in Peripheral Artery Disease) trial[67]. In this report approximately 10% of PAD patients demonstrated worsening symptoms over a 12-month follow-up period, based on changes in their Rutherford classification. Of this fraction of overall patients, a large portion started as either asymptomatic or with mild claudication. The majority of patients with severe claudication at the time of enrollment did not progress to amputation outcomes or worsening symptoms over the 12-month period (approximately 97% of this group). One might naturally assume the lack of progression is due to increases in the number of interventional procedures performed or technical

advances in endovascular or surgical interventions; the number of global limb vascular procedures performed to alleviate PAD morbidity has increased over the past few decades[68], and there has been focus on therapeutic angiogenesis as a treatment for patients. Data from the Rymer et. al. report, however, don't support intervention as the reason for lack of progression in the EUCLID patient cohort. Seven percent of the EUCLID patients that experienced improved symptoms (based on the Rutherford scale) underwent a lower extremity revascularization procedure during the 12-month follow up. Additionally, 14% of the patients in this analysis with worsening symptoms had a revascularization procedure in the 12-month follow period. Existing treatments are largely ineffective[2,69,70] in CLTI patients but the field has yet to truly understand the reasons for this failure. Scientists and clinicians are anxiously awaiting the outcomes of the BEST-CLI (Best Endovascular vs. Best Surgical Therapy in Patients with Critical Limb Ischemia) trial (ClinicalTrials.gov Identifier: NCT02060630), which is scheduled for primary completion in October 2021. This trial should provide critical data on survival outcomes free from major limb amputation events in patients that underwent open surgical or endovascular revascularization procedures. While the originally described primary outcome measure was the occurrence of a major adverse limb event within 48-months, the revised measures are the time to major limb event or patient death in patients with either intervention. The results of this trial will be crucial to the development of novel and/or adjuvant ideas with potential future benefit to this specific clinical presentation. To date, our understanding of the clinical CLTI presentation is evolving, but what we know strongly supports that it is unique. The reasons that patients with PAD have distinct clinical courses despite similar large vessel occlusions suggest that variations in the response to injury within distal leg muscle (the target organ in human PAD) may play a causal role. What is

undoubtedly clear is that we do not fully understand the genetic mechanisms and biological processes that ultimately decide the fate of the CLTI limb.

Myopathy of CLTI

The hemodynamic impairments observed in PAD patients are accompanied by severe skeletal muscle myopathy[11,71–74], defined by abnormal skeletal muscle form and function[75,76]. Individuals with asymptomatic PAD have greater functional impairments and temporal functional decline than those without[77–79]. Myopathy can readily be found in most PAD patients if the search is extensive enough, and includes muscle myofiber atrophy, necrotic lesions, etc. The appearance of muscle lesions has been well reviewed across several decades in this patient population[1,8,42,75], and their functional consequences are well represented in walking or physiologic testing results. Complicating the myopathic presentation is the heterogeneity in manifestation across individual muscles as well as along the long axis of the muscle (proximal to distal). For example, deficits in the contractile function of lower limb muscles are not necessarily uniform across the body[61,80]. The 2002 Walking and Leg Circulation study[77] revealed that lower ankle brachial index (ABI) values were linked to greater likelihood of stopping the 6-minute walk test, poorer physical activity, walking velocity, standing balance and overall functional performance. Exercise rehabilitation has established efficacy in lessening these functional impairments in those who can tolerate it[27,28], making it a viable option for IC patients, but not for CLTI patients. The general physiologic benefits of exercise therapy, however, support the idea that targeting the ischemic skeletal muscle, as well as other downstream tissues, might be key to improving disease outcomes. The unique nature of the CLTI patient skeletal muscle has been well described in recent articles that, together, define the tissues from these patients[42,81,82].

Ryan et al.[42] examined the morphology, transcriptome sequence and mitochondrial function of non-necrotic gastrocnemius muscle from non-PAD, claudicating and CLTI patients. Morphologically, CLTI muscles had significantly smaller myofiber cross-sectional areas and non-uniform myofiber sizes compared with IC and non-PAD patients. Muscle sections obtained for this study did not show differences in muscle fiber type, though fiber type shifts have been observed by other groups[18,72,83,84]. Importantly, transcriptome sequencing revealed a unique gene expression file in CLTI patients when compared with IC (3,999 differentially expressed genes) and non-PAD (3,627 differentially expressed genes) patients. Of note is the finding that IC and non-PAD samples differed by only 397 genes. Similarities in the limb muscle transcriptomes of IC and non-PAD patients might lend insight into why exercise is an effective option for this population, as they seem to retain their transcriptomes related to bioenergetic functional capacities and muscle adaptive abilities. Cong et al.[85] built further upon the findings reported in the Ryan paper using secondary analyses of pathways enriched in CLTI patients. The group reported distinct differences in oxidative phosphorylation, mitochondrial dysfunction, sirtuin signaling pathways, TCA cycle, and fibrosis signaling pathways in CLTI patients compared to the other two groups. A deeper analysis of fibrosis signaling pathways revealed activation of TGFB signaling, collagen deposition and VEGF pathway activation in CLTI patients compared to IC and non-PAD control patients. A secondary cohort was then recruited and histological measurements indicated a greater fibrotic area in CLTI patients compared to IC and non-PAD controls, similar to the findings of Mietus et al[81]. Together, these papers further the idea that CLTI patient limb muscles are histologically, transcriptionally, and morphologically distinct from IC patients.

Across ‘omics analyses, gene ontology has consistently revealed a unique bioenergetics transcriptional program of mitochondrial metabolism in CLTI skeletal muscle, with common

deficits in cellular respiration, mitochondrial inner membrane and NADH dehydrogenase activity. Both the Cong and Ryan papers support the uniqueness of the skeletal muscle mitochondria in CLTI tissues. Additional recent work has clearly outlined unique CLTI metabolomic signatures in serum as well, which is highlighted by changes in amino acid, acylcarnitine, ceramide and cholesteryl ester profiles[82,86]. Of particular interest in these prior studies is the presence of myosteatosis in CLTI patients samples obtained both prior to surgical intervention and at amputation[82], indicating the stubborn nature of this lipid accumulation in this patient population. Whether changes in the mitochondrial axis occur as a manifestation of disease or a mechanism for the myopathy that plagues CLTI patients is still unknown. The exacerbated accumulation of lipid species in the ischemic limb muscle is an ominous characteristic, as this is a defined component of muscle functional decline in general aging populations[87]. Alterations in mitochondrial efficiency are a reported hallmark of myopathic tissues from both IC and CLTI patients[40,42,84]. It is a complicated paradigm to investigate in these tissues, unquestionably, as the presence of mitochondrial dysfunction, oxidative stress, or changes in mitochondrial content amongst necrotic lesions that may not be mounting appropriate regenerative responses in limb muscles seems likely, regardless of the clinical disease presentation. Isolation of tissue mitochondria prior to interrogation also creates confounders, as the organelle data may be influenced in part by mitochondrial contributions from other cell types in the tissues. Ryan et al.[42] attempted to address these issues directly, by ensuring the non-necrotic nature of tissues prior to high resolution respirometry of isolated myofiber bundles isolated from the same anatomic region of the same muscle samples collected from healthy control, IC, and CLTI patients. Solidifying the functional component of this mitochondriopathy, they also established similar mitochondrial contents across tissues from each population using multiple measures of tissue mitochondrial content, including:

lipidomics for cardiolipin species, nuclear/mitochondrial DNA, and citrate synthase. In further support of the critical importance of function versus number, isolated and well-controlled enzymatic experiments paralleled functional oxygen consumption deficits. Overall, the collective metabolic works provide a specific glimpse into the changing landscape of mitochondrial function, irrespective of mitochondrial number in the limb skeletal muscle cells of CLTI patients. The mitochondrial dysfunction observed in CLTI patients is paralleled in preclinical models of PAD[21,35,52,88], although heterogeneity in the models utilized is a rampant problem in the field. Typically, some form of hindlimb ischemia is employed, although the relevance of the chosen model to the CLTI presentation is rarely discussed.

The cytokine phenotype of CLTI patients is an additional unique feature of this population. Most recently, Jalkanen J. et al.[89] detailed elevations in 17 cytokines unique to a cohort of 121 CLTI patients (versus 101 IC or 20 healthy controls). For this study, the authors utilized Rutherford classes I-III for IC and classes IV-VI for CLTI categorization. Interestingly, the authors acknowledge the potential confounding influence of the most severe cases of CLTI on circulating cytokine profile, and therefore excluded patients with infections, gangrenous lesions, or tissue loss from their study. These findings paralleled those by Terra et al.[90] and Stehr et al.[91], which similarly demonstrate unique profiles of circulating cytokines and growth factors in CLTI patients. Circulating cytokine and growth factor profiles do not necessarily reflect the expression levels observed on a tissue compartment level, however. A secondary analysis of the WTSS reported by Ryan et al.[42] focused on the CLTI tissue level interleukin profile reveals 19 targets (interleukin or interleukin-receptor) uniquely increased ($p<0.05$) versus IC tissues. An additional 4 targets meet the threshold analysis ($p<0.05$) for uniquely decreased versus IC tissues. This tissue-based

secondary analysis supports the interleukin profile as both a circulating and tissue level characteristic that distinguishes CLTI patients.

Preclinical Modeling of CLTI

The research discussed above strongly supports the argument that CLTI should be viewed as a distinct manifestation of PAD, accompanied by a unique tissue and circulatory profile. Effective pre-clinical modeling of CLTI should closely mirror the characteristics of this clinical presentation in the affected muscles and tissues. This includes the pathologic manifestation of most or all of the following: 1) tissue loss/lesions with necrosis; 2) skeletal muscle atrophy, which may or may not be accompanied by a shift in myofiber type; 3) skeletal muscle degeneration; 4) impaired or delayed skeletal muscle regeneration; 5) expansion of non-contractile tissue/fibrosis; 6) fat deposition/myosteatosis; 7) reductions in skeletal muscle mitochondrial respiratory capacity and mitochondrial protein expression; 8) sustained deficits in muscle function/contractile performance; and 9) sustained impairments in blood flow to the limb. In the following section we will outline the currently utilized mammalian models of pre-clinical PAD and highlight what is known of their relevance specifically to the CLTI presentation

Pig

Domestic pigs are closely related to humans in terms of their anatomy, physiology, and genetics[92]. For these reasons, porcine models represent an advantageous experimental model for studying therapeutic treatments for a range of diseases[93,94]. Swine are especially useful for modeling cardiovascular diseases, such as coronary artery disease and heart failure, since the pig heart is very similar to that of a human[95]. There are significant differences in the hindlimb vasculature of humans and swine, however, many of which are due to its quadruped nature[96]. Anatomically, pigs

lack a common iliac artery. Instead, there is a trifurcation of the distal aorta into right and left external iliac arteries and the common internal iliac trunk[97]. Running down the lateral portion of the leg, the external iliac branches into the circumflex iliac artery. It then bifurcates into the external (superficial) and internal (deep) femoral arteries which continue down the hindlimb[98]. The external femoral artery further bifurcates into the popliteal and saphenous arteries. Historically, swine hindlimb ischemia (HLI) and ischemia-reperfusion models are common tools for studying vascular specific angiogenic and regenerative processes[97,99,100], however this model is complicated by a lack of significant myopathy post-ischemia induction, difficulties in functional outcome measurements, expense, a lack of genetic/transgenic models, and complications associated with overlaying common risk-factors with surgical ischemic onset. For obvious reasons, the complexities of this model make effective modeling of the CLTI presentation extremely difficult. Recent advancements in the porcine model of PAD include the additions of diet induced co-morbidity, treadmill functional assessments, and angiography and have led to a porcine model with more clinically relevant collateralization and myopathy outcomes[101]. This model will undoubtedly be critical for testing therapeutic interventions (not limited to stem cell therapies) in patients that are poor candidates for interventional surgeries in general and CLTI patients specifically[102–104]. The time to major pathologic manifestation post-surgical induction in pigs is more similar to the human paradigm, allowing for testing of therapeutic interventions post-onset (Is there a reference for this?). This will be critical for the development of effective therapies, particularly until biomarker identification or genetic determinants specific for the CLTI presentation are achieved.

Rabbit

The arterial anatomy of the rabbit hindlimb was described by McNally et al[105] in 1992. At the level of the pelvis, the rabbit aorta branches into the common iliac arteries, which, in turn, give rise to the external and internal iliac arteries. The external iliac artery and its subsequent branches are the main supplies of blood flow in the hindlimb. The external iliac gives rise to the deep circumflex iliac artery as it travels distally from the pelvis. Once it passes behind the inguinal ligament, its name changes to the common femoral artery. The common femoral artery gives rise to the deep femoral artery, inferior epigastric artery and lateral circumflex artery as it travels distally down the thigh. At the midpoint of the femur, the common femoral artery splits into the saphenous, descending geniculate and popliteal arteries. Rabbit HLI includes endovascular coil occlusion, ligation/transection, ameroid constriction, and/or electrocoagulation of the femoral artery[106–112]. The endovascular occlusion model of ischemia was developed in 2005 by Patel et al.[108] to occlude the superficial femoral artery in a way that limited the potential compounding effect of a surgical wound. Complete femoral artery excision in the rabbit was developed to produce a persistent model of animal ischemia[113,114] after it was discovered that iliac, femoral and aortic ligations did not reliably produce adequate ischemia. The complete excision of the femoral artery proved not only to be objective and convenient but produced consistent limb ischemia. Complete femoral artery excision has been shown to result in an acute angiogenic response within the rabbit hindlimb, which is followed by an arteriogenic response. Complete excision also leads to a skeletal muscle myopathy, marked by decreases in muscle fibers, increased adipose tissue and connective tissue within the affected limb, and areas of tissue necrosis[115]. Femoral artery ligation, which involves ligating the femoral artery proximal to the deep femoral artery and distal to the lateral circumflex artery[116], has been shown to reduce muscle cross-sectional area and the number of muscle fibers present in ischemic muscle. Femoral artery and endovascular occlusion similarly

result in an angiogenic response in the hindlimb, though there is limited data on the accompanying myopathy. Despite the vast number of HLI studies that have been performed in rabbits, there is a limited amount of data on the accompanying myopathy and muscle regeneration. From what we know, complete artery excision seems to result in a phenotype that most effectively mirrors CLTI presentation.

Rat

A comprehensive description of the hindlimb vascular anatomy of the rat was published in 1935 by Greene et al[117]. The terminal branches of the aorta split into the right and left common iliac arteries in the rat, which run laterally along inner thigh. The common iliac arteries then bifurcate into the external and internal iliac arteries, which branches into the lateral and medical circumflex arteries. The external iliac gives rise to the pudendoepigastric trunk and then passes behind the inguinal ligament, at which point it's referred to as the femoral artery. The femoral artery runs down the medial side of the thigh, giving rise to four branches: the superficial circumflex iliac, muscular, superficial epigastric, and the highest genicular arteries. It then bifurcates into the saphenous and popliteal arteries at the level of the knee, which continue to branch and form collaterals as they move distally towards the foot. More recently, anatomic heterogeneity in hindlimb vasculature between rats of the same background was identified[118]. The first description of HLI in rats employed a unilateral femoral artery ligation[119]. Since then, multiple groups have altered the standard procedure in an attempt to more accurately model PAD and other disease states[120–125]. The most common rat models employ embolization, ameroid constrictors, and acute vessel ligation/transection. The embolization technique was first developed by Zhuang et al[126] in 2012, and involved the use of synthetic, polymeric hydrogels and a platinum coil, which, following

insertion, would expand over time, occluding the femoral artery. In 2013, Shin et al.[127] investigated the feasibility of N-butyl cyanoacrylate (NBCA) and polyvinyl alcohol (PVA) particles to induce ischemia via enolization, as these particles do not cause susceptibility artifacts during MRI like coils can. Embolization with use of coils, NBCA, or PVA particles results in blood flow reductions and muscle infarction, while minimizing the inflammatory response. Ameroid constrictors have also been used to induce limb ischemia in rats is described as chronic, though this method has not been shown to induce muscle degeneration, nor does it trigger a severe inflammatory response, despite causing persistent deficits in blood flow. Acute ischemia in the rat hindlimb, via vessel ligation/transection, results in necrotic muscle tissue and toes, muscle atrophy, fibrosis, severe inflammation, muscle regeneration and granulation[122,128]. The reaction of rats to acute ischemia more closely models the pathology observed in CLTI patients

Rats are also prone to metabolic syndrome under dietary manipulations, which enhances the relevance of HLI data to clinical populations with heavy co-morbidity burdens. Common diets typically are defined by high fat or high fructose contents. High fat diets (HFD) range in their fat content, from 20-40%[129–131] and are generally employed for 6-10 weeks prior to experimentation. High fructose diets in rats lead to hypertension and dyslipidemia[132,133] and are normally also administered for 6-10 weeks. The preclinical Western diet[134], which is similar to HFD with the addition of cholesterol, has also been utilized in the rat. Several studies have investigated angiogenesis within the context of HLI + streptozotocin-induced type 2 diabetes in rats. These studies have largely focused on the angiogenic response in the hindlimb without attention given to the effect on the skeletal muscle. The impact of HFD on wound healing, cardiac fibrosis[135], and angiogenesis has also been investigated. In each instance, HFD worsened the pathology: including

compromised wound healing[136], exacerbated cardiac fibrosis[135], and impaired angiogenesis[121]. It would be easily assumed that HFD and/or models of type 2 diabetes would worsen HLI myopathy in rats and mimic clinical CLTI more effectively, but this hasn't been directly demonstrated to date.

Mouse

Murine hindlimb ischemia is the most commonly used method for modeling clinical PAD. The primary mouse model of HLI was described in 1998 by Couffinhal et al[57] and based largely on the rabbit model[106]. Today, the mouse model is preferred over larger animal models for its' practicality, cost, and the wide array of transgenic mice that are available[137]. Multiple variations to the mouse limb ischemia procedure have been leveraged to model PAD[23,122,138–140]. Altered variables primarily involve anatomical location of ligation/transection or the rate of ischemic induction. Although these models are all termed "HLI", each produces a uniquely scaled myopathic response and recovery timeline in the limb. One commonality between the models is the methodology traditionally used to evaluate the "response", which includes: blood flow restoration, capillary perfusion, collateral vessel formation, limb muscle contractile force production recovery, and histological evaluation of limb muscles[21,23,52,53,141–143]. The major challenge for the field lies in comparing data from animals that have undergone different forms of HLI, as each can result in vastly different temporal outcomes using these measures. Further complicating the field is the relatively new understanding that common inbred strains of mice display markedly different tissue and blood flow responses, even when subjected to the same form of HLI[21,23,144,145]. For these reasons, much consideration must be given to the details of the model system employed in mouse studies. The acute nature of the ischemic onset and the temporal limitations of HLI in mice are

recognized issues with this system. Despite these complications, using the inherent genetic differences of the existing and commercially available inbred strains of mice, the murine model can be employed as an effective model for CLTI. Ischemic myodegeneration and regeneration are key components of the murine response to limb ischemia[143,146]. Inbred strains that suffer from tissue necrosis, the most severe myodegenerative phenotypes, and/or severe deficits in the recovery of limb blood flow appear to better mimic the physiologic outcomes of CLTI patients, including muscle contractile deficits and severe delays in tissue perfusion recovery. Similar to the rat model, the murine HLI model can be easily paired with preclinical models of PAD comorbidities and risk factors, using both external interventions and/or genetic models of these diseases.

Overlaying PAD co-morbidities with murine HLI to understand how disease states interact is not a novel idea, albeit a relatively uncommonly employed one. When utilized in mice, it often results in outcome measures that parallel CLTI myopathy. The most commonly employed is insulin insensitivity, which can be achieved in multiple ways, including: high fat diet feeding[147–150], Irs1/Irs2/Irs3 knockouts[151], and GPX1 overexpression[152]. Multiple models of type 2 diabetes, obesity and hyperlipidemia have been developed for mice, including HFD feeding[153,154], $Leb^{ob/ob}$[155], $Leb^{db/db}$[156] and $apoE^{-/-}$[157] mice. Ryan et al.[148] found that subjecting C57BL/6 animals to HFD for 16 weeks resulted in a greater degree of limb tissue necrosis, increased myopathic lesion size, reduced muscle regeneration and function, and exacerbated ischemic mitochondrial dysfunction. $ApoE^{-/-}$ mice, which have been widely used to model hypercholesterolemia and atherosclerosis[158,159], have delayed skeletal muscle regeneration after HLI[160]. Smoking alters the angiogenesis related microRNA profile of bone marrow derived stem cells[161] and attenuates the effectiveness of donor

stem cells to improve blood flow restoration in C57BL/6 mice after HLI[162]. Chronic kidney disease (CKD), a common comorbidity for CLTI[163,164] is also effectively modeled in mice[165]. Skeletal muscle from mice with CKD have reduced mitochondrial function, accumulate uremic toxins, and are smaller and weaker than those without[166]. Furthermore, C57BL/6 mice subjected to CKD prior to HLI have exacerbated muscle myopathy despite the absence of capillary regression or blood flow restoration deficits[167]. Taken together, these studies highlight the effectiveness of the murine genetic models or co-morbidity related interventions to effectively mimic CLTI myopathies after HLI. This provides a rich opportunity for testing of future therapeutics aimed at alleviating myopathy in settings which better mirror the complex multi-diseased nature of these patients. When combined with what is now understood about the critical role of background strain/genetics, this approach has the potential to powerfully impact the rigor of the pre-clinical research validating identified therapeutics.

Pre-Clinical Genetics

The idea that inherent genetic makeup can influence susceptibility to cardiovascular disease has gained traction over the past two decades. Multiple genetic loci have been identified that are related to ischemic outcomes in preclinical disease models, from stroke to PAD[43,168–175]. Unquestionably, murine strain-dependent variations in susceptibility to disease have played a key role in advancing our understanding of genetics in cardiovascular diseases[169,171,176]. Barone et al.[177] published the first evaluation of mouse strain differences in cerebral ischemia. Multiple groups followed suit [178–180] and several genetic loci that affect the extent of cerebral ischemic tissue damage have been mapped[169,181]. The general consensus is that C57BL/6 mice are more resistant to middle cerebral artery occlusion than BALB/c mice[179], and that BALB/c mice suffer the largest lesion areas and most severe pathology compared with other strains. Differences between inbred strains

in response to cardiac ischemia have also been investigated. A 2005 study by Gao et al.[182] analyzed left ventricular wall rupture following an acute MI across three common inbred mouse strains and revealed unique risks and timing of ventricular rupture. Salimova et al.[183] examined variations in heart morphology and function across multiple mouse strains and found C57BL/6 animals to be the most susceptible to myocardial rupture and death following left coronary artery ligation[184]. Strain differences in response to peripheral ischemia have been relatively well studied. Markedly different responses occur between BALB/c and C57BL/6 mice when subjected to the same ischemic limb methodology[21,23,53,54,144]: BALB/c mice suffer significant muscle damage, atrophy, mitochondrial deficits, tissue necrosis, reduced collateralization and perfusion recovery in limb skeletal muscles compared to C57BL/6 mice[23,52,145,185]. This is similar to the differences in the tissues of claudicating and CLTI patients.

Dokun et al.[43] initially mapped the genetic basis for tissue loss following HLI in inbred parental strains. Using C57BL/6 and BALB/c mice the authors identified a locus on chromosome 7, termed *Lsq-1,* associated with limb tissue loss following HLI. *Lsq-1* contained 21- and 16- known and predicted genes, respectively. It is important to note that none of the identified genes at the time was known to play a known a role in vascular growth. Additional studies on parental strain genetics that followed focused on collateral vessel formation[186],[187] and identified an additional loci (*Canq1)* on chromosome 7 partly responsible for heritable variation in collateral vessels. Later work[172] reported peak marker overlap between *Canq1* and *Lsq-1*. The majority of mechanistic studies performed since these analyses have focused on targets identified in *Lsq-1*, specifically *ADAM12, IL-21R* and *BAG3*[88,188,189].

ADAM12 (a disintegrin and metalloprotease 12) is a member of the mellatoproteinase family possessing cell-binding and intracellular signaling functions[190]. C57BL/6 mice show significantly higher expression of ADAM12 following HLI compared with BALB/c mice[191] and reductions in ADAM12 attenuated limb blood flow recovery in these mice. Re-expression of ADAM12 in BALB/c mice also partially rescued blood flow. Clinically, ADAM12 polymorphisms have been identified in CLI patients[189], although causality of these polymorphisms for the CLI presentation have not been established in patients. These polymorphisms have also not demonstrated dominant negative outcomes in pre-clinical models. ADAM12 is a critical component of myogenic cell biology[192] and is temporally known to play both positive and negative roles in the regeneration of damaged muscle tissues[193,194]. Interestingly, more recent data demonstrates a role for ADAM12 in the pathologic determination of perivascular cells to profibrotic fibroblasts during acute tissue injury, supporting a role for this target in the exacerbation of the muscle fibrosis phenotype identified by Pipinos as a hallmark of CLTI[81,85]. Focused mining of WTSS data from the Ryan et al[42] reveals an approximate 24-fold increase in ADAM12 in the limb muscles of CLTI patients as compared with healthy adults (p=1.56^{-13}). Together, this data supports ADAM12 as a target for further evaluation in the development of new therapeutics for the degenerative and fibrotic aspects of CLTI patient limb muscles.

Interleukin-21 receptor (IL-21R) is found at the peak of phenotypic association in in the short arm of murine chromosome 7[43]. Follow-up studies by Wang et al[195] determined that C57BL/6 mice upregulate IL-21R expression during HLI, while BALB/c mice do not. IL-21R was originally investigated in immune cells, where it controls lymphoids and the differentiation of myeloid cells[196,197]. Wang et al. established a specific role for this receptor as a modulator of cell survival

and stimulator of angiogenesis in hypoxic endothelial cells[198]. I*n vivo* knockdown of IL-21α in C57BL/6 mice caused impaired perfusion recovery following HLI. Wang et al.[199] later verified increased expression of IL-21R in the endothelium and plasma of skeletal muscle of patients with PAD. While there are no data linking IL-21R specifically to the CLTI presentation, alterations in expression levels in a human PAD population and pre-clinical data on blood flow recovery to the limb support further evaluation of the biological role of IL-21R in PAD in general.

B-cell lymphoma 2–associated anthanogene (BAG3) is a multifunctional adaptor protein that regulates diverse cellular functions and plays critical roles in cancer[200–202], and skeletal and cardiac muscle biology[203]. Mutations in *BAG3* are causally linked to myofibrillar myopathy and dilated cardiomyopathy in humans[204–207], and loss of *Bag3* in mice causes perinatal lethality due to fulminant muscle myopathy[208]. Unique variants in BAG3 occur exclusively in 10% of individuals of African descent with cardiomyopathy[209] and contribute to idiopathic outcomes. Haplotype insufficient BAG3 cardiac muscle results in a heart failure phenotype[210,211] and human variants of BAG3 are causative for impaired hypoxic autophagy and increased apoptosis[88,212,213], providing synergy for expression deficits and dysfunctional variants *in vitro*. BAG3 has also been linked to cadiomyocyte sarcomere function[214]. Recent work has linked haplotype insufficiency of BAG3 to reduced cardiomyocyte sarcomere protein turnover, contributing to the heart failure phenotype and impaired cardiomyocyte contractile function[215]. A murine coding variant in *Bag3* contributes to ischemic muscle necrosis after HLI, and *Bag3* variant gene therapy targeted to ischemic limb muscles rescues both myopathy and vascular density[22] in BALB/c mice. Since limb muscle cells are a critical component of the most effective intervention in PAD patients (exercise), and mutations in BAG3 now appear to be one of the most common to cause disease[204,205,214,216],

investigations into BAG3 have the potential to impact CLTI patients, specifically, but also across all PAD presentations.

Mitochondria function as continuously operating batteries, creating the energy and redox charges essential for establishing and maintaining life for cells. Published[38,39,41,52,142,148,217,218] data suggest that mitochondrial-derived disruptions in skeletal muscle energy charge are primary factors in the etiology of, and susceptibility to, pre-clinical and clinical ischemic myopathy. Intriguingly, the only identified mitochondrial component of *LSq-1* is *mitochondrial complex IV gene cytochrome oxidase 6a2 (Cox6a2)*. Cox6a2 is a component of uniquely altered mitochondria in CLTI patients[42]. It's presence in *LSq-1* is of particular interest for two primary reasons: first, *Cox6a2* is the only locus component expressed solely in striated muscle; and second, it is directly linked to muscle mitochondria. Skeletal muscle contains dense mitochondrial networks responsible for ATP production, maintenance of redox charge and intracellular communication. Compromises in mitochondrial function result in increased oxidative stress, mitochondrial DNA (mtDNA) damage and progressive respiratory chain dysfunction – all of which are implicated across aging and multiple disease states, not limited to PAD[1,36–38,142]. Preclinical studies have shown that therapeutically targeting the mitochondria in a model of CLTI can reduce the ischemia-induced myopathy[38,148]. This provides evidence that targeting skeletal muscle mitochondria could lead to effective treatments for PAD and, specifically, CLTI. Murine mechanisms altering limb muscle mitochondria are also highly translatable to the clinic, as PAD patients often present with metabolic disease (i.e. type 2 diabetes) co-morbidities characterized by reduced muscle mitochondria function[219–221]**.** Similarly, the inbred parental strain driven claudicating phenotype (including mitochondrial sufficiency) associated with C57/BL6J mice after HLI is overridden by

sustained high fat diet (HFD) consumption[148]. For these reasons, the mitochondria are exciting targets for mechanistic interrogation.

Noncoding RNAs in CLTI

Noncoding RNA is a general term encompassing both microRNAs (miRNA) and long noncoding RNA (lncRNA). This biologically diverse class of gene products is poorly understood but rapidly gaining traction as a novel treasure-trove for both biomarkers and therapeutic targets in cardiovascular disease. The human genome encodes 22,000 proteins but it also encodes >2,000 microRNAs and perhaps as many as 60,000 lncRNAs. In general terms, miRs serve to regulate the expression of a gene or several genes within the same pathway by interacting with ribonucleotide interacting proteins in RISC complexes. They largely function to down-regulate gene expression through targeting mRNA for degradation or serving as regulators of translation. Through the same mechanism, miRs can increase a gene or pathway by interacting with an inhibitory RNA or causing negative expression of a transcriptional repressor. When compared to miRs, lncRNAs are less well conserved evolutionarily, more numerous, and have many different potential mechanisms of action. Reports on lncRNAs are growing but they have been identified as playing a causal role in X chromosome inactivation, cell differentiation and pluripotency, mRNA splicing, gene-expression, and miR production and sponging[222–228]. At least somewhat similar to miRs, lncRNAs recruit epigenetic factors to exert effects and can be encoded by-, or act as-, enhancers[222,226,228–231]. LncRNAs can also act as parts of protein machines, chromatin complexes, and even rRNAs in ribosomes. Reports on ncRNA in PAD began almost twenty years ago and even "review articles" on the topic can be found[232–234]. While several studies investigate ncRNA in the pre-clinical murine model system or in culture, there is very little data on the

relevance of these studies to PAD patients in general, and specifically those with CLTI. What follows is a brief review of select ncRNA targets with known relevance specifically to the CLTI presentation (based on clinical data or pre-clinical models matching the requirements we identified above; **Table 2**), for additional new reviews on this specific subject in PAD please see the following references[234,235]:

To the best of our knowledge, very few studies have reported differential lncRNA expression specifically in PAD patient tissue samples. Gastric Adenocarcinoma Associated, Positive CD44 (GAPLINC) increased in a limited (n=3) sample of CLTI patient arterial tissues in a recent investigation[236]. Follow up culture studies performed in HUVEC cells identified a hypoxia sensitive angiogenic phenotype associated with altered expression of this lncRNA. These authors reported a total of 43 differentially expressed lncRNAs in CLTI arterial tissues, with more than half up regulated. Ensemble identifiers can be found in the supplementary material, however the only lncRNA identified by name in the manuscript was GAPLINC. It is also unclear which anatomic arterial segments were used in the study, if the same arterial segment was collected from each patient, what the characteristics of the patients were (sex, co-morbidities, age, Rutherford classification, ABI, etc.) and whether the entire artery was utilized or if segments of the internal arterial tissue rich in endothelium were isolated. Boulberdaa et al. reported Smooth Muscle and Endothelial Cell Enriched Migration/Differentiation-Associated LncRNA (SENCR) expression as decreased (qRTPCR analysis) in the limb muscle tissues of CLTI patients. Detailed analyses demonstrated its' importance in driving HUVEC proliferation, migration, and tube formation *in-vitro*[237]. Recently reported data from our group demonstrates decreased long intergenic non-protein coding RNA 202-1 (LINC00202-1) in black CLTI patients versus black control patients[238].

Additionally, increased expressions of MIR503HG and LINC00941 were discovered in black versus white CLTI patient limb muscles[238]. These findings highlight both the exciting potential this field of research possesses and the vast work that remains in order to understand the clinical relevance and biological mechanisms of action of lncRNA in peripheral tissues. What is missing thus far is a systematic analysis of lncRNA in the limb muscles of a uniform patient population, including both IC and CLTI patients as separate groups, when compared with age-matched non-PAD controls.

Similar to lncRNA, few studies have examined microRNA expression specifically in CLTI patient tissues or in pre-clinical models of CLTI. Profiling of miRNA expressions in bone marrow derived CD34+ cells from patients with both type 2 diabetes and CLTI revealed decreased miRNA-21 as a potent signaling regulator of endothelial cell apoptosis[239]. While there was no CLTI only population in this study, the authors did report the following: 1) no common miRNA expressed in the cells derived from diabetic patients alone and those from diabetic/CLTI patient, and 2) a single miRNA uniquely expressed in the diabetic/CLI patient group alone (has-miR-146a-5p). Another miRNA gaining interest, and one directly implicated in the CLTI phenotype is miR-93[240,241]. Mir-93 is involved in tumor survival and angiogenesis[242], is expressed at lower levels in the limb muscles of in the CLTI-like BALB/c parental strain[240], downregulates the mRNA levels of genes that play a role in cell survival[240], recovery and proliferation following HLI, and its' inhibition in C57BL6 mice attenuates post-HLI recovery *in vivo,* while overexpression improves recovery in BALB/c mice[240]. Follow-up work revealed a specific role for miR93 in macrophage polarization in the ischemic limb muscle tissue and significantly lower miR-93 in PAD limb tissues than controls[241].

Stem Cell Therapy in CLTI

Stem cells have been an exciting area of therapeutic effort for CLTI patients since the early 2000s, primarily focused on improving tissue perfusion and/or collateral vessel growth[243,244]. To date, largely using autologous bone marrow derived and/or expanded stem cells, benefits have been observed in secondary symptom measures with limited efficacy demonstrated in preventing amputation[243,245]. The 3 most recent patient trial publications (since 2019) are detailed in **Table 1**. At the time of this review, there were 36 clinical trials listed as "*completed*" and 6 "*actively recruiting"* (clinicaltrials.gov; *critical limb ischemia*, *stem cell* search terms utilized). Of the 36 "*completed*" trials, only 1 has results listed[246]; ClinicalTrials.gov Identifier: NCT01472289. This study provided a primary assessment of the safety of a "bedside" cell purification and preparation system in a small (*n*=17) cohort of CLTI patients (Rutherford V; 48.8±13.1 SD years of age), with secondary effectiveness measures (ABI, tissue oxygen pressures, walking, pain, amputation rate) across a 12-month follow-up. The Katagiri et al.[247] study is a small (5-patient), short-term (6-month) study of patients 28-64 years of age. These authors reported no major amputations in their small patient group over the experimental term and improvements in ulcer size and walking distances. CLTI patients in the Sharma et al.[248] trial were reported at a mean age of 45.3±15.5 SD in the control group and 41.9±11.0 SD in the cell treated arm. The results of these 3 studies are largely consistent in demonstrating short-term (6- or 12-month) improvements in ABI and transcutaneous oxygen pressure including and no major amputations across the 6-month studies. Only 1 of these studies was designed with control group injections included [249] and all three of these studies represent relatively young patient populations with respect to CLTI (mean age of each study's population in the 40's). Overall, these new reports represent a continuation of the

previous data, with mixed data on amputation prevention over time and consistent improvements in secondary measures.

Recent pre-clinical reports using the CLTI-like BALB/c HLI model have helped to refine our temporal and biological understanding of stem cell biology in the ischemic limb. Beltran-Camacho provide a proteomic readout of tissue changes in the BALB/c (nude) hindlimb after HLI including the administration of human circulating angiogenic stem-cells (CACs)[250]. Intramuscular injections of CACs were insufficient to prevent tissue necrosis within the 4-day experimental period and directed proteomic changes related to cell apoptosis, inflammation, and cellular motility. Moderate alterations were observed in the limb vascular profile, albeit not sufficient to prevent necrotic lesions. A heterogeneous population of bone marrow derived cells (REX-001; including lymphocytes, monocytes, granulocytes and CD34+ hematopoietic stem cells) injected intra-muscularly provided modest improvements in limb blood flow after BALB/c (nude) HLI[251]. No data was provided on myopathic outcome measures in either study, although distribution of REX-001 was largely compartmentalized to the injected limb skeletal muscle. REX-001 is the lead product of Ixaka and is currently being evaluated in Phase III trials across Europe (SALAMANDER trial). Only time will tell if the large number of existing/non reported trials will provide more definitive evidence of stem cell efficacy to prevent amputations and improve morbidity outcomes in the CLTI population. Our understanding of the local environment's influence on stem cell biology is steadily improving[252,253]. This will be key to effectively implementing stem cell strategies in an aged ischemic limb suffering from the type of extensive myopathies that CLTI causes. For the time-being, this remains an exciting area with yet-unrealized potential for this patient population.

Gene Therapy in CLTI

Concerns about the efficacy of gene therapies in human disease or off-target effects of this approach are waning as data becomes more available. As of today, there are 4 FDA approved gene therapies that use lentiviral, retroviral, CAR-T, or Adeno-associated virus (AAV) delivery models. The overwhelming majority of gene therapy approaches for CLTI are focused on driving angiogenesis, using vascular endothelial growth factor (VEGF)[254–256], fibroblast growth factor (FGF)[257–259], or hepatocyte growth factor (HGF)[255,260–262]. There are 3 clinical trials (clinicaltrials.gov; *critical limb ischemia*, *gene therapy* search terms utilized) currently recruiting. Two of the trials utilize variant plasmid delivery of HGF (ClinicalTrials.gov Identifiers: NCT04275323 and NCT04274049). The third is investigating intravascular AAV delivery of telomerase (hTERT) (ClinicalTrials.gov Identifier: NCT04110964) in an attempt to alleviate telomerase-related aging cellular alterations that contribute to the CLTI presentation. Angiogenic gene therapy has not proven efficacious as of yet. Similar to surgical interventions used in this patient population, this approach is still focused on restoring blood flow and not designed to alter the biology of the primarily affected limb tissues with CLI, the limb muscle. The general failures of the angiogenic gene therapy approach in improving patient outcomes, combined with the prevalence of surgical interventions to restore blood flow, warrant new ideas to improve outcomes in the CLTI population.

Skeletal muscle specific gene therapy is a burgeoning field, with AAV-based therapies encompassing a large portion of clinical trials related to muscular dystrophies. The FDA recently (July 2020) awarded the Sarepta Therapeutics SRP-9001 gene therapy for Duchenne Muscular Dystrophy (AAVrh74, using a MHCK7 promoter to drive a micro-dystrophin transgene) “Fast

Track" and "Rare Pediatric Disease" designations. The same AAV vector is being used by Sarepta Therapeutics to generate gene therapies for Sarcoglycanopathies, characterized by mutations in genes encoding one of four proteins in the dystrophin-associated glycoprotein complex that results in similar myopathy to general dystrophy. This is important in the context of CLTI due to the myopathic phenotype associated with dysfunctional muscle regeneration in these patients and provides insight into what might represent a novel strategy for intervention in aged limb muscle. The local density and functionality of muscle tissue level capillaries correlates with limb function in PAD patients[263,264]. Paired with the recent report of a general disconnect between overall limb blood flow and the reperfusion of limb skeletal muscle capillary beds in the BALB/c CLTI pre-clinical model[143], the potential local role that the degenerating/regenerating skeletal muscle provides locally to focal angiogenesis[265] is a promising avenue for exploitation in therapeutic design. The potential upside of this approach is that it could be utilized independently or in combination with existing surgical interventions, with the concept of improving the limb muscle environment to better respond to the interventional restoration of limb blood flow at the site of occlusion.

Conclusions

Much of the research related to and treatments of PAD and CLTI have focused on the vascular nature of the disease, though these methods have largely failed the CLTI population. To advance the field and improve the quality of life for patients with CLTI, we must improve our understanding of the genetic mechanisms and biological processes that underlie its pathophysiology. Additionally, we must look beyond the limb vasculature for potential therapeutic targets. Given the focus of this review on effective pre-clinical research models,

clinical findings and areas of study related to PAD, it's worth noting that there is a considerable amount of promising research underway that could greatly impact our understanding and treatment of PAD pathology in the near future.

Figures and Tables:

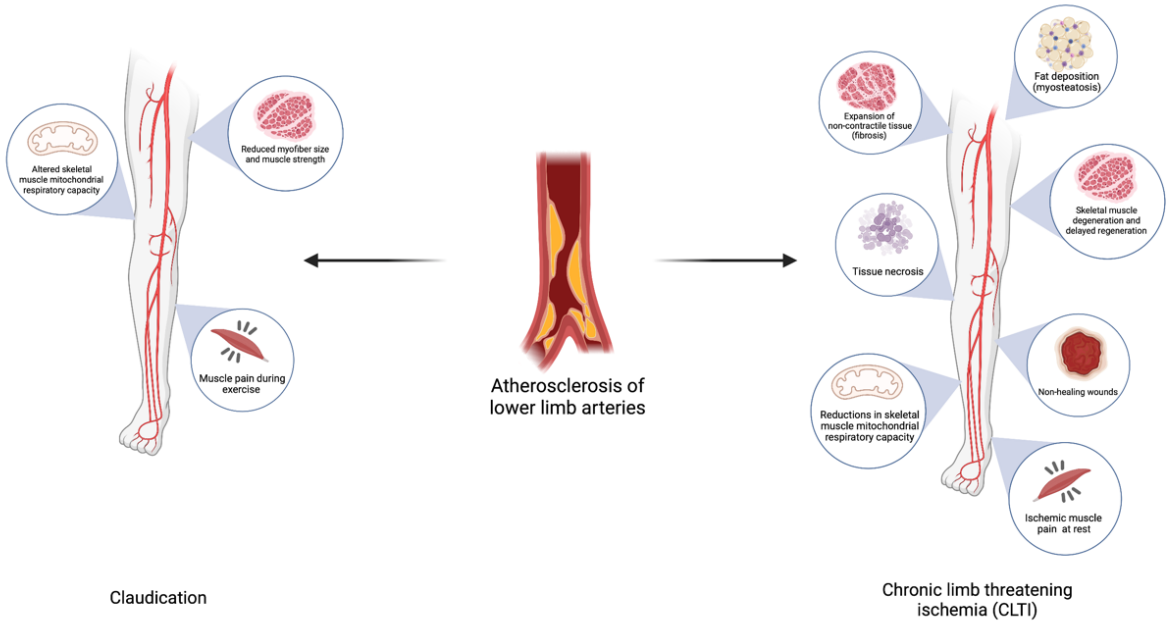

Figure 2: Schematic of Lower limbs and highlight all the known specific details of CLTI limb tissues.

Authors	Study	Ref.	Cells	Route of Admin	No. of participants	Placebo Group	Primary Outcomes	Secondary Outcomes
Ponemone et al	CLI-STEM	Stem Cells Int. 2017; 2017: 4137626.	Autologous bone marrow concentrate	i.m. (gastroc)	17	No	Safety of bed-side processing of cells	From baseline, improvements in: ABI and transcutaneous oxygen pressure, walking distance, leg vessel density, and the presence of ulcers across a 12-month follow-up. 5 patients suffered amputations.
Katagiri et al	TACT-ADRC	Scientific Reports (2020) 10:16045	Adipose-derived regenerative cells (ADRC)	i.m. (gastroc) (hand)	4 (limb) 1 (hand)	No	Amputation free survival rate 100% after 6-months	No change observed in ABI; reductions in ulcer size after 6-months; improved walking distance
Sharma et al	CTRI/ 2010/091/ 000565	J Vasc Interv Radiol 2021; 32:157–163	Bone marrow mononuclear cells (BMMNCs)	Intra-arterial	56 (CLTI) 25 (Claudicating)	Sham Injection	No major amputations in CLTI treatment group (*n*=29) after 6-months, 4 in placebo (*n*=27)	Improvements reported in CLTI patient ABI and transcutaneous oxygen pressure

Table 1. Summary of the most recent patient trial publications.

Gene Symbol	Gene Name	Fold Change (from IC)	P-Value	FDR
IL10RA	interleukin 10 receptor, alpha	3.40179157	1.5E-13	3.28E-12
IL33	interleukin 33	2.97427528	3.1E-16	1.17E-14
IL1R1	interleukin 1 receptor, type I	2.6664224	2.1E-10	2.47E-09
IL2RB	interleukin 2 receptor, beta	2.24846348	9.0E-05	0.00030764
IL2RG	interleukin 2 receptor, gamma	1.85432754	1.7E-03	0.00433152
IL1RAP	interleukin 1 receptor accessory protein	1.81783517	5.7E-04	0.00158702
IL18	interleukin 18	1.78749727	7.2E-03	0.01507219
IL12RB2	interleukin 12 receptor, beta 2	1.75873059	2.0E-03	0.00477414
IL16	interleukin 16	1.69836087	2.0E-06	9.81E-06
IL34	interleukin 34	1.65296092	1.1E-05	4.71E-05
IL4R	interleukin 4 receptor	1.62758736	1.4E-03	0.00344625
IL17RE	interleukin 17 receptor E	1.57870251	2.1E-03	0.0051441
IL18BP	interleukin 18 binding protein	1.54288038	5.1E-04	0.00143768
IL10	interleukin 10	1.53244517	1.0E-02	0.02077954
IL17RA	interleukin 17 receptor A	1.47327674	3.8E-03	0.00859307
IL15	interleukin 15	1.44845432	1.2E-04	0.00038054
IL6R	interleukin 6 receptor	1.26142198	3.1E-02	0.05435785
IL6ST	interleukin 6 signal transducer	1.21319158	1.3E-02	0.02600248
IL17RD	interleukin 17 receptor D	1.1827007	4.1E-03	0.00910874
IL11RA	interleukin 11 receptor, alpha	-1.3463143	6.5E-05	0.00022887

Table 2. Gene list of differential interleukin expression in CLI limb skeletal muscle (n=20) as compared to IC (n=16). List was generated from WTSS data, sorted by Fold Change (From IC) and significance (*p*-value), and the targets meeting the $p<0.05$ threshold are represented. Fold Change representative of target message counts. List generated from secondary analysis of previously published WTSS (See ref [42]).

CHAPTER 3: TEMPORAL ASSOCIATION BETWEEN ISCHEMIC MUSCLE PERFUSION RECOVERY AND THE RESTORATION OF MSUCLE CONTRACTILE FUNCTION AFTER HINDLIMB ISCHEMIA

Emma J. Goldberg[1,2], Cameron A. Schmidt[1,2], Tom D. Green[1,2], Reema R. Karnekar[1,2], Dean J. Yamaguchi[3, 4], Espen E. Spangenburg[1,2], Joseph M. McClung[1,2,3*]

[1]Department of Physiology, Brody School of Medicine, East Carolina University, Greenville, NC, United States,

[2]East Carolina Diabetes and Obesity Institute, East Carolina Heart Institute, Brody School of Medicine, East Carolina University, Greenville, NC, United States,

[3]Department of Cardiovascular Sciences, Brody School of Medicine, East Carolina University, Greenville, NC

[4]Division of Surgery, Brody School of Medicine, East Carolina University, Greenville, NC, United States

*Correspondence should be addressed to J.M.M.: Diabetes and Obesity Institute, Office #4109, Mail Stop 743, East Carolina Heart Institute, Brody School of Medicine at East Carolina University, 115 Heart Drive, Greenville, NC 27834-4354. Tel: 252-737-5034 (office); Fax: 252-744-3460; email: mcclungj@ecu.edu

Abstract

During incomplete skeletal muscle recovery from ischemia, such as that occurs with critical limb ischemia, the temporal relationship between recovery of muscle capillary perfusion and contractile function is poorly defined. We examined this relationship in BALB/cJ mice (N = 24) following unilateral hindlimb ischemia (HLI), which pre- clinically mimics the myopathy observed in critical limb ischemia patients. Specifically, we examined this relationship in two phenotypically distinct muscles (i.e., "oxidative" soleus – Sol and "glycolytic" extensor digitorum longus – EDL) 14- or 56-days after HLI. Although overall limb blood flow (LDPI) reached its' recovery peak (48% of control) by HLI d14, the capillary networks in both the Sol and EDL (whole mount confocal imaging) were disrupted and competent muscle capillary perfusion (perfused lectin+μm2/muscle μm2) remained reduced. Interestingly, both Sol and EDL muscles recovered their distinct capillary structures and perfusion (Con Sol; 0.056 ± 0.02 lectin+μm2/muscle μm2, and Con EDL; 0.039 ± 0.005 lectin+μm2/muscle μm2) by HLI d56 (Sol; 0.062 ± 0.011 lectin+μm2/muscle μm2 and EDL; 0.0035 ± 0.005 lectin+μm2/muscle μm2), despite no further improvement in limb blood flow (LDPI). Both muscles suffered severe myopathy, indicated by loss of dystrophin positive immunostaining and the absence of stimulation induced isometric force production at HLI d14. Dystrophin immunofluorescence returned at HLI d56, although neither myofiber CSA (μm2) nor isometric force production (58 and 28% sustained deficits, Sol and EDL, respectively) recovered completely in either muscle. In summary, we reveal that the temporal relationship between the restoration of muscle capillary perfusion and functional ischemic skeletal muscle regeneration favors competent muscle capillary perfusion recovery in BALB/c mice in a phenotypically non-distinct manner.

Introduction

Peripheral arterial disease (PAD) is a medical condition caused by an occlusion in the peripheral arteries, most commonly those supplying blood to the lower extremities[2]. Dysfunctional hemodynamics in the affected limb result in intermittent, pathologic limb ischemia and severe myopathy, defined by abnormal skeletal muscle function and morphology[19,27,71,72]. This myopathy is universally attributed to the completeness of perfusion reduction and little is known about inherent tissue susceptibility[266], although it is a keystone manifestation of PAD and largely predicts patient morbidity and mortality[49,73,74,267,268].

Arteriogenesis, myogenesis, and angiogenesis are central to restoring ischemic limb function and are believed to be tightly coordinated and temporally dependent processes[269]. Whether or not this temporal association varies between different myofiber phenotypes, however, is not well understood. Oxidative and glycolytic muscle fibers display well-documented differences in their capillary structures and density, which contributes to their individualized relationships with tissue perfusion and oxygen distribution[270,271]. PAD patients experience a selective degradation of fast-twitch (type II) fibers that parallels presentations of increasing disease severity[18,72,272], suggesting possible fiber type specific patterns or timelines of muscle regeneration. We used BALB/c mice and hindlimb ischemia (HLI), which in combination results in tissue pathology that mimics critical limb ischemia patients, to interrogate the time-based relationship between limb blood flow recovery, skeletal muscle capillary perfusion recovery and myopathy in oxidative (soleus, Sol) and glycolytic (extensor digitorum longus, EDL) limb muscles. We hypothesized that myofiber phenotypes with well-documented anatomic differences in capillary density and contractile kinetics would possess distinctive patterns of recovery, providing insight into inherent phenotypic susceptibility to limb ischemia. Our results reveal a similar temporal recovery of Sol and EDL

capillary structures and perfusion after HLI that precede muscle morphological and functional recovery.

Materials and Methods

Animals

Experiments were conducted on adult male (12–18 week old) BALB/cJ mice ($N = 24$) obtained from Jackson Laboratories (Bar Harbor, ME). BALB/cJ mice were chosen for their uniformity of pathology presentation and relevance to critical limb ischemia patients. All work was approved by the Institutional Review Committee of East Carolina University. Animal care followed the Guide for the Care and Use of Laboratory Animals, Institute of Laboratory Animal Resources, Commission on Life Sciences, National Research Council. Washington: National Academy Press, 1996.

Hindlimb Ischemia

Acute unilateral hindlimb ischemia (HLI) was performed as previously described[21]. Mice were sacrificed by cervical dislocation or perfusion fixation 14 or 56 days after ligation (d14–56) under ketamine (90 mg/kg bodyweight) and xylazine (10 mg/kg) anesthesia. Limb blood flow was measured by laser Doppler perfusion imaging (LDPI) using a Moor Instruments LDI2-High Resolution (830 nM) System (Moor, Axminster, United Kingdom), as previously described[21]. Images were obtained at baseline (pre), immediately following surgery (d0) and at d7, d14, d21, and d56. Two hours prior to sacrifice, 50 μL of 1 mg/mL *Griffonia simplicolia* Isolectin-B4 (GS-IB4) DyLight 594 conjugate (Vector Labs, Burlingame, CA) was injected into the right retro-orbital sinus using a 31-guage needle.

Perfusion Fixation

Under ketamine/xylazine anesthesia, the heart was exposed to provide access to the atria and ventricles. The right atrium was punctured and a 21-gauge needle was inserted into the left ventricle. Perfusion began with a solution containing phosphate buffered saline (PBS), 10 μg/mL sodium nitroprusside, and 0.03% heparin[273] and continued until the liver was pale in color and all of the blood was flushed from the animal. Vessels were then briefly fixed by systemic perfusion with 4% paraformaldehyde (PFA). Following fixation, EDL and Sol were carefully dissected, tied at length and immersion fixed in 4 or 2% PFA, respectively, and placed in 1× PBS overnight.

Whole Mount Imaging

For whole muscle imaging, muscles were permeabilized in saponin, washed in 1× PBS, and blocked in 5% goat serum + 1× PBS. Samples were incubated overnight with CD31 primary antibody (1:500 dilution). Samples were then washed in 1× PBS and incubated with AF 488 conjugated anti-rat IgG secondary antibody (1:1000 dilution, Invitrogen, Carlsbad, CA), phalloidin (1:100 dilution, Invitrogen) and Nucblue (2 drops/mL). Muscles were washed and stored in 1× PBS at 4°C.

Histology and Immunofluorescence

Muscles were placed into 30% sucrose solution for cryoprotection before being embedded in optimal cutting temperature medium (OCT) and frozen in liquid nitrogen cooled isopentane. 10 μm sections were cut using a CM-3060S cryostat (Leica) and collected on charged glass slides. Histology was performed as previously described[20,21] and included primary antibodies for rat anti-mouse CD31 (BioRad, Hercules, CA), rabbit anti-mouse dystrophin (BioRad, Hercules, CA),

rabbit-anti mouse laminin (Sigma-Aldrich, St. Louis, MO), MyHC types I (BA-D5), IIa (SC-71), and IIb (BF-F3; Developmental Studies Hybridoma Bank, University of Iowa). Samples were mounted using Vectashield hard mount medium (Vector Labs) and imaged with an Evos FL auto microscope (Thermo Fisher Scientific, Waltham, MA).

Muscle Contractile Function

Contractile function was assessed on control and ischemic Sol and EDL muscles using an Aurora 300B-LR, as previously described[21,274,275]. Force frequency curves were integrated and summed over time to calculate force capacity (N^*s/cm^2).

Statistical Analyses

All outcome measures and analyses were performed by individuals blinded to ischemia or control groups. Group means were compared using multiple *t*-tests. A one-way ANOVA was used to determine differences in LDPI perfusion data between all timepoints. *P* values less than 0.05 were considered statistically significant. All statistical analysis and visualization were carried out using Graphpad Prism (Version 7.0d). Image analysis was carried out using ImageJ version 1.53f (NIH, Bethesda, MD). Image processing was applied uniformly across all images of comparable groups. Representative images were contrast enhanced with a 0.3%-pixel saturation threshold. Images used for quantification were not altered in any way that would affect image histograms.

Results

Limb Blood Flow and Competent Capillary Perfusion Recovery

Vascular structure and muscle capillary perfusion recovery were examined by employing the following: non-invasive LDPI; whole mount phalloidin and CD31+ immunostaining; and transverse muscle section CD31+ and isolectin+ immunostaining and quantification. 60× confocal Z-stacks provided us with qualitative information regarding anatomical muscle transformations throughout the regenerative process (Figures 1A,B). Sprouting angiogenesis was observed in both muscles at HLI d14 (indicated with red arrows in Figure 1B). By HLI d56, both muscles had re-established vascular networks with similar properties as the control muscles: i.e., winding and dense Sol capillaries and parallel organization of the EDL vasculature along the myofiber long axis. LDPI revealed a significant decrease in plantar paw blood flow at all time points following HLI induction (Figure 2A). The flux ratio of the ischemic/control limb (AU) was reduced immediately following HLI (d0) and remained attenuated through HLI d56 (d56 flux ratio mean: 0.5696 ± 0.09169) (Figure 2B). Immunohistochemistry of CD31+ cells and lectin+ vessels in transverse muscle sections (Figure 2C) reveal reduced lectin positive areas (lectin+μm2/muscle μm2; used as an indicator of competent capillary perfusion) in both the ischemic Sol and EDL at HLI d14 (Ctrl. Sol: 0.067 ± 0.0014, Isch. Sol: 0.01 ± 0.01, P = 0.006; Ctrl. EDL: 0.035 ± 0.001, Isch. EDL: 0.0034 ± 0.003 P < 0.001). Both Sol and EDL lectin perfusion areas were restored to contralateral baseline values by HLI d56 (Ctrl. Sol: 0.056 ± 0.02, Isch. Sol: 0.062 ± 0.011, P = 0.73; Ctrl. EDL: 0.039 ± 0.005, Isch. EDL: 0.035 ± 0.005 P = 0.841) (Figure 2D). Restoration of lectin+ area in transverse muscle sections indicates recovery of capillary perfusion in the muscle. CD31+ area (CD31+μm2/muscle μm2; used as an indicator of total capillary number) was significantly reduced in the EDL at HLI d14 (Ctrl. EDL: 0.046 ± 0.01, Isch. EDL: 0.007 ± 0.003 P = 0.041). Interestingly, CD31+ area was increased in the Sol at HLI d14 (Ctrl. Sol: 0.045 ± 0.006, Isch. Sol: 0.082 ± 0.015, P = 0.033). CD31+ positive area returned to control values in both the

Sol and EDL by HLI d56 (Figure 2E). The ratio of lectin+:CD31+ areas (used as an indicator of competent perfused capillary vessels out of the total endothelial signal present) decreased in both the ischemic Sol and EDL at HLI d14 (Ctrl. Sol: 1.21 ± 0.49, Isch Sol: 0.17 ± 0.21 P = 0.04; Ctrl EDL: 0.97 ± 0.38, Isch. EDL: 0.30 ± 0.43, P = 0.049) but was restored to contralateral control values at HLI d56 (Figure 2F).

Muscle Structural and Functional Recovery After HLI

Whole mount imaging qualitatively revealed the extent of myofiber degeneration and regeneration after HLI (indicated with yellow arrows in Figure 3A). Transverse sections of the Sol and EDL (Figure 3B) were utilized to quantify the number of dystrophin+ fibers per μm2. At HLI d14, both ischemic Sol and EDL muscles suffered from significant reductions in the number of dystrophin+ fibers. At d56, dystrophin+ fiber numbers were returned to contralateral control values in both muscles (Figure 3C). Fiber cross-sectional area (CSA, μm2) was measured at HLI d56 and revealed attenuated myofiber sizes (CSA, μm2) in the ischemic Sol and EDL compared with their respective contralateral controls (Ctrl. Sol: 798.1 ± 11.9, Isch. Sol: 506.8 ± 17.76, P = 0.23; Ctrl. EDL: 956.6 ± 22.11, Isch. EDL: 379.9 ± 8.64, P = 0.016) (Figure 3D and Supplementary Figure S2A). Compared to contralateral controls, the distribution of MHC fiber types was not altered in the ischemic Sol or EDL (Figure 3E).

Force frequency (FF) protocols were performed to measure total and specific tension in control, HLI d14 and HLI d56 EDL and Sol (Figures 4A,B). After 14d HLI, neither the Sol nor EDL were capable of measurable force production (when dystrophin immunoreactivity was largely absent). At HLI d56, the ischemic EDL was only able to produce 72% of maximal control force (100 Hz)

and the ischemic Sol produced 42% of maximal control force (80 Hz). This signifies persistent deficits in muscle contractile function, which are more severe in the oxidative Sol. Force frequency curves were integrated and summed over time to calculate force capacity (N∗s/cm2). Force capacity was significantly reduced at both HLI d14 (Ctrl. Sol: 58.60 ± 5.498, Isch. Sol: 2.719 ± 2.332, P = 0.23; Ctrl. EDL: 40.43 ± 2.272, Isch. EDL: 0.7552 ± 0.641, P = 0.016) and d56 (Ctrl. Sol: 58.60 ± 5.498, Isch. Sol: 506.8 ± 3.278, P = 0.23; Ctrl. EDL: 40.43 ± 2.272, Isch. EDL: 29.84 ± 2.756, P = 0.016) (Figure 4C).

The specific force values measured in this study are consistent with values previously recorded by our lab and our collaborators using our experimental procedures[59,71,72,266]; we have consistently measured maximum specific force of Sol and EDL muscles to be between 15 and 25 N/cm2. Variations in specific force values between our lab and others may be due to the inbred mouse strain utilized or the extent to which the muscle is dried prior to obtaining its wet weight. The absolute force values achieved in our experiments (Figures 4D,E), however, are similar to those previously outlined by Brooks and Faulkner[49]. Control EDL and soleus muscles isolated from the 12–18-week-old BALB/cJ mice used in this study reached maximal absolute force values of 364 and 211 mN, respectively, comparable with the 413 and 213 mN absolute force values that were recorded for 2–3-month-old C57BL/6 mice in their study[49].

DISCUSSION

Effectively recovering limb skeletal muscle contractile function within an ischemic environment is dependent upon the successful reestablishment of both tissue perfusion and anatomic muscle architecture. We examined the temporal relationship between the restoration of ischemic limb

blood flow, muscle capillary bed organization, competent vessel perfusion, and myofiber regeneration in physiologically distinct muscles. Our findings reveal that capillary perfusion and muscle structural organization (dystrophin) are restored within 8 weeks of ischemic onset by HLI in oxidative and glycolytic muscles of BALB/cJ mice. Despite peak restoration of overall limb blood flow and complete restoration of muscle capillary perfusion, myofiber sizes and muscle force capacity do not recover on the same timeline in either oxidative or glycolytic muscle phenotypes. Our contractile measurements were performed in a controlled bath facilitating the diffusive flux of oxygen in muscles isolated from an ischemic environment in vivo. Effectively, we removed any confounding influences of differential capillary perfusion in our functional force measurements. 56-days post HLI, despite quantitative restoration of competent capillary perfusion in vivo, muscles are severely functionally and anatomically compromised even in an environment where diffusive oxygen is readily available across the length of the muscle. Combined with the histological evaluations, we interpret this data to reveal that the observed functional deficits are likely a result of the delays in structural/anatomical repair of the muscle fibers. Overall, our data reveal that ischemic myopathy persists similarly in oxidative and glycolytic BALB/c myofibers long after ischemic onset, and that both muscle types share a similar temporal restoration of tissue perfusion.

The temporal recovery of limb blood flow from nadir is a commonly studied process pre-clinically. BALB/cJ mice, in particular, suffer incomplete limb blood flow recovery across multiple models of hindlimb ischemia[20,21,141,145,188]. This deficit is commonly attributed to a differential density of pre-existing intermediate collateral vessels prior to ischemia and/or reduced ability to generate new collaterals via arteriogenesis. In this study, peak recovery of limb/plantar paw blood flow,

measured by LDPI, occurred within 14-days of surgically induced ischemia. The nature of the surgery used in this study (isolation and transection at the proximal end of the femoral artery) is insufficient to induce outward tissue necrosis (paw lesions or auto amputation), even across the 56d period of ischemic recovery. In this instance, the temporal restoration of peak limb/paw blood flow was disconnected from the muscle tissue specific restoration of capillary perfusion. This demonstrates that the recovery of individual muscle tissue capillary perfusion is regulated locally and is distinct from that of the limb/paw blood flow that presumably rescues toe/paw lesion formation in these mice. Given the anatomic disruption we observed in vascular structures at HLI d14, the restoration of locally competent capillaries is likely a key limiting factor in the ability of the limb to shunt any restored flow to anterior and posterior skeletal muscles. In the case of the Soleus muscle, this is uniquely defined by the maintenance of CD31+ signal at HLI d14, despite a lack of competent perfusion of those vessels. In the case of the EDL, this is defined by a reduction of CD31+ signal combined with lack of vessel perfusion.

Clinically, pathologic limb ischemia is accompanied by intermittent bouts of ischemic insult, which cause cycles of myofiber degeneration and regeneration[276]. When successful, regenerative processes result in an innervated, vascularized, contractile skeletal muscle that is indistinguishable from its non-ischemic counterpart[269,277]. In general, myopathic diseases are tightly paralleled with vascular network degradation. A partial explanation for the failure of therapeutic angiogenesis trials in critical limb ischemia patients may be that these therapies fail to stimulate the survival and regeneration of ischemic muscle myofibers, which face a harder path to full restoration than the capillary networks that feed them. Both muscles examined restored functional, individualized vascular networks within 56 days: the Sol remodeled its convoluted network; the EDL remodeled

its myofiber-parallel network. A similar timeline of vascular function and structure recovery in these phenotypically distinct muscles suggests that local signals within each muscle are capable of guiding vascular progenitors and endothelial cells through complex and distinct organizational processes. Despite this, both muscle phenotypes continued to suffer from persistent myopathy through 56 days. This indicates that processes related to vascular reorganization are temporally prioritized over those related to contractile function restoration in the limb, but do not guarantee complete functional recovery of the affected muscles. Although the reason for the temporal prioritization of revascularization in regenerating skeletal muscle is not completely understood, a logical explanation is that sufficient blood supply is required to maintain functional skeletal muscle[278,279]. Additionally, studies have highlighted a role for angiogenesis in increasing the amount of active blood-vessel related stem cells that can participate in skeletal muscle regeneration[280,281]. Dynamic and reciprocal interactions between regenerating skeletal muscle and angiogenesis are accepted as pivotal components of juvenile dermatomyositis (JDM) myopathy and Duchenne muscular dystrophy (DMD)[282] and have led to approaches to treat muscular dystrophies with phosphodiesterase-5 inhibitors like Tadalafil[283] to improve blood flow[284] and muscle regeneration. The results of this study, in a common pre-clinical model of PAD, support the development of dual therapy approaches to improve both the temporal restoration of muscle capillary perfusion and the regeneration of muscle myofibers to restore full functional capacity.

Several articles have reported the selective degradation of faster-twitch fibers during the ischemia that occurs in PAD patients[18,72,272]. A benefit to this adaptation would be clearly evident if slower/oxidative myofibers demonstrated a regenerative or functional advantage under the intermittent ischemic conditions caused by PAD. In this study, we took advantage of the fiber type

homogeneity observed in the predominantly oxidative Sol and predominantly glycolytic EDL mouse muscles. Thus, if oxidative fibers harbored an inherent regenerative advantage, the Sol muscle should recover from ischemic injury more completely and efficiently. Despite muscle type-specific differences in vascular anatomy and contractile characteristics, the oxidative Sol and glycolytic EDL muscles appear to possess similar angiogenic timelines in our model system. It is important to note the context of the studies performed here when interpreting this finding. Mice of the BALB/c parental strain most accurately mirror the myopathy and vasculopathy seen in critical limb ischemia patients in the pre-clinical HLI model[21,88,145,188,285,286] . PAD presents as either intermittent claudication (IC; pain with exertion that is relieved with rest) or critical limb ischemia (CLI; pain at rest with or without tissue necrosis or gangrene). Although less common than IC, CLI carries a substantially higher morbidity and mortality; CLI patients have a risk of major amputation or death that approaches 40% in 1 year[69,287]. Very little is known about the biology of limb skeletal muscle in CLI patients. Recently, we observed no change in myofiber phenotype in the gastrocnemius muscles of CLI patients[42]. CLI patients are largely intolerant to exercise and suffer high rates of morbidity, even after surgical interventions that restore blood flow to the affected limb. This clinical disconnect parallels the temporal disconnect we observed between muscle perfusion reconciliation and persistent myopathy in BALB/c muscles.

CONCLUSION

The timeline required to regenerate a fully functional skeletal muscle is dependent upon the concomitance of both angiogenic and myogenic processes. As we have shown, these processes do not necessarily reach completion within the same timeline. Furthermore, the restoration of tissue perfusion does not guarantee timely muscle functional recovery. Our results may partially explain

why, despite a marked increase in the number of lower extremity revascularization procedures, functionality tied to morbidity and mortality in the PAD patient population remains largely unchanged (Goodney et al., 1946; Sampson et al., 2014). A more precise understanding of the persistent myopathy in the presence of restored limb blood flow and tissue perfusion provides an opportunity to develop adjuvant therapies to better ensure the success of surgical revascularization procedures and potentially identify patients most at risk for severe manifestations of PAD and other myodegenerative diseases.

Figures:

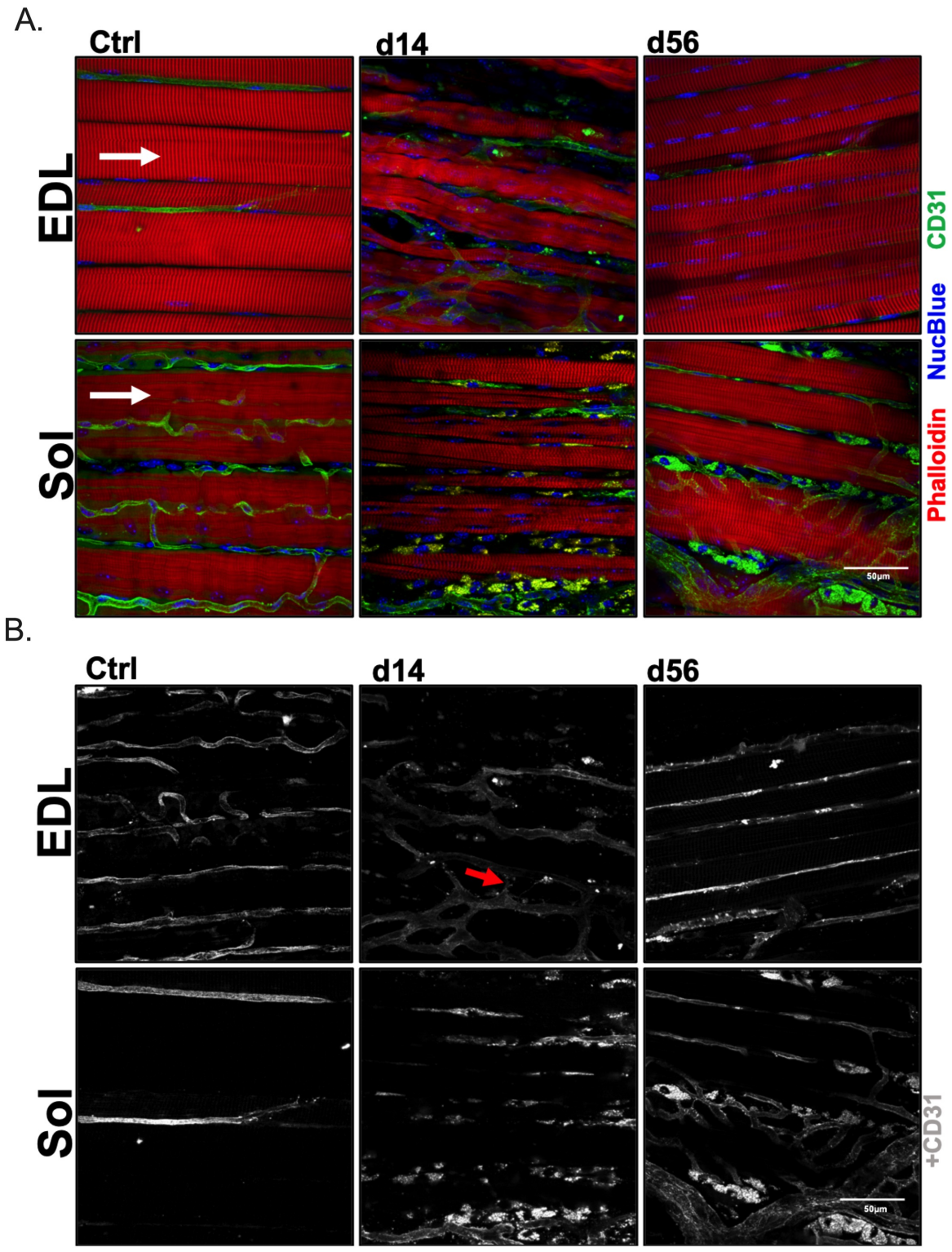
A.
Ctrl
d14
d56
EDL
Sol
CD31
NucBlue
Phalloidin
50µm
B.
Ctrl
d14
d56
EDL
Sol
+CD31
50µm

Figure 2: Myofiber and capillary anatomy during recovery from ischemia. (A) Representative 60× confocal Z-stack images of whole-Mount EDL and Sol muscles immunostained for myofiber structure (phalloidin; red), vascular structure (CD31; green) and nuclei (NucBlue; blue) in control, d14 and d56 limbs. Images qualitatively reveal the complex microenvironment within the limb following an ischemic injury and present a temporal summary of our findings. White arrows indicate myofiber direction. (B) Grayscale representative 60× confocal Z-stack images from panel (A), presenting only CD31+ immunostaining. These whole-Mount EDL and Sol images specifically highlight the vascular structures in the muscles before and following ischemic injury (CD31; gray). Red arrows indicate observed sprouting angiogenesis in the ischemic microenvironment.

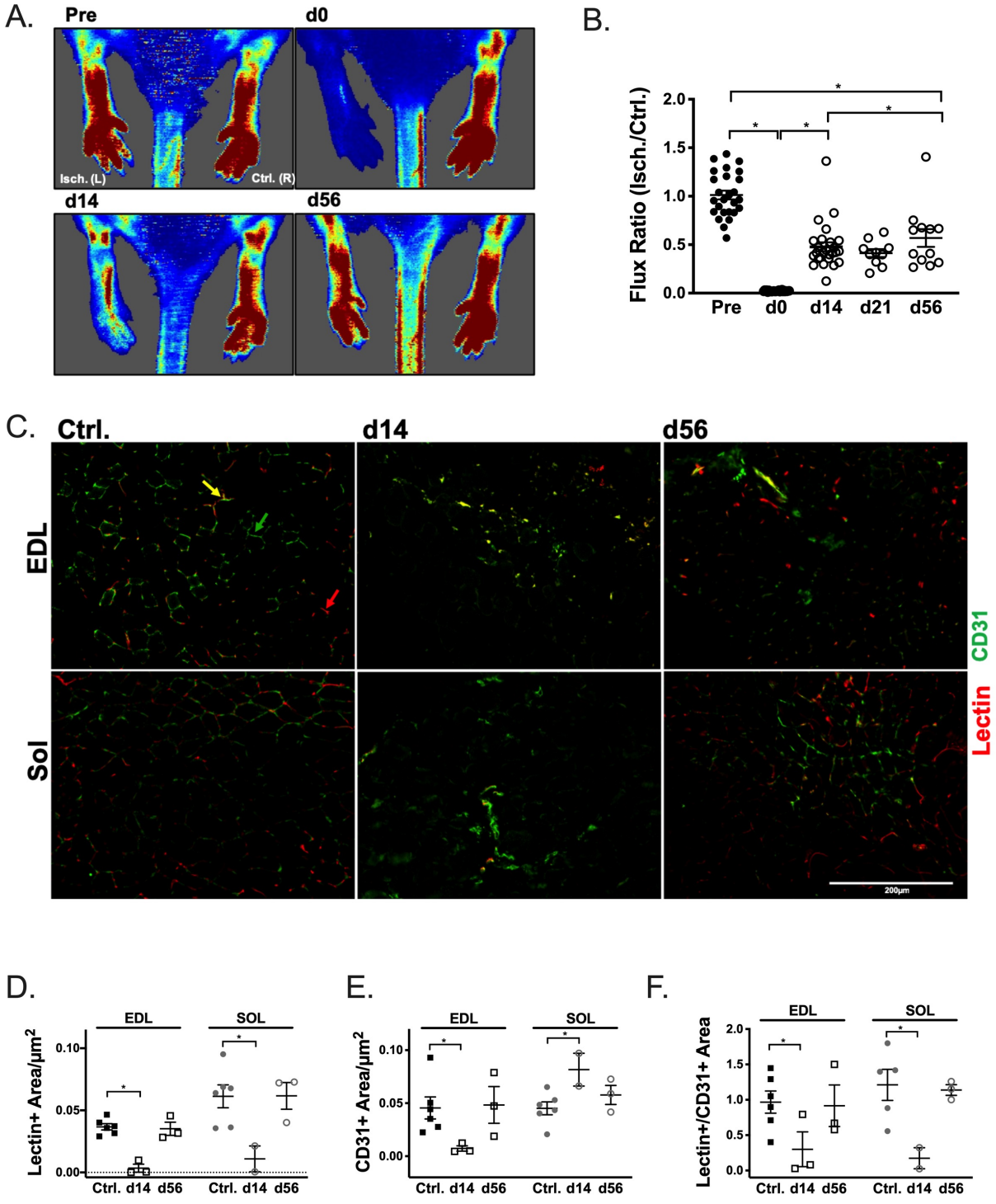
A.
Pre
d0
Isch. (L)
Ctrl. (R)
d14
d56
B.
Flux Ratio (Isch./Ctrl.)
2.0
1.5
1.0
0.5
0.0
Pre
d0
d14
d21
d56
C.
Ctrl.
d14
d56
EDL
Sol
CD31
Lectin
200µm
D.
EDL
SOL
Lectin+ Area/µm2
0.10
0.05
0.00
Ctrl. d14 d56
Ctrl. d14 d56
E.
EDL
SOL
CD31+ Area/µm2
0.10
0.05
0.00
Ctrl. d14 d56
Ctrl. d14 d56
F.
EDL
SOL
Lectin+/CD31+ Area
2.0
1.5
1.0
0.5
0.0
Ctrl. d14 d56
Ctrl. d14 d56

Figure 3: Restoration of peripheral blood flow and muscle capillary perfusion. (A) Representative laser Doppler perfusion images (LDPI) of the ischemic left [Isch. (L)] and control right [Ctrl. (R)] plantar paws in the prone position at baseline, d0, d14, and d56. (B) Quantification of flux measurements at baseline, d0, d14, d21, and d56 represented as a ratio of the left (Isch.) over right (Ctrl.) limbs. (C) Representative 20× immunofluorescent images of systemically DyLight 594 conjugated GS-IB4 lectin, which indicates vessels which were actively perfused at the time of sacrifice (red), and cluster of differentiation 31 (CD31+, PECAM-1; green), which indicates total endothelial cells, in transverse sections of the control, d14 and d56 Sol and EDL. Red arrows indicate lectin+ vessels; green arrows indicate CD31+ vessels and yellow arrows indicate CD31+/lectin+ vessels. (D) Average lectin positive area per μm2 in control, d14 and d56 EDL and Sol. (E) Average cluster of differentiation 31 (CD31), area per μm2 in control, d14 and d56 EDL and Sol. (F) Ratio of lectin positive area:CD31 positive area in control, d14 and d56 EDL and Sol. Error Bars indicate mean ± SEM. $*P < 0.05$.

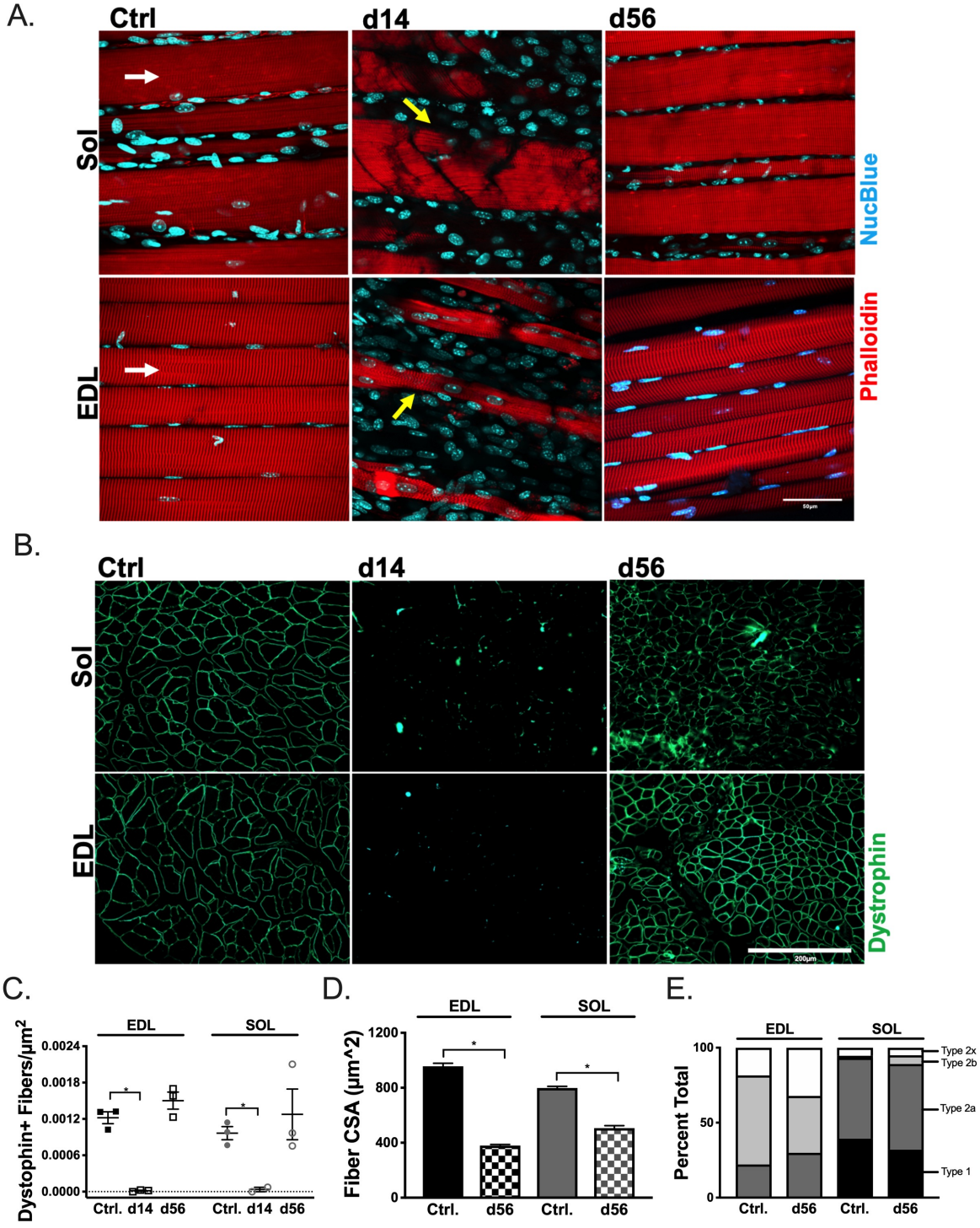
A.
Ctrl
d14
d56
Sol
EDL
NucBlue
Phalloidin
B.
Ctrl
d14
d56
Sol
EDL
Dystrophin
C.
EDL
SOL
Dystophin+ Fibers/µm2
0.0024
0.0018
0.0012
0.0006
0.0000
Ctrl. d14 d56 Ctrl. d14 d56
D.
EDL
SOL
Fiber CSA (µm^2)
1200
800
400
0
Ctrl. d56 Ctrl. d56
E.
EDL
SOL
Percent Total
100
50
0
Type 2x
Type 2b
Type 2a
Type 1
Ctrl. d56 Ctrl. d56

Figure 4: Myofiber structural recovery. (A) Representative 60× Z-stacks of control, d14 and d56 EDL and Sol. Myofiber structure is represented by phalloidin immunostaining (red) and counterstained with NucBlue (blue). White arrows indicate myofiber direction. Yellow arrows indicate damaged myofibers. (B) Representative 20× immunofluorescence images of dystrophin positive immunostaining in transverse sections of control, d14 and d56 EDL and Sol. (C) Average dystrophin-positive immunostained myofibers per μm2 in control, d14 and d56 EDL and Sol. (D) Average CSA (μm2) of myofibers in control and d56 EDL and Sol. (E) Fiber type distribution in control and d56 EDL and Sol (E). $*P < 0.05$.

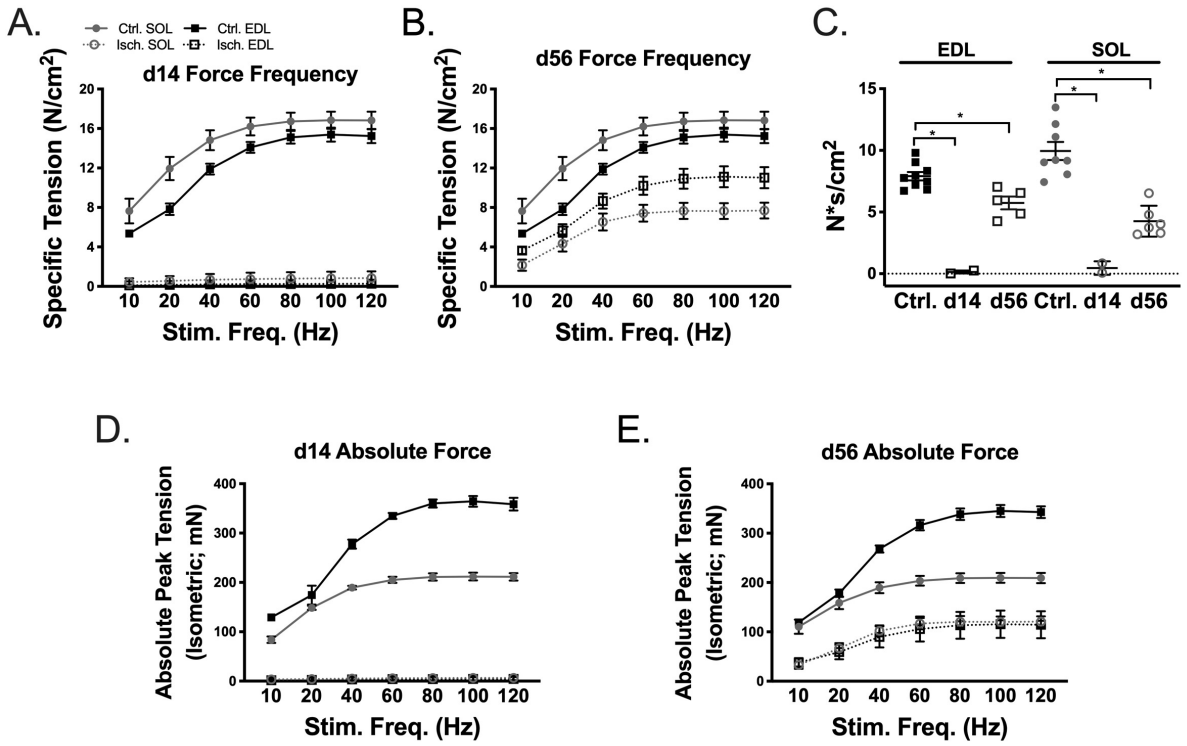

FIGURE 5: Muscle contractile function recovery. Force frequency curves for ischemic and control Sol and EDL muscles at d14 (A) and d56 (B). (C) Force capacity (measured by integrating the force frequency curves and summing the values over time) of control, d14 and d56 EDL and Sol. Absolute peak isometric tension curves for ischemic and control Sol and EDL muscles at d14 (D) and d56 (E). Bars indicate mean ± SEM. $*P < 0.05$

CHAPTER 4: MURINE MODEL OF CYTOCHROME C-OXIDASE 6A2 (COX6A2) GENOMIC DELETION

Emma J. Goldberg[1,2], Zoe S. Terwilliger[1,2], Makenzie G. Kolasa[1,2], Cameron A. Schmidt[1,2], Adam J. Amorese, Tom D. Green[1,2], Reema R. Karnekar[1,2], Dean J. Yamaguchi[3, 5], Kelsey Fisher-Wellman[1, 2], Tonya Zeczycki[4], Espen E. Spangenburg[1,2], Joseph M. McClung[1,2,3*]

[1]Department of Physiology, Brody School of Medicine, East Carolina University, Greenville, NC, United States

[2]East Carolina Diabetes and Obesity Institute, East Carolina Heart Institute, Brody School of Medicine, East Carolina University, Greenville, NC, United States

[3]Department of Cardiovascular Sciences, Brody School of Medicine, East Carolina University, Greenville, NC

[4]Department of Biochemistry and Molecular Biology, Brody School of Medicine, East Carolina University, Greenville, NC, United States

[5]Division of Surgery, Brody School of Medicine, East Carolina University, Greenville, NC, United States

*Correspondence should be addressed to J.M.M.: Diabetes and Obesity Institute, Office #4109, Mail Stop 743, East Carolina Heart Institute, Brody School of Medicine at East Carolina University, 115 Heart Drive, Greenville, NC 27834-4354. Tel: 252-737-5034 (office); Fax: 252-744-3460; email: mcclungj@ecu.edu

Introduction

Peripheral artery occlusive disease (PAD) is a manifestation of systemic atherosclerosis defined by an occlusion in arteries most commonly supplying blood to the lower extremities[1,2]. The clinical course of PAD treatment has largely targeted residual blood flow through revascularization and endovascular procedures[11,68,288]. These treatments have largely proven ineffective[1-3], unfortunately. This is especially true in patients with chronic limb threatening ischemia (CLTI), the most severe clinical manifestation of PAD. A growing body of research indicates CLTI is a distinct manifestation of PAD, and that these patients may be genetically susceptible to severe disease manifestation[42,82,85,86]. Preclinically, common inbred strains of mice (C57BL/6J and BALB/c) mirror this presentation. BALB/c mice suffer from a severe ischemic myopathy and are unable to recover muscle contractile function and paw perfusion within 56 days, while C57BL/6J mice are less affected[21,23,52,143]. A 37-gene quantitative trait locus (QTL), *Lsq-1*, was identified by examining tissue survival and perfusion recovery following hindlimb ischemia (HLI)[43]. Currently, only three genes within *Lsq-1* (ADAM12, IL-21R, and BAG3) are recognized as being crucial for limb blood flow restoration or myopathy resolution in C57BL/6J and BALB/c mice following HLI[88,191,198]. Although these processes require cellular energy (adenosine triphosphate – ATP), there is currently no comprehensive understanding of the mechanism(s) that regulate the generation of this energy charge in the ischemic limb, or what influence genetics may impart in these processes.

The balance of limb skeletal muscle mitochondrial bioenergetics has the potential to significantly advance therapeutic PAD research[38,52,148,217,289]. Skeletal muscle contains dense mitochondrial networks responsible for ATP production, maintenance of redox charge, and intracellular communication. Compromised mitochondrial function results in increased oxidative stress, mitochondrial DNA (mtDNA) damage and progressive respiratory chain impairment – all of which are implicated in aging and multiple disease states including PAD[1,35–38]. Mitochondria also play crucial roles in the energetic failure and initiation of cell death of ischemic cells[290,291] and house the machinery of metabolic pathways that are responsible for ~90% of the cell's resting ATP production. Given these crucial roles, the maintenance or recovery of mitochondrial function in ischemic limb muscles could be a key mechanism for tissue survival and regeneration during an acute ischemic event. *Ex vivo* studies of skeletal muscle myofibers from PAD patients demonstrate decreased oxygen consumption and enzyme activity[35,39–41], substantiating the notion that PAD patients suffer from an inherent mitochondrial dysfunction. One gene target identified in *Lsq-1*, Cox6a2, is a protein subunit of cytochrome c oxidase (CcO; complex IV of the mitochondrial electron transport system). Its presence in *Lsq-1* is unique because it is thought to be expressed solely in mature striated muscles (cardiac and skeletal) and serves as a regulatory component of cytochrome c oxidase, the terminal enzyme in the electron transport system (ETS) responsible for oxygen consumption[292,293].

Previous studies have described the existence of a strain dependent mitochondriopathy that occurs in inbred strains of mice following HLI and segregates mice with poor perfusion recovery[21,52] independent of reductions in mitochondrial content. The extent to which muscle mitochondrial function requires a functional Cox6a2 remains somewhat unclear. Previous

studies have used mice with a null mutation in Cox6a2, resulting in a lifelong loss of Cox6a2 loss in cardiac and skeletal muscle tissue[293,294]. These studies identified only subtle cardiac dysfunction, defined by: impaired maximal diastolic performance; increased whole body energy expenditure; and skeletal muscle ROS production under normal cage conditions. When challenged with a chronic high-fat diet (HFD), Cox6a2-null mice did not gain more weight and were protected from HFD-induced glucose intolerance and insulin resistance. This model inherently contains confounders, however, when investigating the skeletal muscle specific role of Cox6a2. Potential problems include overlapping cardiac complications and potential lifelong compensation for developmental loss of the transcript and protein.

To establish a skeletal muscle cell specific inducible deletion model of Cox6a2 implemented after the mice reached adulthood, we generated Cox6a2$^{f/f}$ mice on a BL6J background and crossed them to inducible skeletal muscle Cre (HSA-MCM) mice (on a BL6NJ background). We aged these mice to adulthood and treated them with tamoxifen to induce genomic deletion of Cox6a2. Our findings validate the HSA-Cre mediated and tamoxifen inducible genetic deletion model of Cox6a2, establishing this line as an effective murine model of Cox6a2 mRNA and protein reduction in limb skeletal muscles. We revealed a role for Cox6a2 in basal mitochondrial function, though physiologic muscle function was not impaired by tamoxifen induced deletion of Cox6a2. Reductions in basal mitochondrial function were not exacerbated by over-nutrition induced by high fat diet. We will employ this genetic model in future mitochondrial sufficiency studies after hindlimb ischemia.

Methods

Animal Generation

Generation of the Cox6a2 knockdown mice was achieved by crossing mature skeletal muscle-specific, tamoxifen inducible HSA-mER-Cre-mER male mice (originally developed by Dr. Karyn Esser, University of Florida, Gainesville, FL, USA, and Dr. John J. McCarthy, University of Kentucky, Lexington, KY) with female mice with flox sites flanking exons 1-3 of the Cox6a2 gene (*Cox6a2$^{f/f}$*). This initial breeding scheme resulted in HSA-mER-Cre-mER^{+}-Cox6a2$^{f/-}$ males, which were then crossed with female *Cox6a2$^{f/f}$* mice to generate HSA-mER-Cre-mER^{+}-Cox6a2$^{f/f}$ mice. The HSA-mER-Cre-mER mice have a c57/Bl6NJ background, and Cox6a2$^{f/f}$ mice were generated on a c57/Bl6J background.

Animal Genotyping

All animals were genotyped based on the presence of HSA-mER-Cre-mER, and heterozygote or homozygote Cox6a2 flox expression using genomic DNA. Primer sets for mER-Cre-mER F-5'-GCATGGTGGAGATCTTTGA-3' and R-5'-CGACCGGCAAACGGACAGAAGC -3' were used to screen for HSA-mER-Cre-mER^{+} animals. Animals were additionally genotyped for Cox6a2 flox using primer sets F-5'- GAAGTCATTCCGTGCCACTGT-3' and R-5'-CCTGCTTGCTCCAGCCC-3', where the Cox6a2 flox amplification band is ~2038bp and the wild-type band is ~1891bp.

Cox6a2 Recombination DNA analysis

Successful recombination was validated in all experimental animals. Tamoxifen induced recombination was confirmed through PCR analysis if genomic DNA with a DNA Isolation kit. Primers F-5'-GAAGTCATTCCGTGCCACTGT-3' and R-5'-

TATGGATAAGAACTAACACAAGACTG were used to generate an amplicon that was 295bp in length, indicating deletion of the flox region of Cox62.

Experimental Approach

Eight- to ten-week-old HSA-mER-Cre-mER^{+}-Cox6a2$^{f/f}$ and HSA-mER-Cre-mER^{+}-Cox6a2$^{f/-}$ mice were injected for five consecutive days with either 2mg day^{-1} tamoxifen or vehicle solution. Three weeks later, the mice were subjected to a second round of five-day tamoxifen delivery. Animals of the genotype HSA-mER-Cre-mER^{+}-Cox6a2$^{f/f}$ administered tamoxifen or sunflower seed oil and ethanol are referred to as KO and WT mice, respectively. Animals of the genotype HSA-mER-Cre-mER^{+}-Cox6a2$^{f/-}$ administered tamoxifen will be referred to as HET mice. Cohorts of HSA-mER-Cre-mER^{+} and Cox6a2$^{f/f}$ administered tamoxifen were additionally assessed to ensure no off-target effects (supplemental info). To date, we have found no off target effects of tamoxifen delivery in any of our outcome measurements, including skeletal muscle contractile function, mitochondrial respiration, and bodyweight. All animals were housed in a temperature (22˚C) and light controlled (12-hour light/12-hour dark) room with free access to food and water. All animal experiments adhered to the Guide for the Care and Use of Laboratory Animals from the Institute for Laboratory Animal Research, National Research Council, Washington, D.C., National Academy Press, 1996, and any updates. All procedures were approved by the Institutional Animal Care and Use Committee of East Carolina University

High Fat Diet and Glucose and Insulin Tolerance Testing

Mice of the genotype HSA-mER-Cre-mER^{+}-Cox6a2$^{f/f}$ were placed on either a 45% Kcal HFD (Research Diets; D12451) or a 10% kcal low-fat diet (LFD; Research Diets D12450) at 4-6 weeks

of age and were maintained on the diet until sacrifice at 20-22 weeks of age. Tamoxifen was administered at weeks 6 and 10 of the diet, resulting in the loss of skeletal muscle Cox6a2. Whole-body glucose tolerance was determined during the 14th week of diet feeding from intraperitoneal (IP) injection of glucose (1g of glucose/kg body mass) after a 4-h morning fast. Insulin tolerance testing was performed during the 15th week of diet feeding using IP injections of insulin (1.0 U insulin/kg body mass) after a 4-h fast. Blood glucose levels were measured with a glucometer (Nova Biomedical; Waltham, MA, USA) before glucose or insulin injection. For the GTTs, blood glucose was measured before injection (0), 15, 30 , 60 and 120 min after glucose injection. For ITTs, blood glucose was measured before insulin injection (0), and at 15, 30, 60 and 90 min after the injection.

Immunofluorescence and Histology

Tibialis anterior, extensor digitorum longus (EDL) and soleus muscles from WT, Het and KO mice were excised and embedded in Tissue-Tek optimal cutting temperature medium. Samples were then frozen in liquid-nitrogen cooled isopentane and stored at -80˚ until processing. 10um transverse sections were cut on 3060S cryostat, collected on charged slides and stored at -20˚C until use for histology or IHC. Standard hematoxylin and eosin (H&E) staining was performed, as previously described[145]. IHC was performed as previously described[21]. Briefly, sections were fixed in 1:1 acetone/methanol for 5min at -20˚C, rehydrated in PBS, and blocked in 5% goat serum in PBS for 1hr at room temperature. Sections were then incubated overnight in primary antibodies for rabbit anti-mouse dystrophin (1:100 dilution; Thermo Rb-9024; targeted to the protein C-terminus) and rat anti-mouse CD31 (platelet endothelial cell adhesion molecule 1; 1:1000 dilution; BioRad, Hercules, CA). The following day, slides were washed with PBS and incubated for 1

hour with Alexa-Fluor 488-conjugated anti-rat, and 647-conjugated anti-rabbit secondary antibodies (1:250, Invitrogen, Carlsbad, CA). Samples were mounted using Vectashield hard mount medium (Vector Labs) and imaged with an Evos FL auto microscope (Thermo Fisher, Waltham, MA) with a plan fluorite 20x objective lens. Images were taken across each muscle section. Images were analyzed by a blinded investigator using ImageJ version 1.53f. Technical replicates were averaged, and data is represented by mean fluorescence positive area.

Western Blotting

Isolated mitochondria pellets were resuspended in RIPA buffer containing protease inhibitors. Proteins were separated on NuPAGE Bis-Tris gels (Thermo Fisher), which were then transferred onto polyvinylidene difluoride (PVDF) membranes (Trans-Blot Turbo Transfer System; Bio-Rad). PVDF membranes were blocked at room temperature for 90 minutes in 5% dry milk, and then incubated overnight with a primary antibody for Coxa2 at 4˚C. Following primary incubation, membranes were incubated at room temperature for 1h with goat-anti rabbit HRP-conjugated secondary antibodies at 1:10,000 (Invitogren). Proteins were visualized via chemiluminescence with care being taken to ensure signal detection was in a linear range and not saturated (Clarity Western ECL Substrate, Bio-Rad). The images were quantified using Image Lab and normalized to total protein content.

Muscle Contractile Function

Muscle contractile function was assessed *in vitro* for soleus and EDL muscles of WT, Het and KO mice, as previously described[21,143,274] using an Aurora 300B-LR system (Aurora Scientific, Aurora, ON, Canada). Resting tension and muscle length were adjusted for each muscle to obtain the

optimal twitch contraction force prior to force frequency and fatigue resistance protocols. The length and mass of each muscle were recorded for calculation of physiological CSA and specific force, expressed as (N/cm^2)[295]. Force frequency curves from each stimulation frequency were integrated over time and then added together to calculate force capacity ($N*s/cm^2$).

Skeletal Muscle Mitochondrial Isolation

Skeletal muscle mitochondria was isolated using differential centrifugation as previously described[296,297] with some modifications. The following buffers were utilized: buffer A (PBS and 10 mm EDTA at pH 7.4); buffer B (50 mmMOPS, 100 mm KCl, 1 mm EGTA, 5 mm $MgSO_4$); and buffer C (buffer B and 2 g/liter BSA). Gastrocnemius complexes (medial/lateral gastrocnemius heads, plantaris and soleus) were excised and immediately placed in ice cold Buffer A. Samples were then minced and exposed to 5% trypsin for 5 minutes on ice. The samples were then centrifuged at 600xg for 5 minutes at 4˚C and the supernatant was removed. The remaining pellet was resuspended in Buffer B and homogenized via a drill-driven Teflon pestle and borosilicate glass vessel. Homogenates were centrifuged at 800xg for 10min at 4˚C. The supernatant was filtered through two layers of gauze and centrifuged at 10,000xg for 10min at 4˚C. Pellets were then washed in 1.4mL of Buffer A, transferred to microcentrifuge tubes and centrifuged at 10,000×*g* for 10 min at 4 °C. Final mitochondrial pellets were resuspended in 100–200µL of Buffer A, and protein content was determined using a BCA protein assay. Freshly isolated mitochondria were immediately used for functional experiments, and the remaining pellet was flash frozen and used for complex specific activity assays, Western blot analyses and Blue-Native Page analyses.

High Resolution Respirometry

High-resolution O_2 consumption rate measurements were conducted at 37˚C in a 1mL reaction volume using the OROBOROS Oxygraph-2K (Oroboros Instruments) as previously described[296,297]. The base assay buffer used for all experiments was Buffer D (105 mM potassium-MES, 30 mM KCl, 10 mM KH2PO4, 5 mM MgCl2, 1 mM EGTA, 2.5 g/L BSA and 5 mM creatine monohydrate; pH = 7.2), which was then modified for either the creatine kinase (CK), or the hexokinase (HK) clamp.

Creatine Kinase Clamp Experiments

A modified version of the CK clamp was used to determine steady state JO_2 across a physiologically relevant range of ATP free energies of hydrolysis, as previously described[296,297]. 20ug of fresh mitochondria were added to Buffer D, followed by respiratory substrates to stimulate State 4 respiration. The substrate conditions tested were: 1) 5mM pyruvate and 2mM malate (P/M); 2) 5uM rotenone and 10mM succinate (R/S); and 3) 5mM pyruvate, 2mM malate, 5mM glutamate, 0.2mM octanoyl-carnitine and 5mM succinate (Multi). The CK clamp was initiated by the addition of 5mM ATP, 1mM PCr and 20U/mL CK, simulating a high energy demand for ATP re-synthesis. PCr was then sequentially added to 6, 15 and 21mM to create a low energy demand state. FCCP was added at the end of the protocol to stimulate maximal uncoupled respiration.

Hexokinase Clamp Experiments

Freeze fractured mitochondria were challenged with the HK clamp, which measures respiration under conditions of saturating ADP as previously described[297]. Buffer D supplemented with cytochrome C and 5mM ADP was loaded into the chambers, followed by 10ug of freeze thawed mitochondria. Hexokinase (1U/mL) and glucose (5mM) were then added to the chamber, followed by NADH to directly measure NADH-linked respiration. This respiration was then inhibited by rotenone (0.002mM), and succinate-linked respiration was stimulated by the addition of succinate

(10mM). Antimycin A (0.0025uM) was then added, inhibiting succinate-linked respiration, and complex IV was stimulated through the addition of the cytochrome C-specific electron donor N,N,N',N'-tetramethyl- p-phenylenediamine (TMPD; 0.5 mM) and ascorbate (2 mM).

Analysis of mtDNA/nDNA Ratio

To measure mitochondrial content/density, the ratio of mitochondrial DNA (mtDNA) to nuclear DNA (nDNA) was quantified as previously described[42,298]. Genomic DNA was isolated from skeletal muscle of WT and KO animals using a Nucleospin tissue kit (Takara). qPCR was performed using 50ng of gDNA. The ratio of mtDNA/nDNA was calculated by dividing the MT- expression by the GAPDH expression.

Blue-Native Page

200ug of isolated mitochondria were spun down at 10,000xg for 10 minutes at 4˚C. Pelleted mitochondria were then resuspended in Native PAGE Sample Buffer (Invitrogen, Carlsbad, CA) supplemented with protease inhibitors. Mitochondria were then solubilized using an 8:1 digitonin to protein ratio (Sigma-Aldrich, St. Louis, MO) for 20 minutes on ice. Samples were then centrifuged at 20,000xg for 15 minutes at 4˚C. Supernatants were transferred to new tubes and protein was quantified via a BCA assay. 30ug of protein was combined with 5% G-250 sample additive and loaded onto a 3-12% NativePage Bis-Tris gel (Invitrogen, Carlsbad, CA). The gel was run in dark buffer at 150V for 30 minutes, after which dark buffer was switched out with light buffer. The gel was then run at 250V for an additional 60min. The gel was fixed in a 40% methanol/10% acetic acid solution for 15min at room temperature and destained in 8%

acetic acid until the desired background was reached. The gel was imaged on a Bio-Rad Chemidoc imaging system. Densitometry was performed using ImageLab software v6.0.1.

Statistics.

Comparisons between KO and WT mice were performed by Student's *t*-tests. Comparisons of KO, WT and Het groups were analyzed using one-way ANOVAs. Nonparametric Mann-Whitney testing was used to determine differences between the distributions of necrosis scores between groups. Statistical analyses were conducted using Prism, version 9.3.1 (GraphPad Software Inc., San Diego, CA, USA). In all cases, $P < 0.05$ was considered statistically significant. Data are presented as mean ± SEM.

Results

Mouse Model of Skeletal Muscle-Specific Cox6a2 Loss

Measurements of genomic DNA demonstrated that exons 1-3 of the *Cox6a2* gene were deleted in the skeletal muscle of tamoxifen-injected mice from two rounds of injection. This recombination event was specific to skeletal muscle, as evidenced by the lack of recombination in non-skeletal muscle tissue (Figure 1C). No recombination was observed in vehicle-injected mice, and partial recombination was observed in tamoxifen-treated HET mice (Figure 1D). Recombination resulted in a significant loss of Cox6a2 mRNA (Figure 1E). Cox6a1 mRNA was measured in skeletal muscle of KO, WT and HET mice, and we found that its expression in KO mice was increased compared with the other two groups (Figure 1E). Cox6a2 protein abundance was measured in isolated skeletal muscle mitochondria, and recombination was successful in reducing its expression by an average of 55% compared to WT mice (Figures 1F, G). Together, these data

confirm that our inducible model of Cox6a2 loss results in skeletal muscle specific loss of Cox6a2 protein. Importantly, bodyweight was unchanged between groups and no outward phenotype was observed (Figures 1H, I). Initial examination revealed a single round of tamoxifen injection resulted in partial (70%) but less complete recombination and reductions in mRNA for Cox6a2.

HET mice do not display a bioenergetic or physiologic phenotype

To determine if the inducible, hemizygous loss of Cox6a2 was sufficient to induce a bioenergetic or physiologic phenotype, we assessed mitochondrial respiration and muscle contractile force in HET mice administered tamoxifen and vehicle (Figures 2A-E). There were no significant differences in mitochondrial oxygen consumption or force production found between these groups. Together, these data indicate that the hemizygous loss of Cox6a2 is not adequate to induce a phenotype. Thus, for the remainder of the results section we will focus on the KO and WT mice.

Mitochondria from KO animals display lower mitochondrial respiration and content

The mitochondrial content of WT and KO skeletal muscle was analyzed using mitochondrial DNA/nuclear DNA ratios. Analysis of the mtDNA/nDNA ratio indicated a reduction of mitochondrial content in the limb skeletal muscle of KO animals compared to WT animals (Figure 3A). For this reason, further analyses of mitochondrial function were performed in isolated skeletal muscle mitochondria to eliminate this confounding variable.

To comprehensively assess the effects of Cox6a2 knockdown in skeletal muscle mitochondria, oxygen consumption rates (JO_2) rates were measured in response to various substrate conditions using the creatine kinase (CK) and hexokinase (HK) clamps. The CK clamp measures JO_2 rates

across a physiologic span of ATP free energies of hydrolysis (ΔG_{ATP}), or energy demand states. Freshly isolated mitochondria from KO mice displayed significantly lower JO_2 compared with both WT mice at all ΔG_{ATP} values under all substrate conditions tested (Figures 3B-D). Maximal uncoupled JO_2, assessed via FCCP addition, was only significantly reduced under the succinate/rotenone condition in KO animals, though maximal JO_2 rates were not completely rescued in the Pyr/Mal or multisubstrate conditions (Figure 3D).

The HK clamp, which measures JO_2 rates under conditions of saturating ADP, was utilized on freeze/thawed KO and WT mitochondria to investigate the effect of Cox6a2 knockdown on NADH- and succinate-linked respiration. Ascorbate/TMPD was added at the end of this protocol as a measure of Complex IV-linked respiration. KO mitochondria displayed significantly lower JO_2 rates for NADH- and succinate-linked respiration, as well as for Ascorbate/TMPD linked respiration (Figure 3F).

Mitochondrial Supercomplex and ATP Synthase Content are not Affected by Cox6a2 Loss

Using isolated mitochondria from KO and WT mice, blue native PAGE experiments were performed to quantify the content of mitochondrial supercomplexes as well as mitochondrial complex V (ATP synthase). The loss of Cox6a2 in KO mice did not alter the abundance of mitochondrial supercomplexes or CV present in skeletal muscle mitochondria (Figures 3G-I).

Skeletal muscle morphology, but not contractile function, is not altered in KO mice,

To determine the impact of Cox6a2 knockdown on skeletal muscle contractile function, *in vitro* force production protocols were performed on EDL muscles from KO and WT mice. EDL muscles

from KO mice were significantly smaller than those of WT animals (Figure 4A), however neither the absolute nor specific force production was found to be different between the groups (Figures 4B, C). Force capacity, determined by summing the integration of the force frequency curves, was also unchanged in KO mice (Figure 4D).

To examine whether Cox6a2 loss affects skeletal muscle morphology, the cross-sectional area (CSA) of the tibialis anterior (TA) muscle from KO and WT mice was measured. KO mice displayed significantly larger muscle fiber area compared with WT mice (Figures 4E-G). TAs were also fiber typed based on myosin heavy chain content. We did not observe a shift in fiber type proportion in our KO animals compared with WT animals (Figures 4E, H). Together these data indicate that the loss of skeletal muscle Cox6a2 affects skeletal muscle morphology by increasing CSA of the TA muscle, but does not impact muscle contractile function. Transverse muscle sections were immunostained with an antibody for CD31 to visualize vascular networks at baseline (Figure 4E). No differences were found between $CD31^{+}$ area of WT and KO mice, indicating that the loss of Cox6a2 did not affect skeletal muscle vasculature at baseline (Figure 4I).

Chronic HFD feeding KO mice results in increased bodyweight, but does not affect glucose or insulin tolerance

To determine if the loss of Cox6a2 affects how mice respond differently to a HFD challenge, mice of the genotype mice HSA-mER-Cre-mER^{+}-$Cox6a2^{f/f}$ were fed either a 45% HFD or a 10 % LFD for 16 weeks. Cox6a2 knockdown was induced by tamoxifen injection on weeks 6 and 10 of the diet feeding. Mice on the HFD gained significantly more weight than those on the LFD, with significant differences in bodyweight between the groups beginning one week following the diet

start date, but no differences in bodyweight were observed at baseline (Figure 5A). GTTs and ITTs were performed on the 14th and 15th weeks of diet feeding. KO HFD mice did not exhibit higher glucose responses compared to KO LFD mice at any time point tested during either the GTT or the ITT (Figures 5B, C), indicating that high-fat diet feeding KO mice did not affect glucose or insulin tolerance.

Chronic high fat feeding KO mice increases maximal NADH- and succinate-linked respiration

OROBOROS Oxygraph-2K measurements of mitochondrial respiration were performed on KO mice after 16 weeks of consuming either a HFD or LFD. HFD fed KO mice did not exhibit differences in mitochondrial respiration under physiologic conditions, i.e., when challenged with the CK clamp (Figures 5D-F). When freeze thawed isolated mitochondria from HFD and LFD fed KO animals was exposed to the HK clamp, the HFD KO mice displayed significantly higher Max uncoupled JO_2 was not different between HFD and LFD fed mice (Figure 4G). NADH- and complex IV-linked respiration compared with their LFD fed counterparts (Figure 4H). These data suggest that chronic HFD feeding KO mice influences mitochondrial enzyme activity, though whether this results in functional consequences remains unknown. Mitochondrial content, assessed by the ratio of mtDNA/nDNA revealed no differences in mitochondrial content between HFD and LFD animals (Figure 4I).

Discussion

Using our novel KO mouse model of skeletal muscle specific Cox6a2 loss, we demonstrate that inducible deletion of skeletal muscle Cox6a2 results in a bioenergetic phenotype defined by reduced mitochondrial respiration that independent of substrate and the reduction in mitochondrial

content. These deficits are accompanied by reduced EDL muscle weight, increased skeletal muscle fiber size in the TA muscle, but no significant changes in EDL contractile function were observed. Specific force values of the KO animal EDLs, however, did trend upward. Moreover, we observed a reduction in the mtDNA/nDNA ratio within the skeletal muscle and increase in Cox6a1 mRNA in KO animals. Together, our data demonstrate that inducible genetic deletion of Cox6a2 leads to a skeletal muscle mitochondrial bioenergetic phenotype. Challenging KO mitochondria in various ways allowed us to confidently and comprehensively conclude that the loss of Cox6a2 in skeletal muscle results in a lesion within the electron transport system. Loss of Cox6a2 lowered mitochondrial JO_2 independent of substrate condition or ΔG_{ATP}, suggesting that the lesion was not complex- or substrate-specific. Although not statistically significant, maximal uncoupled FCCP rates were not rescued in KO mice compared with WT animals, which indicates that the observed respiratory impairments were not caused by lesions in ATP synthase. The hexokinase experiment performed on freeze-fractured mitochondria fed NADH and succinate directly into the ETS. Since the respiratory deficits were maintained in the freeze-fractured KO mitochondria, we were able to rule out lesions in the dehydrogenases associated with Complexes I & II. Together, our data suggest an important role for skeletal muscle Cox6a2 in bioenergetic function, and that its loss results in a mitochondrial dysfunction that is most likely due to a lesion in complex IV.

The complete loss of protein is rarely observed in inducible skeletal muscle-specific knockout models[299,300] since skeletal muscle contains numerous cell types, i.e., smooth muscle, neurons, fibroblasts, and satellite cells[301]. The model system utilized in this study is no different, as Cox6a2 protein could still be detected via Western blot in skeletal muscle mitochondria of KO animals.

One explanation for this protein persistence is that the satellite cell population is contributing to the Cox6a2 pool via cell fusion within the muscle[302,303]. Satellite cell fusion occurs in response to the daily wear and tear that the muscle endures with up to 30% of mature myofibers acquiring satellite cells within a two week period[304]. Following tamoxifen administration, KO animals undergo a full 21-day tamoxifen washout period. During this time, it is possible that the activated satellite cells fusing to mature myofibers re-introduce Cox6a2 to the muscles of our KO animals. We did not observe any abnormal signs of muscle regeneration, i.e., increased centralized nuclei, in KO animals. Thus, it doesn't appear that the loss of Cox6a2 is inducing satellite cell activation and fusion. One way to address this matter in the future could be to introduce mice to a tamoxifen diet[305,306], resulting in a constant level of circulating tamoxifen that would delete the gene for Cox6a2 as soon as its expression began. Persistent protein has been attributed to the existence of unidentified alternative transcriptional start sites[307,308] that can evade Cre/lox-mediated gene inactivation. This type of evasion is more prevalent in systems where the loxP sites flank a single exon of a large gene. The Cox6a2 gene contains three exons[309] and the loxP sites used in our model system flank the entirety of exons 1 and 2, and part of exon 3. Based on the design of our model, the likelihood that the remaining portion of Cox6a2 exon 3 is responsible for the lingering protein is highly unlikely. Additionally, since the mitochondrial targeting sequence of Cox6a2 resides in exon 1, it would be nearly impossible for any hypothetically translated protein to enter the mitochondria. Finally, it's possible that the remaining Cox6a2 mRNA following tamoxifen injection is sufficient in translating protein. On average, two rounds of tamoxifen delivery are able to reduce Cox6a2 mRNA by 90%. Seeing as Cox6a2 plays an important role in complex IV stability and catalytic activity, the remaining mRNA may be upregulating translation in attempt to prevent physiologic distress.

Cox6a is is one of the thirteen subunits of cytochrome C oxidase (CcO; complex IV) and exists as two distinct isoforms: Cox6a2 and Cox6a1. Cox6a2 is expressed in mature, striated muscle and in specific fast-firing interneurons[310], while Cox6a1 is ubiquitously expressed[311,312]. Both isoforms of Cox6a are believed to be added at the end stages of complex assembly and are involved in the stabilization of cytochrome C oxidase and cytochrome c oxidase dimers[311]. One major functional difference between the Cox6 isoforms is the ability of Cox6a2 to bind ADP[313–315] and increase the catalytic activity of CcO. Hence, it makes sense that the Cox6a2 isoform of Cox6a is expressed in tissues with high metabolic activity. Based on its role in CcO, it is surprising that the loss of Cox6a2 does not result in more severe physiologic outcomes. It is possible that Cox6a1 is partially compensating for the Cox6a2 loss, as we observed a nearly twofold increase in Cox6a1 mRNA in KO skeletal muscle, but this increase in mRNA expression does not necessarily translate to an increase in functional Cox6a1 protein. Thus far, we have not been able to identify an antibody against Cox6a1 that we feel confident in using to address the question of whether Cox6a1 protein is changed in KO mice. Since Cox6a1 is ubiquitously expressed, it's impossible to tell if its expression is coming from the skeletal muscle, or if it's coming from the mitochondria of other cell types within the muscle. Regardless, it's clear that even if Cox6a1 can partially compensate for reductions in Cox6a2 and help with complex IV stabilization, it is unable to make up for the lost catalytic ability of Cox6a2, resulting in the observed bioenergetic phenotype.

Only a handful of papers, including ours, have investigated the consequences of Cox6a2 loss[293,310,311,316] *in vivo* and, to our knowledge, this is the first report of an inducible, skeletal

muscle-specific model of Cox6a2 knockdown. The earliest model system of Cox6a2 loss employs a null mutation that results in the lifelong loss of Cox6a2 in cardiac and skeletal muscle tissue[294]. These mice harbor subtle cardiac dysfunction[294], reduced mitochondrial respiration and complex IV activity, but do not display changes in muscle contractile force. A more recent study of these Cox6a2 null mice[310] observed that the loss of Cox6a2 in parvalbumin-positive interneurons leads to behavioral abnormalities. In all studied tissue types, the loss of Cox6a2 results increased in oxidative stress and ROS production, coupled with reduced mitochondrial respiration. Studies on both embryonic and inducible Cox6a2 loss *in vivo* consistently indicate a role for Cox6a2 in normal, physiologic mitochondrial respiration, though the consequences of its loss do not appear to be catastrophic to development or homeostasis.

In this study and in another, ubiquitous Cox6a2-null or skeletal muscle specific KO mice were challenged with a chronic HFD[293]. While Cox6a2-null mice did not show increases in bodyweight compared with their LFD-fed counterparts, muscle specific KO mice gained a significant amount of bodyweight in response to HFD. This suggests that the lean, obesity-resistant phenotype observed in the whole body Cox6a2-null can't be attributed solely to the loss of Cox6a2 in the skeletal muscle. Regardless, HFD-fed from both model systems appeared to be protected from glucose intolerance and insulin resistance under the conditions employed. The current study examined skeletal muscle mitochondrial complex I and II enzyme activity following chronic overnutrition, observing a rescue effect in HFD-fed Cox6a2 KO mice compared with those fed a LFD. Although it's not possible to tell if this rescue effect is physiologically beneficial, it does suggest that when faced with a HFD challenge, the mitochondria of KO mice are able to adapt and compensate. These are not the first reports of an inherent mitochondrial dysfunction preventing

obesity or insulin resistance[317–319] development and it is well documented that mitochondria are capable of responding to stress[320,321]. Thus, we believe that the observed rescue of mitochondrial enzyme activity and protection from metabolic syndrome are compensatory mechanisms induced by the chronic overnutrition stressor.

Cytochrome c oxidase deficiency is a common hallmark of mitochondrial chain defects in human pathology[316,322–327], and multiple CcO subunits have been implicated in disease including Cox4I2[328], Cox6a1[329], Coxb1[330] and Cox7b[331]. A 2019 study[322] first implicated Cox6a2 variants in the development of a COX deficiency in two separate patients, marked only by striated muscle weakness. A recent study from our lab[42] identified differences in Cox6a2 protein abundance between patients with CLTI and healthy controls that is associated with decreased expression of complex I and IV proteins. Although a causative role for Cox6a2 in the bioenergetic signature observed in this study was not identified, the unique CLTI mitochondriopathy has significant implications that could greatly impact therapeutic developments. These recent findings further support the idea that understanding mitochondrial stability and function is vital in treating pathology. The role that Cox6a2 plays in the development of these disease states and whether it is a viable therapeutic target needs additional interrogation.

Conclusions

In the present study, we reveal a role for skeletal muscle specific Cox6a2 in mitochondrial respiration. The reduction of Cox6a2 protein from mature skeletal muscle does not appear to cause muscle functional deficits. A possible explanation for this is that in the absence of a significant stressor, Cox6a2 loss is not sufficient to induce a physiologic phenotype. Future studies employing

other challenges, including ischemic injury, should be performed to better evaluate the effect of Cox6a2 loss. Data from *in vitro* studies have implicated a vital role for Cox6a2 in myoblast differentiation into myotubes. Thus, examining the role of Cox6a2 in myoregeneration, i.e., in the satellite cell population, is an important next step to better understanding the effects of Cox6a2 in skeletal muscle. Additionally, knocking down Cox6a1 in the skeletal muscle is important to determine whether it is playing a protective, compensatory role. Overall, our results reveal an important role for Cox6a2 in regulating the activity of Complex IV.

Figures:

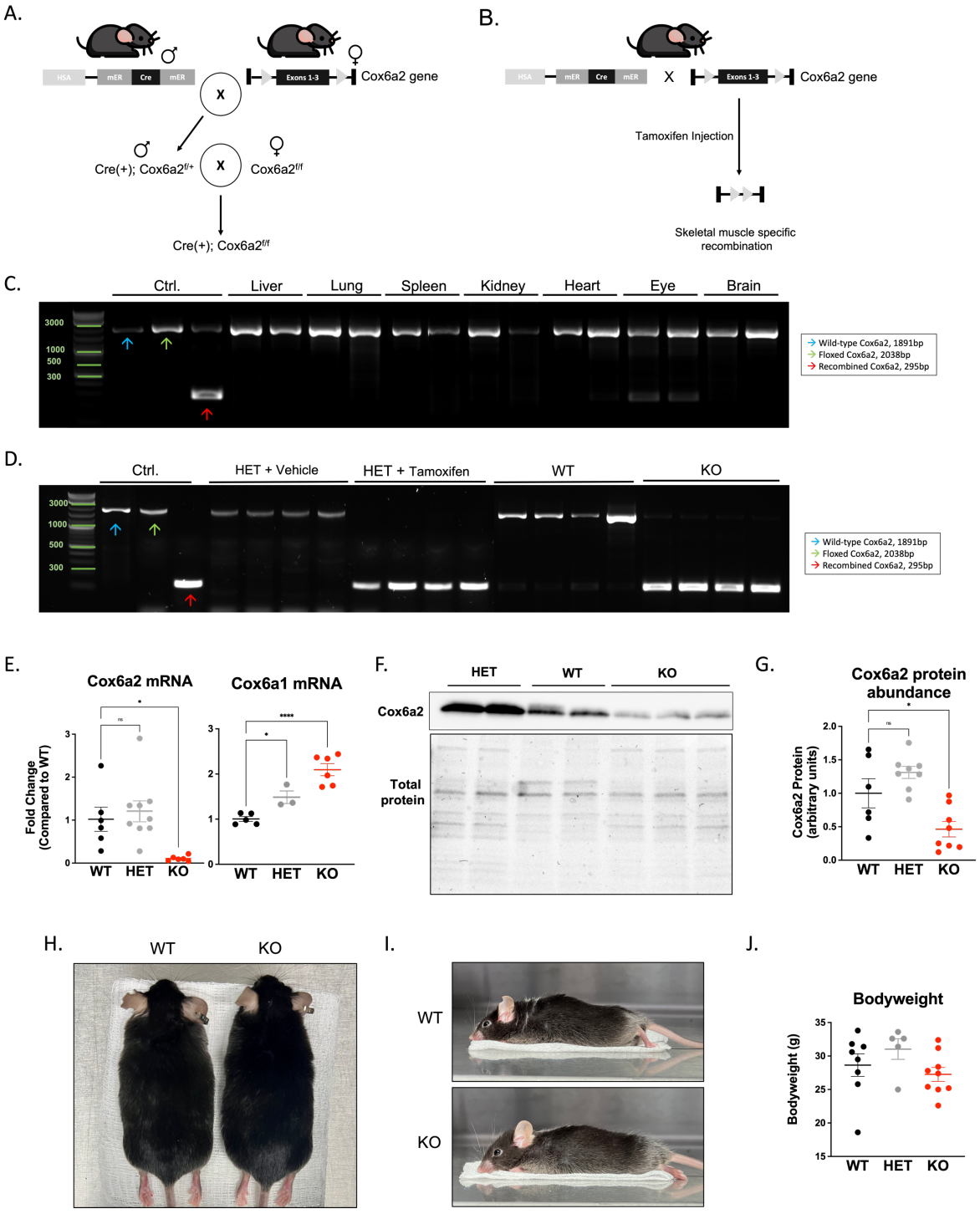

Figure 6: Induction and validation of skeletal muscle-specific Cox6a2 knockdown. (A) Breeding scheme to generate a skeletal muscle-specific Cox6a2 KO mouse. (B) Injection of

tamoxifen resulted in the deletion of exons 1-3 of the *Cox6a2* gene. (C) Recombination of the *Cox6a2* gene was not observed in any non-muscle tissue from KO animals. (D) Recombination was not observed in vehicle treated mice. Successful recombination was observed in HET mice treated with tamoxifen and KO mice treated with tamoxifen. (E) Cox6a2 and Cox6a1 mRNA was measured in WT, HET and KO mice. There were no differences in Cox6a2 mRNA between HET and WT mice. Cox6a2 mRNA for the KO mice was significantly reduced. Cox6a1 mRNA was similar between WT and HET mice, and was significantly increased in KO animals. (F) Representative Western blot of Cox6a2 in HET, WT and KO mice. (G) Cox6a2 protein abundance was semi-quantified from Western blots, revealing a significant decrease in Cox6a2 protein in KO animals and no change in HET animals compared to WT. (H, I) Representative images of WT and KO mice. KO mice did not show any outward phenotype. (J) Bodyweight between WT, HET and KO groups was similar. Data are presented as mean +/- SEM. *P<0.05, **P<0.01

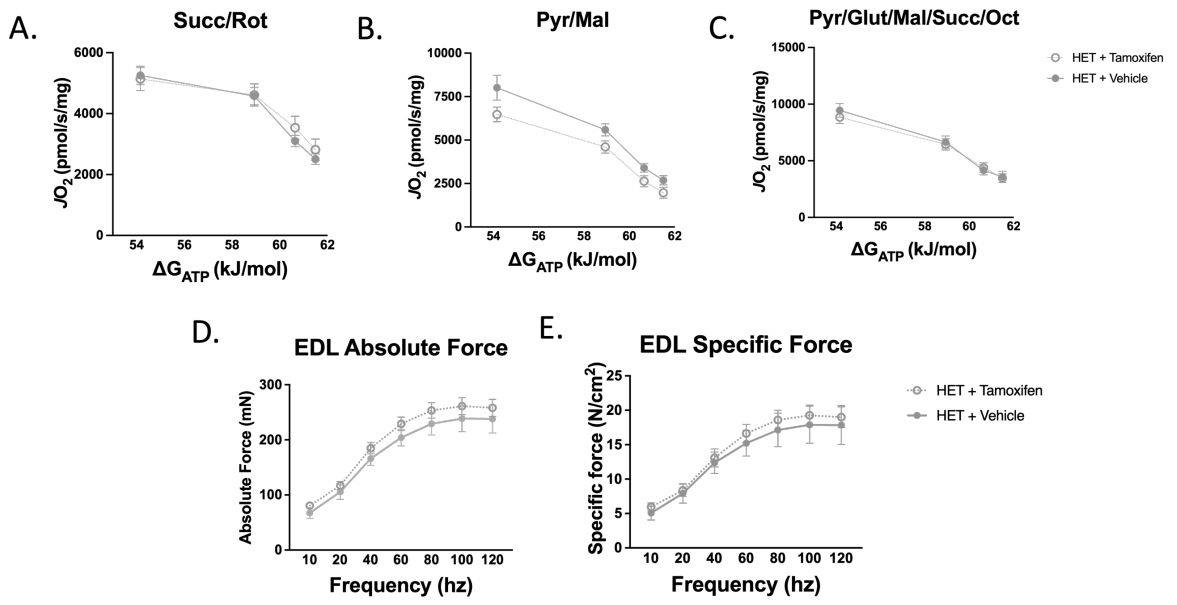

Figure 7: HET mice do not display a bioenergetic phenotype. JO_2 was assessed using the creatine kinase clamp in HET mice treated with tamoxifen and vehicle. (A-C) No differences in JO_2 were observed between HET mice treated with tamoxifen or vehicle under any substrate condition. (D, E) Absolute and specific force from EDL muscles showed no differences between HET mice treated with tamoxifen or vehicle. Data are presented as mean +/- SEM. *P<0.05, **P<0.01

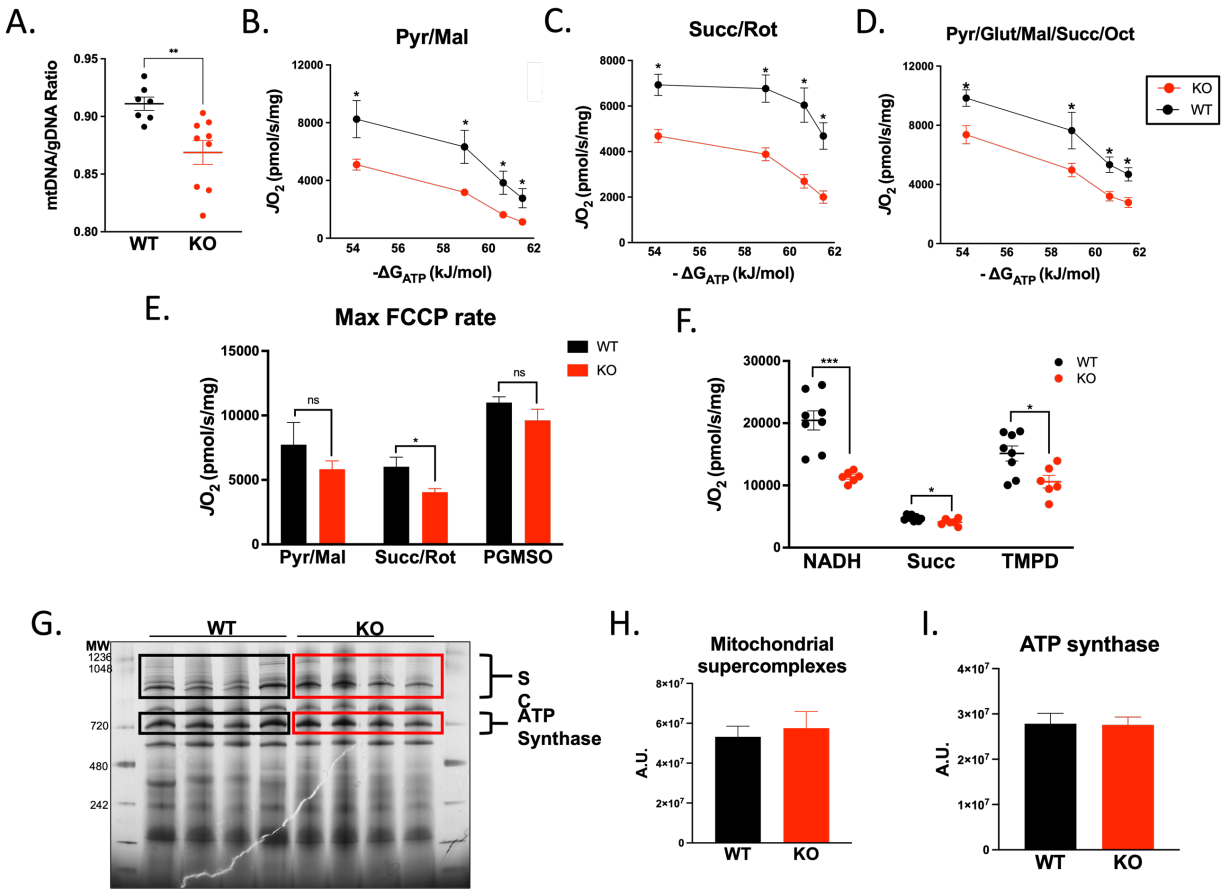

Figure 8: KO mice display a bioenergetic phenotype. (A) Mitochondrial content was assessed by the ratio of mitochondrial DNA/nuclear DNA from whole skeletal muscle. KO mice showed a significant reduction in mitochondrial content. (B-D) JO_2 was assessed using the creatine kinase clamp under multiple substrate conditions in WT and KO mice. KO mitochondria display significantly reduced respiration under all substrate conditions at all ΔG_{ATP}. (E) Max uncoupled JO_2 assessed by FCCP addition was measured in KO and WT mice under all substrate conditions. FCCP was unable to rescue JO_2 in KO mice. (F) Freeze-fractured mitochondria were challenged with the Hexokinase clamp. KO mitochondria displayed significantly lower NADH-, succinate- and TMPD-linked respiration compared with WT mice. (G) Whole blue native PAGE gel highlighting mitochondrial supercomplexes and ATP synthase. (H, I) Cox6a2 loss did not affect mitochondrial supercomplex or ATP synthase abundance. Data are presented as mean +/- SEM. *P<0.05, **P<0.01

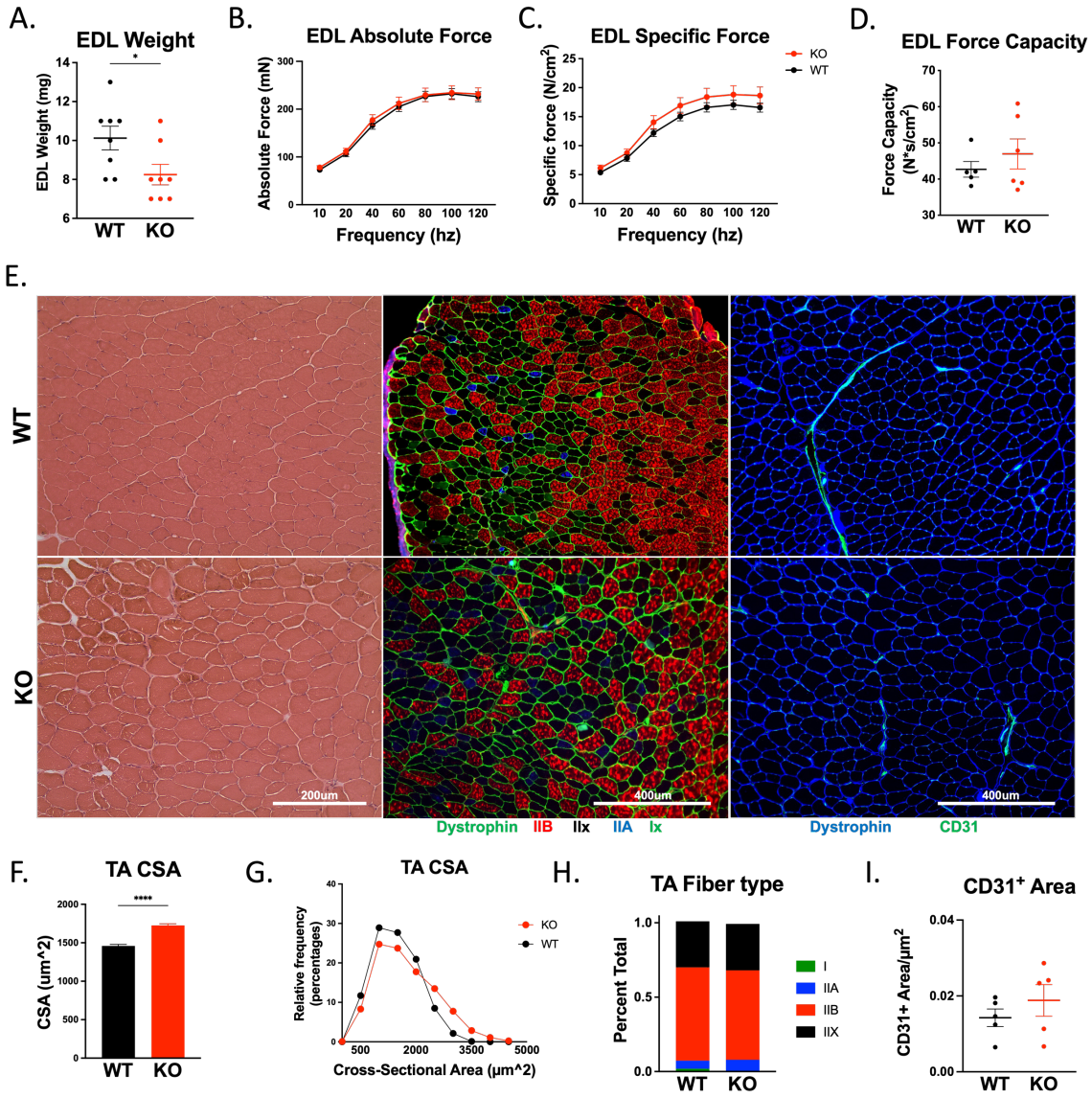

Figure 9: Cox6a2 KO mice do not display a skeletal muscle functional phenotype (A) EDL weights were significantly reduced in KO animals compared with WT animals. (B, C) Force frequency curves were generated on WT and KO EDL muscles. No differences in force production were observed. (D) Specific force capacity was obtained by summing the time-tension integrals for each force frequency contraction in the EDL. Force capacity was not different between WT and KO mice. (E) Representative images of tibialis anterior (TA) muscles from WT and KO animals with various histological and immunohistochemical stains. (F, G) CSA of WT and KO animals was measured on hematoxylin and eosin-stained cross-sections. The CSA of KO animals was significantly larger than that of WT animals. (H) Myosin heavy chain antibodies were used to assess if the loss of Cox6a2 resulted in fiber type switching. The proportion of fiber types were similar between WT and KO animals. (I) CD31, a marker of endothelial cells, was used to investigate the impact of Cox6a2 loss on the endothelium. No differences in $CD31^{+}$area was observed. Data are presented as mean +/- SEM. *P<0.05, **P<0.01 ***P<0.001

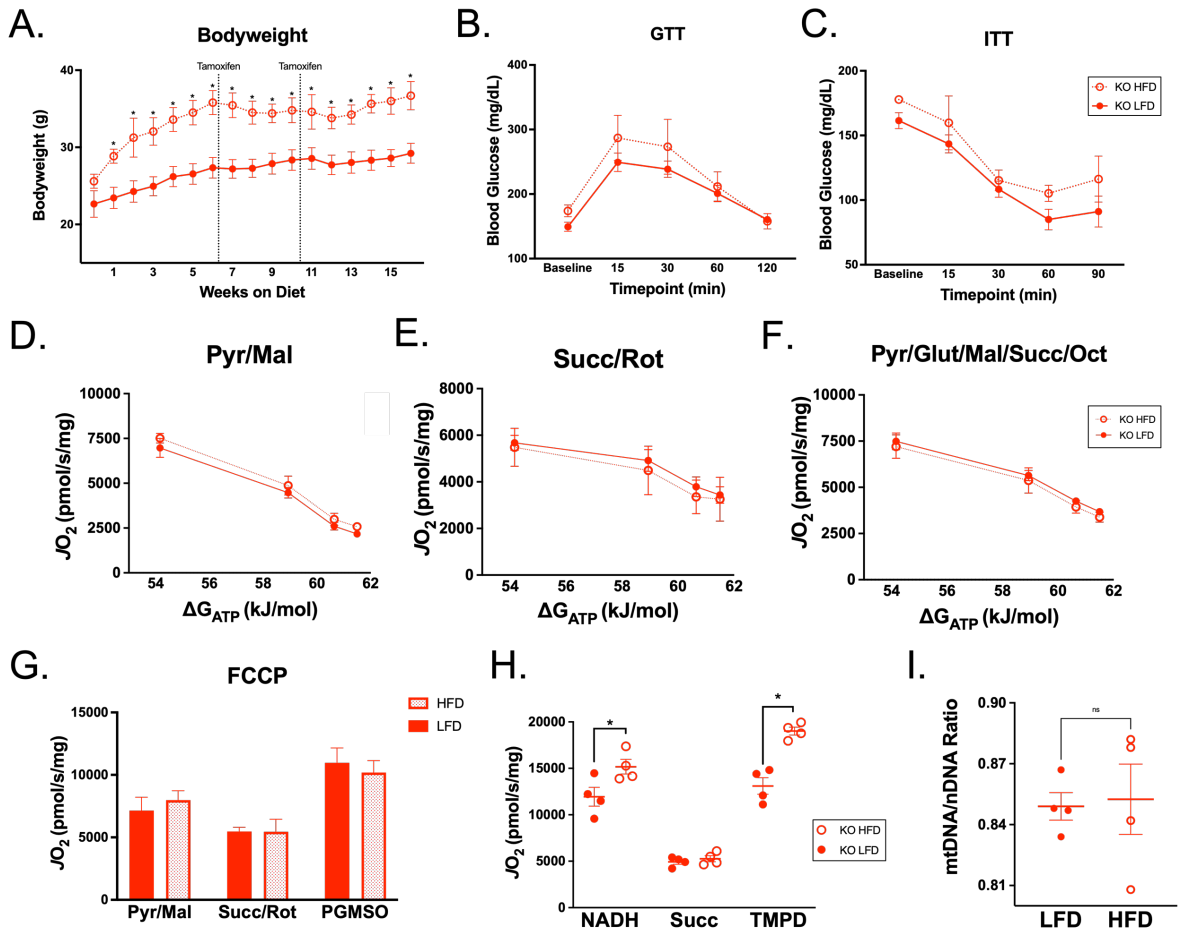

Figure 10: Impact of Cox6a2 loss on chronic overnutrition. (A) Mice of the genotype mice HSA-mER-Cre-mER^{+}-Cox6a2$^{f/f}$ were placed either a 45% HFD or a 10 % LFD at 4-6 weeks of age, and kept on the diet for 16 weeks. Cox6a2 knockdown was induced by tamoxifen injection on weeks 6 and 10 of the diet feeding. Bodyweight of HFD fed mice was significantly higher than that of the LFD fed mice at all timepoints following the diet start date, but no differences in bodyweight were observed at baseline. (B, C) GTTs and ITTs were performed on weeks 14 and 15 of the diet. HFD mice did not show changes in glucose or insulin tolerance. (D-F) isolated mitochondria from HFD and LFD-fed KO mice were challenged with the CK clamp. No differences in mitochondrial respiration were observed between groups. (G) Maximal uncoupled FCCP rates were similar between HFD and LFD fed mice. (H) Freeze-fractured mitochondria from HFD and LFD fed KO mice were challenged with the HK clamp. HFD-fed mitochondria displayed significantly higher NADH- and TMPD-linked respiration. (I) Mitochondrial content was assessed by the ratio of mitochondrial DNA/nuclear DNA from whole skeletal muscle from HFD and LFD fed KO mice. No changes in mitochondrial content were observed. Data are presented as mean +/- SEM. *P<0.05, **P<0.01 ***P<0.001

Chapter 5: SUMMARY AND FUTURE DIRECTIONS

Summary

The primary purpose of this dissertation was to gain an understanding of whether capillary reperfusion and contractile function recovery are temporally related, and how a skeletal muscle-specific mitochondrial protein, Cox6a2, affects skeletal muscle bioenergetic function. We hypothesized that muscles with well-documented differences in capillary density and contractile kinetics would display distinct patterns of regeneration. Additionally, we hypothesized that the loss of skeletal muscle Cox6a2 would result in contractile force deficits and mitochondrial dysfunction, which would be exacerbated by a high fat diet stressor. Results from our studies provide evidence that restoration of capillary perfusion does not guarantee a timely or complete recovery of muscle contractile function. We additionally demonstrated that isolated mitochondria from Cox6a2 KO mice display reduced respiration under basal conditions, though these deficits did not translate into physiologic muscle function deficits

The data generated by this dissertation are supportive of what is observed in the clinical PAD population. Namely, our results confirm that revascularization of ischemic tissue is not sufficient to rescue the associated myopathy that plagues patients with PAD. Further, our novel mouse model supports the idea that patients with CLTI harbor a unique skeletal muscle mitochondriopathy that could be correlated with the loss of Cox6a2. Skeletal muscle mitochondria from CLTI patients displays significantly reduced Cox6a2 expression and shows severe deficits in mitochondrial respiration, similar to what we observed in KO mice. These findings should inform new approaches to understating underlying causes of CLTI manifestation and provide potential targets for further exploration.

Future Directions

In this dissertation, we examined whether the temporal relationship between capillary reperfusion and contractile function restoration following ischemia is different between skeletal myofiber types, and if the two processes are tightly associated. We also assessed whether Cox6a2 is required for normal mitochondrial bioenergetic function under basal conditions and during a period of chronic overnutrition. Our data suggest that the loss of this mitochondrial protein results in respiratory and enzyme kinetic deficits, but whether this has a functional consequence remains to be explored. Future experiments on Cox6a2 KO mice should include a comprehensive look at mitochondrial supercomplex formation, and how Cox6a2 loss affects this. Additional mitochondrial function assays, including membrane potential, ATP production and H_2O_2 emission, should also be conducted to better understand how Cox6a2 loss affects mitochondrial efficiency and function.

To better understand the role of Cox6a2 in the ischemic environment, HLI studies should be performed on Cox6a2 KO mice. This would provide vital information on whether Cox6a2 in the mature skeletal muscle is required for ischemic tissue survival. An important limitation in our current Cox6a2 KO model, however, is that following HLI, regenerating myofibers could reintroduce Cox6a2 into the skeletal muscle. As previously discussed, this could be a result of satellite cell differentiation, as these cells were not affected by tamoxifen treatment. One possible way to circumvent this issue would be to use Pax7-MCM to generate a satellite cell-specific knockdown of Cox6a2. These mice, when subjected to HLI, would be unable to express Cox6a2

in their differentiating myofibers, answering the question of whether Cox6a2 is required for *in vivo* myoregeneration.

In this dissertation, Cox6a2 KO animals were subjected to a physiologically relevant high fat diet challenge. Neither of these challenges induced a functional muscle phenotype despite the existence of a basal bioenergetic phenotype. Future challenges that could provide a better understanding of the role Cox6a2 plays in mature skeletal muscle could include challenging the mice with distance treadmill or wheel running *in vivo*, or subjecting *ex vivo* muscles to longer fatigue protocols. Due to the lower respiratory capacity of the KO muscles at baseline, it's possible that the muscles will exhibit a functional phenotype when challenged with a maximal aerobic capacity challenge.

REFERENCES:

1. Pipinos, I. I. *et al.* The Myopathy of Peripheral Arterial Occlusive Disease: Part 1. Functional and Histomorphological Changes and Evidence for Mitochondrial Dysfunction. *Vasc. Endovascular Surg.* **41**, 481–489 (2008).
2. Norgren, L. *et al.* Inter-society consensus for the management of peripheral arterial disease. *International angiology : a journal of the International Union of Angiology* (2007). doi:10.1016/j.jvs.2006.12.037
3. Song, P. *et al.* Global, regional, and national prevalence and risk factors for peripheral artery disease in 2015: an updated systematic review and analysis. *Lancet Glob. Heal.* **7**, e1020–e1030 (2019).
4. Fowkes, F. G. R. *et al.* Comparison of global estimates of prevalence and risk factors for peripheral artery disease in 2000 and 2010 : a systematic review and analysis. *Lancet* **382**, 1329–1340 (2013).
5. Farber, A. Chronic limb-threatening Ischemia. *N. Engl. J. Med.* **379**, 171–180 (2018).
6. Conte, M. S. *et al.* Global Vascular Guidelines on the Management of Chronic Limb-Threatening Ischemia. *Eur J Vasc Endovasc Surg* **58**, 1–109 (2019).
7. Dua, A. & Lee, C. J. Epidemiology of Peripheral Arterial Disease and Critical Limb Ischemia. *Tech. Vasc. Interv. Radiol.* **19**, 91–95 (2016).
8. Mcdermott, M. M. Lower Extremity Manifestations of Peripheral. *Circ. Res.* **116**, 1540–1551 (2015).
9. Goodney, P. P., Beck, A. W., Nagle, J., Welch, H. G. & Zwolak, R. M. National trends in lower extremity bypass surgery, endovascular interventions, and major amputations. *J. Vasc. Surg.* **50**, 54–60 (2009).

10. Hirsch, A. T. *et al.* ACC/AHA 2005 Guidelines for the Management of Patients With Peripheral Arterial Disease (Lower Extremity, Renal, Mesenteric, and Abdominal Aortic): A Collaborative Report from the American Association for Vascular Surgery/Society for Vascular Surgery,∗Soc. *J. Am. Coll. Cardiol.* **47**, e1–e192 (2006).

11. Brass, E. P. & Hiatt, W. R. Acquired skeletal muscle metabolic myopathy in atherosclerotic peripheral arterial disease. *Vasc. Med.* **5**, 55–59 (2000).

12. Duprez, D. A. Pharmacological interventions for peripheral artery disease. *Expert Opin. Pharmacother.* **8**, 1465–1477 (2007).

13. Larsen, O. A. & Lassen, N. A. Effect of daily muscular exercise in patients with intermittent claudication. *Scand. J. Clin. Lab. Investig. Suppl.* **99**, 168–171 (1967).

14. Pernow, B. & Zetterquist, S. Metabolic evaluation of the leg blood flow in claudicating patients with arterial obstructions at different levels. *Scand. J. Clin. Lab. Invest.* **21**, 277–287 (1968).

15. Gardner, A. W., Skinner, J. S., Cantwell, B. W. & Smith, L. K. Prediction of claudication pain from clinical measurements obtained at rest. *Med. Sci. Sports Exerc.* (1992). doi:10.1249/00005768-199202000-00002

16. McDermott, M. M. G. *et al.* Impairments of Muscles and Nerves Associated with Peripheral Arterial Disease and Their Relationship with Lower Extremity Functioning: The InCHIANTI Study. *J. Am. Geriatr. Soc.* **52**, 405–410 (2004).

17. Gardner, A. W. & Killewich, L. A. Lack of functional benefits following infrainguinal bypass in peripheral arterial occlusive disease patients. *Vasc. Med.* **6**, 9–14 (2001).

18. Steinacker, J. M. *et al.* Expression of myosin heavy chain isoforms in skeletal muscle of patients with peripheral arterial occlusive disease. *J. Vasc. Surg.* **31**, 443–449 (2000).

19. Brass, E. P., Hiatt, W. R. & Green, S. Skeletal muscle metabolic changes in peripheral arterial disease contribute to exercise intolerance: A point-counterpoint discussion. *Vasc. Med.* **9**, 293–301 (2004).

20. Schmidt, C. A. *et al.* Diminished force production and mitochondrial respiratory deficits are strain-dependent myopathies of subacute limb ischemia. *J. Vasc. Surg.* **65.5**, 1504–1514 (2017).

21. Schmidt, C. A. *et al.* Strain-Dependent Variation in Acute Ischemic Muscle Injury. *Am. J. Pathol.* **188**, 1246–1262 (2018).

22. Mcclung, J. M. *et al.* A BAG3 Coding Variant in Mice Determines Susceptibility to Ischemic Limb Muscle Myopathy by Directing Autophagy. **136**, 281–296 (2018).

23. McClung, J. M. *et al.* Subacute limb ischemia induces skeletal muscle injury in genetically susceptible mice independent of vascular density. *J. Vasc. Surg.* **64**, 1101-1111.e2 (2016).

24. Jacobsen, N. L., Norton, C. E., Shaw, R. L., Cornelison, D. D. W. & Segal, S. S. Myofibre injury induces capillary disruption and regeneration of disorganized microvascular networks. *J. Physiol.* **600**, 41–60 (2022).

25. McDermott, M. M. *et al.* Treadmill Exercise and Resistance Training in Patients With Peripheral Arterial Disease With and Without Intermittent Claudication. *Jama* **301**, 165 (2009).

26. McDermott, M. M. *et al.* Physical activity, walking exercise, and calf skeletal muscle characteristics in patients with peripheral arterial disease. *J. Vasc. Surg.* **46**, 87–93 (2007).

27. McDermott, M. M. Medical Management of Functional Impairment in Peripheral Artery Disease: A Review. *Prog. Cardiovasc. Dis.* **60**, 586–592 (2018).

28. Mcdermott, M. M. Exercise rehabilitation for peripheral artery disease: a review. *J. Cardiopulm. Rehabil. Prev.* **38**, 63–69 (2019).

29. White, S. H. *et al.* Walking performance is positively correlated to calf muscle fiber size in peripheral artery disease subjects, but fibers show aberrant mitophagy: An observational study. *J. Transl. Med.* **14**, 1–15 (2016).

30. Flück, M. Functional, structural and molecular plasticity of mammalian skeletal muscle in response to exercise stimuli. *J. Exp. Biol.* **209**, 2239–2248 (2006).

31. Jelenik, T. & Roden, M. Mitochondrial plasticity in obesity and diabetes mellitus. *Antioxidants Redox Signal.* **19**, 258–268 (2013).

32. Adhihetty, P. J., Irrcher, I., Joseph, A., Ljubicic, V. & Hood, D. A. Plasticity of skeletal muscle mitochondria in response to contractile activity. *J. Appl. Physiol.* **88**, 99–107 (2003).

33. Bahat, A. & Gross, A. Mitochondrial plasticity in cell fate regulation. *J. Biol. Chem.* **294**, 13852–13863 (2019).

34. Mishra, P. & Chan, D. C. Metabolic regulation of mitochondrial dynamics. *J. Cell Biol.* **212**, 379–387 (2016).

35. Zhu, Z. *et al.* Chronically ischemic mouse skeletal muscle exhibits myopathy in association with mitochondrial dysfunction and oxidative damage. *Am. J. Physiol. Integr. Comp. Physiol.* **295**, R290–R296 (2008).

36. Balaban, R. S., Nemoto, S. & Finkel, T. Mitochondria, oxidants, and aging. *Cell* **120**, 483–495 (2005).

37. Harper, M., Bevilacqua, L., Hagopian, K., Weindruch, R. & Ramsey, J. J. Ageing , oxidative stress , and mitochondrial uncoupling. 321–331 (2004).

38. Ryan, T. E. *et al.* Mitochondrial Regulation of the Muscle Microenvironment in Critical Limb Ischemia. *Front. Physiol.* **6**, 1–9 (2015).

39. Pipinos, I. I. *et al.* Mitochondrial defects and oxidative damage in patients with peripheral arterial disease. *Free Radic. Biol. Med.* **41**, 262–269 (2006).

40. Pipinos, I. I. *et al.* Abnormal mitochondrial respiration in skeletal muscle in patients with peripheral arterial disease. *J. Vasc. Surg.* **38**, 827–832 (2003).

41. Sabbah, H. N. *et al.* Abnormal mitochondrial respiration in skeletal muscle in patients with peripheral arterial disease. *J. Vasc. Surg.* **38**, 827–832 (2003).

42. Ryan, T. E. *et al.* Extensive skeletal muscle cell mitochondriopathy distinguishes critical limb ischemia patients from claudicants. *JCI Insight* **3**, (2018).

43. Dokun, A. O. *et al.* A quantitative trait locus (LSq-1) on mouse chromosome 7 is linked to the absence of tissue loss after surgical hindlimb ischemia. *Circulation* **117**, 1207–1215 (2008).

44. Lend, G. C. & Fowkes, F. G. R. The Edinburgh Claudication Questionnaire: An improved version of the WHO/Rose questionnaire for use in epidemiological surveys. *J. Clin. Epidemiol.* **45**, 1101–1109 (1992).

45. F. G. R. Fowkes *et al.* Ankle Brachial Index Combined with Framingham Risk Score to Predict Cardiovascular Events and Mortality: A Meta-analysis. *J. Am. Med. Assoc.* **300**, 197–208 (2017).

46. Hamburg, N. M. & Creager, M. A. Pathophysiology of intermittent claudication in peripheral artery disease. *Circ. J.* **81**, 281–289 (2017).

47. Katwal, A. B. & Dokun, A. O. Peripheral Arterial Disease in Diabetes : Is There a Role for. *Curr. Diab. Rep.* **11**, 218–225 (2012).

48. McDermott, M. M. *et al.* Decline in Functional Performance Predicts Later Mobility Loss and Mortality in Peripheral Arterial Disease. *J. Am. Coll. Cardiol.* **57**, 962–970 (2011).

49. Dolan, N. C. *et al.* Peripheral artery disease, diabetes, and reduced lower extremity functioning. *Diabetes Care* **25**, 113–120 (2002).

50. Fowkes, F. G. R. *et al.* Peripheral artery disease: Epidemiology and global perspectives. *Nat. Rev. Cardiol.* **14**, 156–170 (2017).

51. Das C, Lucia MS, H. K. and T. J. The Genetic Basis of Peripheral Arterial Disease: Current Knowledge, Challenges and Future Directions. *Physiol. Behav.* **176**, 139–148 (2015).

52. Schmidt CA, Ryan TE, Lin CT, Inigo MMR, Green TD, Brault JJ, S. E. and M. J. Diminished Force Production and mitochondrial respiratory deficits are strain-dependent myopathies of subacute limb ischemia. *J. Vasc. Surg.* **27**, 138–144 (2016).

53. Fukino, K., Sata, M., Seko, Y., Hirata, Y. & Nagai, R. Genetic background influences therapeutic effectiveness of VEGF. *Biochem. Biophys. Res. Commun.* **310**, 143–147 (2003).

54. Scholz, D. *et al.* Contribution of arteriogenesis and angiogenesis to postocclusive hindlimb perfusion in mice. *J. Mol. Cell. Cardiol.* **34**, 775–787 (2002).

55. Fowkes, F. G. R. *et al.* Peripheral artery disease: Epidemiology and global perspectives. *Nat. Rev. Cardiol.* **14**, 156–170 (2017).

56. Voskuil, M. *et al.* Modulation of collateral artery growth in a porcine hindlimb ligation model using MCP-1. *Am. J. Physiol. - Hear. Circ. Physiol.* **284**, 1422–1428 (2003).

57. Couffinhal, T. *et al.* Mouse Model of Angiogenesis. *Am. J. ofPathologyAm J Pathol* **152**, 1667–1679 (1998).

58. Dormandy, J., Heeck, L. & Vig, S. The fate of patients with critical leg ischemia. *Semin. Vasc. Surg.* **12**, 142—147 (1999).

59. Norgren, L. *et al.* Inter-Society Consensus for the management of peripheral arterial disease (TASC II). *J. Vasc. Surg.* **45**, S5–S67 (2007).

60. Annex, B. H. Therapeutic angiogenesis for critical limb ischaemia. *Nat. Rev. Cardiol.* **10**, 387–396 (2013).

61. Aquino, R. *et al.* Natural history of claudication: Long-term serial follow-up study of 1244 claudicants. *J. Vasc. Surg.* **34**, 962–970 (2001).

62. Rosenbloom, M. S. *et al.* Risk Factors Affecting the Natural History of Intermittent Claudication. *Arch. Surg.* **123**, 867–870 (1988).

63. Sigvant, B., Lundin, F. & Wahlberg, E. The Risk of Disease Progression in Peripheral Arterial Disease is Higher than Expected: A Meta-Analysis of Mortality and Disease Progression in Peripheral Arterial Disease. *Eur. J. Vasc. Endovasc. Surg.* **51**, 395–403 (2016).

64. Mätzke, S. & Lepäntalo, M. Claudication does not always precede critical leg ischemia. *Vasc. Med.* **6**, 77–80 (2001).

65. Annex, B. H. Therapeutic angiogenesis for critical limb ischaemia. *Nat. Rev. Cardiol.* **10**, 387–396 (2013).

66. Dormandy, J., Heeck, L. & Vig, S. The fate of patients with critical leg ischemia. *Semin. Vasc. Surg.* **12**, 142—147 (1999).

67. Rymer, J. A. *et al.* Association of disease progression with cardiovascular and limb outcomes in patients with peripheral artery disease insights from the EUCLID trial. *Circ. Cardiovasc. Interv.* 93–101 (2020). doi:10.1161/CIRCINTERVENTIONS.120.009326

68. Isbell, D. C. *et al.* Delayed Calf Muscle Phosphocreatine Recovery After Exercise Identifies Peripheral Arterial Disease. *J. Am. Coll. Cardiol.* **47**, 2289–2295 (2006).

69. Hirsch, A. T. *et al.* Peripheral Arterial Disease Detection , Awareness , and Treatment in Primary Care. *J. Am. Med. Assoc.* **286**, 1317–1324 (2001).

70. Aoife N Keeling *et al.* Clinical correlates of size and number of collateral vessels in peripheral artery disease. *Physiol. Behav.* **176**, 139–148 (2017).

71. Hiatt, W. R., Armstrong, E. J., Larson, C. J. & Brass, E. P. Pathogenesis of the Limb Manifestations and Exercise Limitations in Peripheral Artery Disease. *Circ. Res.* **116**, 1527–1539 (2015).

72. Regensteiner, J. G. *et al.* Chronic changes in skeletal muscle histology and function in peripheral arterial disease. *Circulation* **87**, 413–421 (1993).

73. Evans, N. S. *et al.* Associations of calf skeletal muscle characteristics and peripheral nerve function with self-perceived physical functioning and walking ability in persons with peripheral artery disease. *Vasc. Med.* **16**, 3–11 (2011).

74. McDermott, M. M. *et al.* Calf muscle characteristics, strength measures, and mortality in peripheral arterial disease: A longitudinal study. *J. Am. Coll. Cardiol.* **59**, 1159–1167 (2012).

75. McDermott, M. M. *et al.* Skeletal muscle pathology in peripheral artery disease a brief review. *Arterioscler. Thromb. Vasc. Biol.* 2577–2585 (2020). doi:10.1161/ATVBAHA.120.313831

76. Kim, K., Anderson, E. M., Scali, S. T. & Ryan, T. E. Skeletal muscle mitochondrial dysfunction and oxidative stress in peripheral arterial disease: A unifying mechanism and therapeutic target. *Antioxidants* **9**, 1–23 (2020).

77. McDermott, M. M. *et al.* The ankle brachial index is associated with leg function and physical activity: The Walking and Leg Circulation Study. *Ann. Intern. Med.* **139**, 306 (2003).

78. Mary M. McDermott, MD, Jack M. Guralnik, MD, PhD, Luigi Ferrucci, MD, PhD, Lu Tian, ScD, Kiang Liu, PhD, Yihua Liao, MS, David Green, MD, PhD, Robert Sufit, MD, Frederick Hoff, MD, Takashi Nishida, MD, Leena Sharma, MD, William H. Pearce, MD, Joseph R. Sc, M. Asymptomatic Peripheral Arterial Disease Is Associated With More Adverse Lower Extremity Characteristics Than Intermittent Claudication Mary. *Physiol. Behav.* **176**, 139–148 (2011).

79. McDermott, M. M. *et al.* Leg symptom categories and rates of mobility decline in peripheral arterial disease. *J. Am. Geriatr. Soc.* **58**, 1256–1262 (2010).

80. McDermott, M. M. *et al.* Associations between lower extremity ischemia, upper and lower extremity strength, and functional impairment with peripheral arterial disease. *J. Am. Geriatr. Soc.* **56**, 724–729 (2008).

81. Mietus, C. J. *et al.* Abnormal Microvascular Architecture, Fibrosis, and Pericyte Characteristics in the Calf Muscle of Peripheral Artery Disease Patients with Claudication and Critical Limb Ischemia. *J. Clin. Med.* **9**, 2575 (2020).

82. Khattri, R. B. *et al.* Unique Metabolomic Profile of Skeletal Muscle in Chronic Limb Threatening Ischemia. *J. Clin. Med.* **10**, 548 (2021).

83. Gerhard-Herman, M. D. *et al. 2016 AHA/ACC guideline on the management of patients with lower extremity peripheral artery disease: Executive Summary: A report of the American college of cardiology/American Heart Association task force on clinical practice guidelines*. *Circulation* **135**, (2017).

84. Koutakis, P. *et al.* Oxidative damage in the gastrocnemius of patients with peripheral artery disease is myofiber type selective. *Redox Biol.* **2**, 921–928 (2014).

85. Cong, G. *et al.* Fibrosis Distinguishes Critical Limb Ischemia Patients from Claudicants in a Transcriptomic and Histologic Analysis. *J. Clin. Med.* **9**, (2020).

86. Ismaeel, A. *et al.* Altered Metabolomic Profile in Patients with Peripheral Artery Disease. *J. Clin. Med.* **8**, 1463 (2019).

87. Hilton, T. N., Tuttle, L. J., Bohnert, K. L., Mueller, M. J. & Sinacore, D. R. Excessive adipose tissue infiltration in skeletal muscle in individuals with obesity, diabetes mellitus, and peripheral neuropathy: association with performance and function. *Phys. Ther.* **88**, 1336–1344 (2008).

88. McClung, J. M. *et al.* BAG3 (Bcl-2-Associated Athanogene-3) coding variant in mice determines susceptibility to ischemic limb muscle myopathy by directing autophagy. *Circulation* **136**, 281–296 (2017).

89. Jalkanen, J., Maksimow, M., Hollmén, M., Jalkanen, S. & Hakovirta, H. Compared to Intermittant Claudication Critical Limb Ischemia Is Associated with Elevated Levels of Cytokines. *PLoS One* **11**, 1–11 (2016).

90. Teraa, M. *et al.* Bone Marrow Alterations and Lower Endothelial Progenitor Cell Numbers in Critical Limb Ischemia Patients. *PLoS One* **8**, (2013).

91. Stehr, A. *et al.* VEGF: A Surrogate Marker for Peripheral Vascular Disease. *Eur. J. Vasc. Endovasc. Surg.* **39**, 330–332 (2010).

92. Meurens, F., Summerfield, A., Nauwynck, H., Saif, L. & Gerdts, V. The pig: A model for human infectious diseases. *Trends Microbiol.* **20**, 50–57 (2012).

93. Walters, E. M. & Prather, R. S. Advancing Swine Models for Human Health and

Diseases. **110**, 212–215 (2013).

94. Walters, E. M., Wells, K. D., Bryda, E. C., Schommer, S. & Prather, R. S. Swine models, genomic tools and services to enhance our understanding of human health and diseases. *Lab Anim. (NY).* **46**, 167–172 (2017).

95. Keeran, K. J. *et al.* A chronic cardiac ischemia model in swine using an ameroid constrictor. *J. Vis. Exp.* **2017**, 1–6 (2017).

96. Lelovas, P. P., Kostomitsopoulos, N. G. & Xanthos, T. T. A comparative anatomic and physiologic overview of the porcine heart. *J. Am. Assoc. Lab. Anim. Sci.* **53**, 432–438 (2014).

97. Gao, Y. *et al.* Collateral development and arteriogenesis in hindlimbs of domestic swine after ligation of arterial inflow. *Biomed. Res.* **02155**, 1–28 (2006).

98. Lopes-Berkas, V. C. & Jorgenson, M. A. Measurement of peripheral arterial vasculature in domestic Yorkshire swine by using quantitative vascular angiography. *J. Am. Assoc. Lab. Anim. Sci.* **50**, 628–634 (2011).

99. Grundmann, S. *et al.* Granulocyte-macrophage colony-stimulating factor stimulates arteriogenesis in a pig model of peripheral artery disease using clinically applicable infusion pumps. *J. Vasc. Surg.* **43**, 1263–1269 (2006).

100. Clemens, M. S. *et al.* Extracorporeal Filtration of Potassium in a Swine Model of Bilateral Hindlimb Ischemia-Reperfusion Injury with Severe Acute Hyperkalemia. *Mil. Med.* **183**, E335–E340 (2018).

101. Long, C. A. *et al.* AN ENDOVASCULAR MODEL OF ISCHEMIC MYOPATHY FROM PERIPHERAL ARTERY DISEASE. *Physiol. Behav.* **176**, 100–106 (2016).

102. Gao, Y. *et al.* Collateral Development and Arteriogenesis in Hindlimbs of Swine After

Ligation of Arterial Inflow. *J. Surg. Res.* **249**, 168–179 (2020).

103. Polhemus, D. J. *et al.* Therapeutic potential of sustained-release sodium nitrite for critical limb ischemia in the setting of metabolic syndrome. *Am. J. Physiol. - Hear. Circ. Physiol.* **309**, H82–H92 (2015).

104. Long, C. A. *et al.* An endovascular model of ischemic myopathy from peripheral arterial disease. *J. Vasc. Surg.* **66**, 891–901 (2017).

105. McNally, M. A., Small, J. O., Mollan, R. A. B. & Wilson, D. J. Arteriographic study of the rabbit lower limb. *Anat. Rec.* **233**, 643–650 (1992).

106. Ito, W. D. *et al.* Angiogenesis but not collateral growth is associated with ischemia after femoral artery occlusion. *Am. J. Physiol. - Hear. Circ. Physiol.* **273**, (1997).

107. Petrasek, P. F., Homer-Vanniasinkam, S. & Walker, P. M. Determinants of ischemic injury to skeletal muscle. *J. Vasc. Surg.* **19**, 623–631 (1994).

108. Patel, T. H., Kimura, H., Weiss, C. R., Semenza, G. L. & Hofmann, L. V. Constitutively active HIF-1α improves perfusion and arterial remodeling in an endovascular model of limb ischemia. *Cardiovasc. Res.* **68**, 144–154 (2005).

109. Ito, W. D. *et al.* Angiogenesis but not collateral growth is associated with ischemia after femoral artery occlusion. *Am. J. Physiol.* **273**, H1255–H1265 (1997).

110. Murohara, T. *et al.* Nitric oxide synthase modulates angiogenesis in response to tissue ischemia. *J. Clin. Invest.* **101**, 2567–2578 (1998).

111. Lee, G. *et al.* Acute and chronic complications of laser angioplasty: Vascular wall damage and formation of aneurysms in the atherosclerotic rabbit. *Am. J. Cardiol.* **53**, 290–293 (1984).

112. Del Giudice, C. *et al.* Evaluation of a new model of hind limb ischemia in rabbits. *J. Vasc.*

Surg. **68**, 849–857 (2018).

113. Hong, J. H. *et al.* An experimental model of ischemia in rabbit hindlimb. *J. Korean Med. Sci.* **16**, 630–635 (2001).

114. Takeshita, S. *et al.* Therapeutic angiogenesis. A single intraarterial bolus of vascular endothelial growth factor augments revascularization in a rabbit ischemic hind limb model. *J. Clin. Invest.* **93**, 662–670 (1994).

115. Olea, F. D. *et al.* Repeated, but not single, VEGF gene transfer affords protection against ischemic muscle lesions in rabbits with hindlimb ischemia. *Gene Ther.* **16**, 716–723 (2009).

116. Wafai, R., Tudor, E. M., Angus, J. A. & Wright, C. E. Vascular effects of FGF-2 and VEGF-B in rabbits with bilateral hind limb ischemia. *J. Vasc. Res.* **46**, 45–54 (2008).

117. Greene, E. C. *The anatomy of the rat*. *Journal of Heredity* **16**, (1935).

118. Kigata, T. & Shibata, H. Anatomical variations of the arterial branches from the rat iliac arteries. *J. Vet. Med. Sci.* **81**, 1–8 (2019).

119. Challiss, R. A. J., Hayes, D. J., Petty, R. F. H. & Radda, G. K. An investigation of arterial insufficiency in rat hindlimb. A combined 31P-n.m.r. and bloodflow study. *Biochem. J.* **236**, 461–467 (1986).

120. McNeil, P. L. & Khakee, R. Disruptions of muscle fiber plasma membranes. Role in exercise-induced damage. *Am J Pathol* **140**, 1097–1109 (1992).

121. Taniyama, Y. *et al.* Therapeutic angiogenesis induced by human hepatocyte growth factor gene in rat and rabbit hindlimb ischemia models: Preclinical study for treatment of peripheral arterial disease. *Gene Ther.* **8**, 181–189 (2001).

122. Tang, G. L., Chang, D. S., Sarkar, R., Wang, R. & Messina, L. M. The effect of gradual or

acute arterial occlusion on skeletal muscle blood flow, arteriogenesis, and inflammation in rat hindlimb ischemia. *J. Vasc. Surg.* **41**, 312–320 (2005).

123. Lundberg, G., Luo, F., Blegen, H., Kalin, B. & Wahlberg, E. A rat model for severe limb ischemia at rest. *Eur. Surg. Res.* **35**, 430–438 (2003).

124. Luyt, C. E. *et al.* Low-molecular-weight fucoidan promotes therapeutic revascularization in a rat model of critical hindlimb ischemia. *J. Pharmacol. Exp. Ther.* **305**, 24–30 (2003).

125. Brevetti, L. S. *et al.* Exercise-induced hyperemia unmasks regional blood flow deficit in experimental hindlimb ischemia. *J. Surg. Res.* **98**, 21–26 (2001).

126. Zhuang, Z. W., Shi, J., Rhodes, J. M., Tsapakos, M. J. & Simons, M. Challenging the Surgical Rodent Hindlimb Ischemia Model with the Miniinterventional Technique. *Bone* **23**, 1–7 (2012).

127. Shin, C. Il *et al.* Rat model of hindlimb ischemia induced via embolization with polyvinyl alcohol and N-butyl cyanoacrylate. *Korean J. Radiol.* **14**, 923–930 (2013).

128. Paek, R. *et al.* Correlation of a simple direct measurement of muscle pO2 to a clinical ischemia index and histology in a rat model of chronic severe hindlimb ischemia. *J. Vasc. Surg.* **36**, 172–179 (2002).

129. Holmes, A., Coppey, L. J., Davidson, E. P. & Yorek, M. A. Rat Models of Diet-Induced Obesity and High Fat/Low Dose Streptozotocin Type 2 Diabetes: Effect of Reversal of High Fat Diet Compared to Treatment with Enalapril or Menhaden Oil on Glucose Utilization and Neuropathic Endpoints. *J. Diabetes Res.* **2015**, (2015).

130. Woods, S. C., Seeley, R. J., Rushing, P. A., D'Alessio, D. & Tso, P. A Controlled High-Fat Diet Induces an Obese Syndrome in Rats. *J. Nutr.* **133**, 1081–1087 (2003).

131. Buettner, R. *et al.* Defining high-fat-diet rat models: Metabolic and molecular effects of

different fat types. *J. Mol. Endocrinol.* **36**, 485–501 (2006).

132. Dupas, J. *et al.* Metabolic Syndrome and Hypertension Resulting from Fructose Enriched Diet in Wistar Rats. *Biomed Res. Int.* **2017**, (2017).

133. Dziadek, K., Kopeć, A., Piątkowska, E. & Leszczyńska, T. High-fructose diet-induced metabolic disorders were counteracted by the intake of fruit and leaves of sweet cherry in wistar rats. *Nutrients* **11**, (2019).

134. Bortolin, R. C. *et al.* A new animal diet based on human Western diet is a robust diet-induced obesity model: Comparison to high-fat and cafeteria diets in term of metabolic and gut microbiota disruption. *Int. J. Obes.* **42**, 525–534 (2018).

135. Eid, R. A. *et al.* A high-fat diet rich in corn oil induces cardiac fibrosis in rats by activating JAK2/STAT3 and subsequent activation of ANG II/TGF-1β/Smad3 pathway: The role of ROS and IL-6 trans-signaling. *J. Food Biochem.* **43**, 1–18 (2019).

136. Yang, P. *et al.* Compromised wound healing in ischemic type 2 diabetic rats. *PLoS One* **11**, 1–19 (2016).

137. Aref, Z., de Vries, M. R. & Quax, P. H. A. Variations in surgical procedures for inducing hind limb ischemia in mice and the impact of these variations on neovascularization assessment. *Int. J. Mol. Sci.* **20**, 1–14 (2019).

138. Bredee, J. An Improved Ameroid Constrictor. *J. Surg. Res.* **9**, 117–122 (1969).

139. Hellingman, A. A. *et al.* Variations in surgical procedures for hind limb ischaemia mouse models result in differences in collateral formation. *Eur. J. Vasc. Endovasc. Surg.* **40**, 796–803 (2010).

140. Yang, Y. *et al.* Cellular and molecular mechanism regulating blood flow recovery in acute versus gradual femoral artery occlusion are distinct in the mouse. *J. Vasc. Surg.* **48**, 1546–

1558 (2008).

141. Padgett, M. E., McCord, T. J., McClung, J. M. & Kontos, C. D. Methods for acute and subacute murine hindlimb ischemia. *J. Vis. Exp.* **2016**, 1–8 (2016).

142. Pipinos, I. I. *et al.* Chronically ischemic mouse skeletal muscle exhibits myopathy in association with mitochondrial dysfunction and oxidative damage. *Am. J. Physiol. - Regul. Integr. Comp. Physiol.* **295**, 290–296 (2008).

143. Goldberg, E. J. *et al.* Temporal Association Between Ischemic Muscle Perfusion Recovery and the Restoration of Muscle Contractile Function After Hindlimb Ischemia. *Frontiers in Physiology* **10**, 804 (2019).

144. Chalothorn, D., Faber, J. E. & Carolina, N. Strain-dependent variation in collateral circulatory function in mouse hindlimb. *Physiol. Genomics* **42**, 469–479 (2010).

145. McClung, J. M. *et al.* Skeletal muscle-specific genetic determinants contribute to the differential strain-dependent effects of hindlimb ischemia in mice. *Am. J. Pathol.* **180**, 2156–2169 (2012).

146. Paoni, N. F. *et al.* Time course of skeletal muscle repair and gene expression following acute hind limb ischemia in mice. *Physiol. Genomics* **11**, 263–272 (2002).

147. Hazarika, S. *et al.* Impaired angiogenesis after hindlimb ischemia in type 2 diabetes mellitus: Differential regulation of vascular endothelial growth factor receptor 1 and soluble vascular endothelial growth factor receptor 1. *Circ. Res.* **101**, 948–956 (2007).

148. Ryan, T. E. *et al.* Targeted expression of catalase to mitochondria protects against ischemic myopathy in high-fat diet-fed mice. *Diabetes* **65**, 2553–2568 (2016).

149. Peravali, R. *et al.* In experimental peripheral arterial disease, type 2 diabetes alters post-ischemic gene expression. *J. Clin. Transl. Endocrinol.* **17**, 100199 (2019).

150. Sandu, O. *et al.* Insulin resistance and type 2 diabetes in high-fat-fed mice are linked to high glycotoxin intake. *Diabetes* **54**, 2314–2319 (2005).

151. Nandi, A., Kitamura, Y., Kahn, C. R. & Accili, D. Mouse Models of Insulin Resistance. *Physiol. Rev.* **84**, 623–647 (2004).

152. McClung, J. P. *et al.* Development of insulin resistance and obesity in mice overexpressing cellular glutathione peroxidase. *Proc. Natl. Acad. Sci. U. S. A.* **101**, 8852–8857 (2004).

153. Meng, Q. *et al.* Development of a mouse model of metabolic syndrome, pulmonary hypertension, and heart failure with preserved ejection fraction. *Am. J. Respir. Cell Mol. Biol.* **56**, 497–505 (2017).

154. Heydemann, A. An Overview of Murine High Fat Diet as a Model for Type 2 Diabetes Mellitus. *J. Diabetes Res.* **2016**, (2016).

155. Ingalls, A. M., Dickie, M. M. & Snell, G. D. Obese, a new mutation in the house mouse. *J. Hered.* **41**, 315–317 (1950).

156. Coleman, D., Hummel, K. & Dickie, M. Diabetes, a New Mutafton in the Mouse. *Science (80-.).* **153**, 1127–1128 (1966).

157. Zhang, S. H., Reddick, R. L., Piedrahita, J. A. & Maeda, N. Spontaneous hypercholesterolemia and arterial lesions in mice lacking apolipoprotein E. *Science (80-.).* **258**, 468–471 (1992).

158. Zadelaar, S. *et al.* Mouse models for atherosclerosis and pharmaceutical modifiers. *Arterioscler. Thromb. Vasc. Biol.* **27**, 1706–1721 (2007).

159. Lo Sasso, G. *et al.* The Apoe-/- mouse model: A suitable model to study cardiovascular and respiratory diseases in the context of cigarette smoke exposure and harm reduction. *J.*

Transl. Med. **14**, 1–16 (2016).

160. Kang, J. *et al.* Apolipoprotein E-/- mice have delayed skeletal muscle healing after hind limb ischemia-reperfusion. *J. Vasc. Surg.* **48**, 701–708 (2008).

161. Desjarlais, M., Dussault, S., Rivera, J. C., Chemtob, S. & Rivard, A. MicroRNA Expression Profiling of Bone Marrow–Derived Proangiogenic Cells (PACs) in a Mouse Model of Hindlimb Ischemia: Modulation by Classical Cardiovascular Risk Factors. *Front. Genet.* **11**, 1–17 (2020).

162. Barwinska, D. *et al.* Cigarette Smoking Impairs Adipose Stromal Cell Vasculogenic Activity and Abrogates Potency to Ameliorate Ischemia. *Physiol. Behav.* **176**, 139–148 (2017).

163. Simons, J. P. *et al.* Survival prediction in patients with chronic limb-threatening ischemia who undergo infrainguinal revascularization. *Eur. J. Vasc. Endovasc. Surg.* **58**, S120-S134.e3 (2019).

164. Hishida, M., Menez, S. & Matsushita, K. Peripheral Artery Disease in CKD: Anatomically Peripheral But Clinically Central. *Am. J. Kidney Dis.* **75**, 687–689 (2020).

165. Bao, Y. W., Yuan, Y., Chen, J. H. & Lin, W. Q. Kidney disease models: tools to identify mechanisms and potential therapeutic targets. *Zool. Res.* **39**, 72–86 (2018).

166. Thome, T. *et al.* Impaired muscle mitochondrial energetics is associated with uremic metabolite accumulation in chronic kidney disease. *JCI Insight* **6**, (2021).

167. Berru, F. N. *et al.* Chronic kidney disease exacerbates ischemic limb myopathy in mice via altered mitochondrial energetics. *Sci. Rep.* **9**, 1–15 (2019).

168. Rubattu, S. *et al.* Reciprocal congenic lines for a major stroke QTL on rat chromosome 1. *Physiol. Genomics* **27**, 108–113 (2006).

169. Keum, S. & Marchuk, D. A. A locus mapping to mouse chromosome 7 determines infarct volume in a mouse model of ischemic stroke. *Circ. Cardiovasc. Genet.* **2**, 591–598 (2009).

170. Chung, C. M. *et al.* A genome-wide association study reveals a quantitative trait locus of adiponectin on CDH13 that predicts cardiometabolic outcomes. *Diabetes* **60**, 2417–2423 (2011).

171. Helisch, A. *et al.* Impact of mouse strain differences in innate hindlimb collateral vasculature. *Arterioscler. Thromb. Vasc. Biol.* **26**, 520–526 (2006).

172. Sealock, R., Zhang, H., Lucitti, J. L., Moore, S. M. & Faber, J. E. Congenic fine-mapping identifies a major causal locus for variation in the native collateral circulation and ischemic injury in brain and lower extremity. *Circ. Res.* **114**, 660–671 (2014).

173. Basile, D. P. *et al.* Chromosome substitution modulates resistance to ischemia reperfusion injury in Brown Norway rats. *Kidney Int.* **83**, 242–250 (2013).

174. Brosnan, M. J. *et al.* Genes encoding atrial and brain natriuretic peptides as candidates for sensitivity to brain ischemia in stroke-prone hypertensive rats. *Hypertension* **33**, 290–297 (1999).

175. Gobé, G. *et al.* Relationship between expression of Bcl-2 genes and growth factors in ischemic acute renal failure in the rat. *J. Am. Soc. Nephrol.* **11**, 454–467 (2000).

176. Chalothorn, D. & Faber, J. E. Strain-dependent variation in collateral circulatory function in mouse hindlimb. *Physiol. Genomics* **42**, 469–79 (2010).

177. Barone, F. C., Knudsen, D. J., Nelson, A. H., Feuerstein, G. Z. & Willette, R. N. Mouse strain differences in susceptibility to cerebral ischemia are related to cerebral vascular anatomy. *J. Cereb. Blood Flow Metab.* **13**, 683–692 (1993).

178. Majid, A. *et al.* Differences in vulnerability to permanent focal cerebral ischemia among 3 common mouse strains. *Stroke* **31**, 2707–2714 (2000).

179. Cheng, M. H., Lin, L. L., Liu, J. Y. & Liu, A. J. The outcomes of stroke induced by middle cerebral artery occlusion in different strains of mice. *CNS Neurosci. Ther.* **18**, 794–795 (2012).

180. Majid, A. *et al.* Differences in Vulnerability to Permanent Focal Cerebral Ischemia Among 3 Common Mouse Strains. 509–518 (2011).

181. Lee, H. K., Widmayer, S. J., Huang, M. N., Aylor, D. L. & Marchuk, D. A. Novel neuroprotective loci modulating ischemic stroke volume in wild-derived inbred mouse strains. *Genetics* **213**, 1079–1092 (2019).

182. Gao, X. M., Xu, Q., Kiriazis, H., Dart, A. M. & Du, X. J. Mouse model of post-infarct ventricular rupture: Time course, strain- and gender-dependency, tensile strength, and histopathology. *Cardiovasc. Res.* **65**, 469–477 (2005).

183. Salimova, E. *et al.* Variable outcomes of human heart attack recapitulated in genetically diverse mice. *npj Regen. Med.* **4**, (2019).

184. Salto-Tellez, M. *et al.* Myocardial infarction in the C57BL/6J mouse: A quantifiable and highly reproducible experimental model. *Cardiovasc. Pathol.* **13**, 91–97 (2004).

185. Ryan, T. E. *et al.* PFKFB3-mediated glycolysis rescues myopathic outcomes in the ischemic limb. *JCI Insight* **5**, 1–16 (2020).

186. Wang, S., Zhang, H., Dai, X., Sealock, R. & Faber, J. E. Genetic Architecture Underlying Variation in Extent and Remodeling of the Collateral Circulation. *Circ. Res.* **107**, 558–568 (2010).

187. Wang, S., Zhang, H., Wiltshire, T., Sealock, R. & Faber, J. E. Genetic Dissection of the

Canq1 Locus Governing Variation in Extent of the Collateral Circulation. *PLoS One* **7**, (2012).

188. Dokun, A. O. *et al.* ADAM12 : a genetic modifier of preclinical peripheral arterial disease. *Am. J. Physiol.* **309**, 790–803 (2014).

189. Okeke, E. & Dokun, A. O. Role of genetics in peripheral arterial disease outcomes; significance of limb-salvage quantitative locus-1 genes. *Exp. Biol. Med.* **243**, 190–197 (2018).

190. Kveiborg, M., Albrechtsen, R., Couchman, J. R. & Wewer, U. M. Cellular roles of ADAM12 in health and disease. *Int. J. Biochem. Cell Biol.* **40**, 1685–1702 (2008).

191. Dokun, A. O. *et al.* ADAM12: A genetic modifier of preclinical peripheral arterial disease. *Am. J. Physiol. - Hear. Circ. Physiol.* **309**, H790–H803 (2015).

192. Lafuste, P. *et al.* ADAM12 and α9β1 integrin are instrumental in human myogenic cell differentiation. *Mol. Biol. Cell* **16**, 861–870 (2005).

193. Jørgensen, L. H., Jensen, C. H., Wewer, U. M. & Schrøder, H. D. Transgenic overexpression of ADAM12 suppresses muscle regeneration and aggravates dystrophy in aged mdx mice. *Am. J. Pathol.* **171**, 1599–1607 (2007).

194. Mice, D. *et al.* Short Communication ADAM12 Alleviates the Skeletal Muscle Pathology in. *J. Clin. Invest.* **161**, 1535–1540 (2002).

195. Tao Wang *et al.* Loss of Interleukin-21 Receptor Activation in Hypoxic Endothelial Cells Impairs Perfusion Recovery after Hindlimb Ischemia. *Physiol. Behav.* **176**, 139–148 (2017).

196. Leonard, W. J. & Wan, C. K. IL-21 Signaling in Immunity. *F1000Research* **5**, 1–10 (2016).

197. Fröhlich, A. *et al.* IL-21 receptor signaling is integral to the development of Th2 effector responses in vivo. *Blood* **109**, 2023–2031 (2007).

198. Wang, T. *et al.* Loss of Interleukin-21 Receptor Activation in Hypoxic Endothelial Cells Impairs Perfusion Recovery after Hindlimb Ischemia. *Physiol. Behav.* **176**, 1570–1573 (2018).

199. Wang, T. *et al.* Endothelial interleukin-21 receptor up-regulation in peripheral artery disease. *Physiol. Behav.* **176**, 139–148 (2017).

200. Li, N. *et al.* Bcl-2-associated athanogene 3(BAG3) is associated with tumor cell proliferation, migration, invasion and chemoresistance in colorectal cancer. *BMC Cancer* **18**, 1–15 (2018).

201. Shields, S. *et al.* Correction: BAG3 promotes tumour cell proliferation by regulating EGFR signal transduction pathways in triple negative breast cancer (Oncotarget (2018) 9 (15673-15690) DOI: 10.18632/oncotarget.24590). *Oncotarget* **10**, 3144 (2019).

202. Stürner, E. & Behl, C. The role of the multifunctional bag3 protein in cellular protein quality control and in disease. *Front. Mol. Neurosci.* **10**, 1–18 (2017).

203. Myers, V. D. *et al.* The Multifunctional Protein BAG3: A Novel Therapeutic Target in Cardiovascular Disease. *JACC Basic to Transl. Sci.* **3**, 122–131 (2018).

204. Selcen, D. *et al.* Mutation in BAG3 Causes Severe Dominant Childhood Muscular Dystrophy. **65**, 83–89 (2010).

205. Lee, H. C. *et al.* BAG3-related myofibrillar myopathy in a Chinese family. *Clin. Genet.* **81**, 394–398 (2012).

206. Villard, E. *et al.* A genome-wide association study identifies two loci associated with heart failure due to dilated cardiomyopathy. *Eur. Heart J.* **32**, 1065–1076 (2011).

207. Norton, N. *et al.* Genome-wide studies of copy number variation and exome sequencing identify rare variants in BAG3 as a cause of dilated cardiomyopathy. *Am. J. Hum. Genet.* **88**, 273–282 (2011).

208. Homma, S. *et al.* BAG3 deficiency results in fulminant myopathy and early lethality. *Am. J. Pathol.* **169**, 761–773 (2006).

209. Myers, V. D. *et al.* Association of Variants in BAG3 with Cardiomyopathy Outcomes in African American Individuals. *JAMA Cardiol.* **3**, 929–938 (2018).

210. Myers, V. D. *et al.* Haplo-insufficiency of Bcl2-associated Athanogene 3 in Mice Results in Progressive Left Ventricular Dysfunction, β- Adrenergic Insensitivity and Increased Apoptosis. *Physiol. Behav.* **176**, 139–148 (2019).

211. Knezevic, T. *et al.* BAG3: a new player in the heart failure paradigm. *Heart Fail. Rev.* **20**, 423–434 (2015).

212. Gamerdinger, M., Carra, S. & Behl, C. Emerging roles of molecular chaperones and co-chaperones in selective autophagy: Focus on BAG proteins. *J. Mol. Med.* **89**, 1175–1182 (2011).

213. Carra, S., Seguin, S. J. & Landry, J. HspB8 and Bag3: A new chaperone complex targeting misfolded proteins to macroautophagy. *Autophagy* **4**, 237–239 (2008).

214. Martin, T. G. *et al.* BAG3-dependent autophagy maintains sarcomere function in cardiomyocytes. *Kemamp. Koneksi Mat. (Tinjauan Terhadap Pendekatan Pembelajaran Savi)* **53**, 1689–1699 (2019).

215. Martin, T. *et al.* Cardiomyocyte Contractile Impairment in Heart Failure Results from Reduced BAG3-mediated Sarcomeric Protein Turnover. (2020). doi:10.1101/2020.04.10.022319

216. Kostera-Pruszczyk, A. *et al.* BAG3-related myopathy, polyneuropathy and cardiomyopathy with long QT syndrome. *J. Muscle Res. Cell Motil.* **36**, 423–432 (2015).

217. Ryan, T. E. *et al.* Mitochondrial therapy improves limb perfusion and myopathy following hindlimb ischemia Terence. *J. Mol. Cell. Cardiol.* **143**, 951–959 (2015).

218. Kemp, G. J. Mitochondrial dysfunction in chronic ischemia and peripheral vascular disease. *Mitochondrion* **4**, 629–640 (2004).

219. Pinti, M. V. *et al.* Mitochondrial dysfunction in type 2 diabetes mellitus: An organ-based analysis. *Am. J. Physiol. - Endocrinol. Metab.* **316**, E268–E285 (2019).

220. Vijgen, G. H. E. J. *et al.* Impaired skeletal muscle mitochondrial function in morbidly obese patients is normalized one year after bariatric surgery. *Surg. Obes. Relat. Dis.* **9**, 936–941 (2013).

221. Yokota, T. *et al.* Oxidative stress in skeletal muscle impairs mitochondrial respiration and limits exercise capacity in type 2 diabetic mice. *Am. J. Physiol. - Hear. Circ. Physiol.* **297**, 1069–1077 (2009).

222. Dennis, M. K. *et al.* Long non-coding RNAs with enhancer-like function in humans. *Cell* **127**, 358–366 (2012).

223. Koerner, M. V, Pauler, F. M., Huang, R. & Barlow, D. P. The function of non-coding RNAs in genomic imprinting. **136**, 1771–1783 (2010).

224. Guttman, M. *et al.* lincRNAs act in the circuitry controlling pluripotency and differentiation. *J. Aerosp. Technol. Manag.* **1**, 201–209 (2009).

225. Hung, T. *et al.* Extensive and coordinated transcription of noncoding RNAs within cell cycle promoters. **43**, 621–629 (2013).

226. Willingham, A. T. *et al.* Molecular biology: A strategy for probing the function of

noncoding RNAs finds a repressor of NFAT. *Science (80-.).* **309**, 1570–1573 (2005).

227. Vidisha Tripathi *et al.* The Nuclear-Retained Noncoding RNA MALAT1 Regulates Alternative Splicing by Modulating SR Splicing Factor Phosphorylation. *Mol. Cell. Biochem.* **39**, 925–938 (2009).

228. Gupta, R. A. *et al.* Long non-coding RNA HOTAIR reprograms chromatin state to promote cancer metastasis. *Nature* **464**, 1071–1076 (2010).

229. Negishi, M. *et al.* A new lncRNA, APTR, associates with and represses the CDKN1A/p21 promoter by recruiting polycomb proteins. *PLoS One* **9**, (2014).

230. Blum, R., Vethantham, V., Bowman, C., Rudnicki, M. & Dynlacht, B. D. Genome-wide identification of enhancers in skeletal muscle: The role of MyoD1. *Genes Dev.* **26**, 2763–2779 (2012).

231. Vidisha Tripathi *et al.* The Nuclear-Retained Noncoding RNA MALAT1 Regulates Alternative Splicing by Modulating SR Splicing Factor Phosphorylation. *Mol. Cell. Biochem.* **39**, 925–938 (2009).

232. Yu, B. & Wang, S. Angio-LncRs: LncRNAs that regulate angiogenesis and vascular disease. *Theranostics* **8**, 3654–3675 (2018).

233. Hung, J., Miscianinov, V., Sluimer, J. C., Newby, D. E. & Baker, A. H. Targeting Non-coding RNA in Vascular Biology and Disease. *Front. Physiol.* **9**, 1–16 (2018).

234. Pérez-Cremades, D., Cheng, H. S. & Feinberg, M. W. Noncoding RNAs in critical limb ischemia. *Arterioscler. Thromb. Vasc. Biol.* 523–533 (2019). doi:10.1161/ATVBAHA.119.312860

235. Jaé, N. & Dimmeler, S. Noncoding RNAs in Vascular Diseases. *Circulation research* **126**, 1127–1145 (2020).

236. He, Y. *et al.* Long non-coding RNA GAPLINC promotes angiogenesis by regulating miR-211 under hypoxia in human umbilical vein endothelial cells. *J. Cell. Mol. Med.* **23**, 8090–8100 (2019).

237. Boulberdaa, M. *et al.* A role for the long noncoding RNA SENCR in commitment and function of endothelial cells. *Mol. Ther.* **24**, 978–990 (2016).

238. Terwilliger, Z. S. *et al.* Racial differences in the limb skeletal muscle transcriptional programs of patients with critical limb ischemia. *Vasc. Med. (United Kingdom)* **26**, 247–258 (2021).

239. Spinetti, G. *et al.* MicroRNA-21/PDCD4 Proapoptotic Signaling from Circulating CD341 Cells to Vascular Endothelial Cells: A Potential Contributor to Adverse Cardiovascular Outcomes in Patients with Critical Limb Ischemia. *Diabetes Care* **43**, 1520–1529 (2020).

240. Hazarika, S. *et al.* MicroRNA-93 controls perfusion recovery after hindlimb ischemia by modulating expression of multiple genes in the cell cycle pathway. *Circulation* **127**, 1818–1828 (2013).

241. Shu, X. *et al.* MicroRNA-93 regulates angiogenesis in peripheral arterial disease by targeting CDKN1A. *Mol. Med. Rep.* **19**, 5195–5202 (2019).

242. Fang, L. *et al.* MiR-93 enhances angiogenesis and metastasis by targeting LATS2. *Cell Cycle* **11**, 4352–4365 (2012).

243. Conte, M. S. *et al.* Global vascular guidelines on the management of chronic limb-threatening ischemia. *J. Vasc. Surg.* **69**, 3S-125S.e40 (2019).

244. Soria-Juan, B. *et al.* Cost-effective, safe, and personalized cell therapy for critical limb ischemia in type 2 diabetes mellitus. *Front. Immunol.* **10**, 1–17 (2019).

245. Peeters Weem, S. M. O., Teraa, M., De Borst, G. J., Verhaar, M. C. & Moll, F. L. Bone

Marrow derived Cell Therapy in Critical Limb Ischemia: A Meta-analysis of Randomized Placebo Controlled Trials. *Eur. J. Vasc. Endovasc. Surg.* **50**, 775–783 (2015).

246. Ponemone, V. *et al.* Safety and Effectiveness of Bone Marrow Cell Concentrate in the Treatment of Chronic Critical Limb Ischemia Utilizing a Rapid Point-of-Care System. *Stem Cells Int.* **2017**, (2017).

247. Katagiri, T. *et al.* Therapeutic angiogenesis using autologous adipose-derived regenerative cells in patients with critical limb ischaemia in Japan: a clinical pilot study. *Sci. Rep.* **10**, 1–12 (2020).

248. Sharma, S. *et al.* Randomized, Double-Blind, Placebo-Controlled Trial to Evaluate Safety and Therapeutic Efficacy of Angiogenesis Induced by Intraarterial Autologous Bone Marrow–Derived Stem Cells in Patients with Severe Peripheral Arterial Disease. *J. Vasc. Interv. Radiol.* **32**, 157–163 (2021).

249. Sharma, S. *et al.* Randomized, Double-Blind, Placebo-Controlled Trial to Evaluate Safety and Therapeutic Efficacy of Angiogenesis Induced by Intraarterial Autologous Bone Marrow–Derived Stem Cells in Patients with Severe Peripheral Arterial Disease. *J. Vasc. Interv. Radiol.* **32**, 157–163 (2021).

250. Beltran-Camacho, L. *et al.* Identification of the initial molecular changes in response to circulating angiogenic cells-mediated therapy in critical limb ischemia. *Stem Cell Res. Ther.* **11**, 1–20 (2020).

251. Rojas-Torres, M. *et al.* REX-001, a BM-MNC Enriched Solution, Induces Revascularization of Ischemic Tissues in a Murine Model of Chronic Limb-Threatening Ischemia. *Front. Cell Dev. Biol.* **8**, 1–16 (2020).

252. Lukjanenko, L. *et al.* Aging Disrupts Muscle Stem Cell Function by Impairing

Matricellular WISP1 Secretion from Fibro-Adipogenic Progenitors. *Cell Stem Cell* **24**, 433-446.e7 (2019).

253. Ferguson, L. P., Diaz, E. & Reya, T. The Role of the Microenvironment and Immune System in Regulating Stem Cell Fate in Cancer. *Trends in Cancer* **xx**, 1–11 (2021).

254. Giacca, M. & Zacchigna, S. VEGF gene therapy: Therapeutic angiogenesis in the clinic and beyond. *Gene Ther.* **19**, 622–629 (2012).

255. Barć, P. *et al.* Double VEGF/HGF Gene Therapy in Critical Limb Ischemia Complicated by Diabetes Mellitus. *J. Cardiovasc. Transl. Res.* (2020). doi:10.1007/s12265-020-10066-9

256. Baumgartner, I. *et al.* Constitutive expression of phVEGF165 after intramuscular gene transfer promotes collateral vessel development in patients with critical limb ischemia. *Circulation* **97**, 1114–1123 (1998).

257. Belch, J. *et al.* Effect of fibroblast growth factor NV1FGF on amputation and death: A randomised placebo-controlled trial of gene therapy in critical limb ischaemia. *Lancet* **377**, 1929–1937 (2011).

258. Nikol, S. *et al.* Therapeutic angiogenesis with intramuscular NV1FGF improves amputation-free survival in patients with critical limb ischemia. *Mol. Ther.* **16**, 972–978 (2008).

259. Comerota, A. J. *et al.* Naked plasmid DNA encoding fibroblast growth factor type 1 for the treatment of end-stage unreconstructible lower extremity ischemia: Preliminary results of a phase I trial. *J. Vasc. Surg.* **35**, 930–936 (2002).

260. Shigematsu, H. *et al.* Randomized, double-blind, placebo-controlled clinical trial of hepatocyte growth factor plasmid for critical limb ischemia. *Gene Ther.* **17**, 1152–1161

(2010).

261. Powell, R. J., Goodney, P., Mendelsohn, F. O., Moen, E. K. & Annex, B. H. Safety and efficacy of patient specific intramuscular injection of HGF plasmid gene therapy on limb perfusion and wound healing in patients with ischemic lower extremity ulceration: Results of the HGF-0205 trial. *J. Vasc. Surg.* **52**, 1525–1530 (2010).

262. Makarevich, P. *et al.* Combined transfer of human VEGF165 and HGF genes renders potent angiogenic effect in ischemic skeletal muscle. *PLoS One* **7**, (2012).

263. Robbins, J. L. *et al.* Relationship between leg muscle capillary density and peak hyperemic blood flow with endurance capacity in peripheral artery disease. *J. Appl. Physiol.* **111**, 81–86 (2011).

264. Duscha, B., Robbins, J., Jones, W. & Kraus, W. Angiogenesis in Skeletal Muscle Precede Improvements in Peak. *Arter. Vasc Biol.* **31**, 2742–2748 (2013).

265. Latroche, C. *et al.* Coupling between Myogenesis and Angiogenesis during Skeletal Muscle Regeneration Is Stimulated by Restorative Macrophages. *Stem Cell Reports* **9**, 2018–2033 (2017).

266. Callum, K. & Bradbury, A. ABC of arterial and venous disease: Acute limb ischaemia. *BMJ* **320**, 764–7 (2000).

267. Singh, N. *et al.* Leg Strength Predicts Mortality in Men But Not in Women With Peripheral Arterial Disease. *J. Vasc. Surg.* **52**, 624–631 (2011).

268. Jain, A. *et al.* The Walking Impairment Questionnaire stair-climbing score predicts mortality in men and women with peripheral arterial disease. *J. Vasc. Surg.* **55**, 1662–1673 (2012).

269. Ceafalan, L. C., Popescu, B. O. & Hinescu, M. E. Cellular players in skeletal muscle

regeneration. *Biomed Res. Int.* **2014**, 1–21 (2014).

270. Saltin, B. & Gollnick, P. D. Skeletal Muscle Adaptability: Significance for Metabolism and Performance. *Compr. Physiol.* (2011). doi:10.1002/cphy.cp100119

271. Liu, G., Mac Gabhann, F. & Popel, A. S. Effects of Fiber Type and Size on the Heterogeneity of Oxygen Distribution in Exercising Skeletal Muscle. *PLoS One* **7**, (2012).

272. Koutakis, P. *et al.* Oxidative damage in the gastrocnemius of patients with peripheral artery disease is myofiber type selective. *Redox Biol.* **2**, 921–928 (2014).

273. Dickie, R. *et al.* Three-dimensional visualization of microvessel architecture of whole-mount tissue by confocal microscopy. *Microvasc. Res.* **72**, 20–26 (2006).

274. Spangenburg, E. E., Le Roith, D., Ward, C. W. & Bodine, S. C. A functional insulin-like growth factor receptor is not necessary for load-induced skeletal muscle hypertrophy. *J. Physiol.* **586**, 283–291 (2008).

275. Tarpey, M. D. *et al.* Characterization and utilization of the flexor digitorum brevis for assessing skeletal muscle function. *Skelet. Muscle* **8**, 1–15 (2018).

276. Chargé, S. B. P. & Rudnicki, M. A. Cellular and Molecular Regulation of Muscle Regeneration. *Physiol. Rev.* **84**, 209–238 (2004).

277. Musarò, A. The Basis of Muscle Regeneration. *Adv. Biol.* **2014**, 1–16 (2014).

278. Messina, S. *et al.* VEGF overexpression via adeno-associated virus gene transfer promotes skeletal muscle regeneration and enhances muscle function in mdx mice. *FASEB J.* **21**, 3737–3746 (2007).

279. Deasy, B. M. *et al.* Effect of VEGF on the Regenerative Capacity of Muscle Stem Cells in Dystrophic Skeletal Muscle. *Mol. Ther.* **17**, 1788–1798 (2009).

280. Dellavalle, A. *et al.* Pericytes of human skeletal muscle are myogenic precursors distinct

from satellite cells. *Nat. Cell Biol.* **9**, 255–267 (2007).

281. Zheng, B. *et al.* Prospective identification of myogenic endothelial cells in human skeletal muscle. *Nat. Biotechnol.* **25**, 1025–1034 (2007).

282. Latroche, C. *et al.* Skeletal Muscle Microvasculature : A Highly Dynamic Lifeline. *Physioogy (Bethesda)* **30**, 417–427 (2015).

283. Asai, A. *et al.* Primary Role of Functional Ischemia , Quantitative Evidence for the Two-Hit Mechanism , and Phosphodiesterase-5 Inhibitor Therapy in Mouse Muscular Dystrophy. (2007). doi:10.1371/journal.pone.0000806

284. Martin, E. A. *et al.* Tadalafil alleviates muscle ischemia in patients with Becker muscular dystrophy Elizabeth. *Sci. Transl. Med.* **4**, 155–162 (2014).

285. Ryan, T. E. *et al.* Targeted expression of Catalase to Mitochondria Protects Against Ischemic Myopathy in High Fat Fed Mice. *Diabetes* **db160387**, (2016).

286. Surovi Hazarika, MD, PhD Charles R Farber, PhD, Ayotunde O Dokun, MD, PhD, Achillieas N Pitsillides, PhD, Tao Wang, MD, PhD, R John Lye, PhD3, and Brian H Annex, M. MicroRNA-93 Controls Perfusion Recovery Following Hind-Limb Ischemia by Modulating Expression of Multiple Genes in the Cell Cycle Pathway. *Circulation* **127**, 1–26 (2013).

287. Taylor, S. M. *et al.* Comparison of Interventional Outcomes According to Preoperative Indication : A Single Center Analysis of 2 , 240 Limb Revascularizations. *ACS* **208**, 770–778 (2009).

288. Pipinos, I. I., Shepard, A. D., Anagnostopoulos, P. V., Katsamouris, A. & Boska, M. D. Phosphorus 31 nuclear magnetic resonance spectroscopy suggests a mitochondrial defect in claudicating skeletal muscle. *J. Vasc. Surg.* **31**, 944–952 (2000).

289. Thompson, J. R. *et al.* Protein concentration and mitochondrial content in the gastrocnemius predicts mortality rates in patients with peripheral arterial disease. *Ann. Surg.* **261**, 605–610 (2015).

290. Dayanand, K. Regulated necrotic cell death: The passive aggressive side of Bax and Bak. *Circ. Res.* **176**, 139–148 (2015).

291. Shirihai, O. & Song, M. How mitochondrial dynamism orchestrates mitophagy. *Circ. Res.* **116**, 1835–1849 (2016).

292. Spinazzi, M., Casarin, A., Pertegato, V., Salviati, L. & Angelini, C. Assessment of mitochondrial respiratory chain enzymatic activities on tissues and cultured cells. *Nat. Protoc.* **7**, 1235–1246 (2012).

293. Quintens, R. *et al.* Mice Deficient in the Respiratory Chain Gene Cox6a2 Are Protected against High-Fat Diet-Induced Obesity and Insulin Resistance. *PLoS One* **8**, (2013).

294. Radford, N. B. *et al.* Cardiac dysfunction in mice lacking cytochrome-c oxidase subunit VIaH. *Am. J. Physiol. - Hear. Circ. Physiol.* **282**, 726–733 (2002).

295. Barton, E. R. & Lynch, G. Measuring isometric force of isolated mouse muscles in vitro. *Treat-Nmd.Eu* 1–14 (2008).

296. Fisher-wellman, K., Davidson, M., Narowski, T., Koves, T. R. & Deborah, M. Mitochondrial Diagnostics : A high-throughput assay platform for comprehensive assessment of mitochondrial energy flux.

297. McLaughlin, K. L. *et al.* Novel approach to quantify mitochondrial content and intrinsic bioenergetic efficiency across organs. *Sci. Rep.* **10**, 1–15 (2020).

298. Andres, A. M. *et al.* Mitophagy and mitochondrial biogenesis in atrial tissue of patients undergoing heart surgery with cardiopulmonary bypass. *JCI Insight* **2**, (2017).

299. Jackson, K. C. *et al.* Induced Cre-mediated knockdown of Brca1 in skeletal muscle reduces mitochondrial respiration and prevents glucose intolerance in adult mice on a high-fat diet. *FASEB J.* **32**, 3070–3084 (2018).

300. White, A. T., LaBarge, S. A., McCurdy, C. E. & Schenk, S. Knockout of STAT3 in skeletal muscle does not prevent high-fat diet-induced insulin resistance. *Mol. Metab.* **4**, 569–575 (2015).

301. Yablonka-Reuven, Z. & Nameroff, M. Skeletal muscle cell populations: Separation and partial characterization of fibroblast-like cells from embryonic tissue using density centrifugation. *Histochemistry* **87**, 27–38 (1987).

302. Bentzinger, C. F., Wang, Y. X., Dumont, N. A. & Rudnicki, M. A. Cellular dynamics in the muscle satellite cell niche. *Nat. Publ. Gr.* **14**, 1062–1072 (2013).

303. Yin, H., Price, F. & Rudnicki, M. A. SATELLITE CELLS AND THE MUSCLE STEM CELL NICHE. *Physiol. Rev.* **93**, 23–67 (2013).

304. Pawlikowski, B., Pulliam, C., Betta, N. D., Kardon, G. & Olwin, B. B. Pervasive satellite cell contribution to uninjured adult muscle fibers. *Skelet. Muscle* **5**, 1–13 (2015).

305. Andersson, K. B., Winer, L. H., Mørk, H. K., Molkentin, J. D. & Jaisser, F. Tamoxifen administration routes and dosage for inducible Cre-mediated gene disruption in mouse hearts. *Transgenic Res.* **19**, 715–725 (2010).

306. Kiermayer, C., Conrad, M., Schneider, M., Schmidt, J. & Brielmeier, M. Optimization of Spatiotemporal Gene Inactivation in Mouse Heart by Oral Application of Tamoxifen Citrate. *Genesis* **45**, 76–82 (2007).

307. Turlo, K. A., Gallaher, S. D., Vora, R., Laski, F. A. & Iruela-Arispe, M. L. When Cre-mediated recombination in mice does not result in protein loss. *Genetics* **186**, 959–967

(2010).

308. Han, B. & Zhang, J.-T. Regulation of Gene Expression by Internal Ribosome Entry Sites or Cryptic Promoters: the eIF4G Story. *Mol. Cell. Biol.* **22**, 7372–7384 (2002).

309. Bachman, N. J. *et al.* Structure of the human gene (COX6A2) for the heart/muscle isoform of cytochrome c oxidase subunit VIa and its chromosomal location in humans, mice, and cattle. *Genomics* **42**, 146–151 (1997).

310. Sanz-Morello, B. *et al.* Complex IV subunit isoform COX 6A2 protects fast-spiking interneurons from oxidative stress and supports their function . *EMBO J.* **39**, 1–21 (2020).

311. Fornuskova, D. *et al.* Novel insights into the assembly and function of human nuclear-encoded cytochrome c oxidase subunits 4, 5a, 6a, 7a and 7b. *Biochem. J.* **428**, 363–374 (2010).

312. Cogliati, S. *et al.* Mechanism of super-assembly of respiratory complexes III and IV. *Nature* **539**, 579–582 (2016).

313. Anthony, G., Reimann, A. & Kadenbach, B. Tissue-specific regulation of bovine heart cytochrome-c oxidase activity by ADP via interaction with subunit VIa. *Proc. Natl. Acad. Sci. U. S. A.* **90**, 1652–1656 (1993).

314. Aoyama, H. *et al.* The Whole Structure of the 13-Subunit Oxidized Cytochrome c Oxidase at 2.8 A. *Science (80-.).* **272**, 1136–1144 (1995).

315. Frank, V. & Kadenbach, B. Regulation of the H+/e- stoichiometry of cytochrome c oxidase from bovine heart by intramitochondrial ATP/ADP ratios. *FEBS Lett.* **382**, 121–124 (1996).

316. Deficiencies, O. *et al.* Oxphos Deficiencies Caused By Defects on RESPIRATORY COMPLEX SUBUNITS OR ASSEMBLY FACTORS Alessandra. 76–91 (2016).

doi:10.1016/j.mito.2015.01.009.MITOCHONDRIAL

317. Pereira, R. O. *et al.* OPA 1 deficiency promotes secretion of FGF 21 from muscle that prevents obesity and insulin resistance . *EMBO J.* **36**, 2126–2145 (2017).

318. Fox, R. *et al.* Mitochondrial DNA polymerase editing mutation, PolgD257A, reduces the diabetic phenotype of Akita male mice by suppressing appetite. *Proc. Natl. Acad. Sci. U. S. A.* **108**, 8779–8784 (2011).

319. Pospisilik, J. A. *et al.* Targeted Deletion of AIF Decreases Mitochondrial Oxidative Phosphorylation and Protects from Obesity and Diabetes. *Cell* **131**, 476–491 (2007).

320. Valera-Alberni, M. & Canto, C. Mitochondrial stress management: A dynamic journey. *Cell Stress* **2**, 253–274 (2018).

321. Picard, M. & McEwen, B. S. Psychological Stress and Mitochondria: A Systematic Review. *Physiol. Behav.* **80**, 141–153 (2018).

322. Inoue, M. *et al.* COX6A2 variants cause a muscle-specific cytochrome c oxidase deficiency. *Ann. Neurol.* **86**, 193–202 (2019).

323. Abdulhag, U. N. *et al.* Mitochondrial complex IV deficiency, caused by mutated COX6B1, is associated with encephalomyopathy, hydrocephalus and cardiomyopathy. *Eur. J. Hum. Genet.* **23**, 159–164 (2015).

324. Shoubridge, E. A. Cytochrome c Oxidase De®ciency. *Am. J. Med. Genet. (Semin. Med. Genet.* **106**, 46–52 (2001).

325. Rak, M. *et al.* Mitochondrial cytochrome c oxidase deficiency. *Clin. Sci.* **130**, 393–407 (2016).

326. Von Kleist-Retzow, J. C. *et al.* A high rate (20%-30%) of parental consanguinity in cytochrome-oxidase deficiency. *Am. J. Hum. Genet.* **63**, 428–435 (1998).

327. Skladal, D., Halliday, J. & Thorburn, D. R. Minimum birth prevalence of mitochondrial respiratory chain disorders in children. *Brain* **126**, 1905–1912 (2003).

328. Shteyer, E. *et al.* Exocrine Pancreatic Insufficiency, Dyserythropoeitic Anemia, and Calvarial Hyperostosis Are Caused by a Mutation in the COX4I2 Gene. *Am. J. Hum. Genet.* **84**, 412–417 (2009).

329. Tamiy, G. *et al.* A Mutation of COX6A1 causes a recessive axonal or mixed form of charcot-marie-tooth disease. *Am. J. Hum. Genet.* **95**, 294–300 (2014).

330. Massa, V. *et al.* Severe Infantile Encephalomyopathy Caused by a Mutation in COX6B1, a Nucleus-Encoded Subunit of Cytochrome C Oxidase. *Am. J. Hum. Genet.* **82**, 1281–1289 (2008).

331. Indrieri, A. *et al.* Mutations in COX7B cause microphthalmia with linear skin lesions, an unconventional mitochondrial disease. *Am. J. Hum. Genet.* **91**, 942–949 (2012).

Appendix A: Supplemental Figures

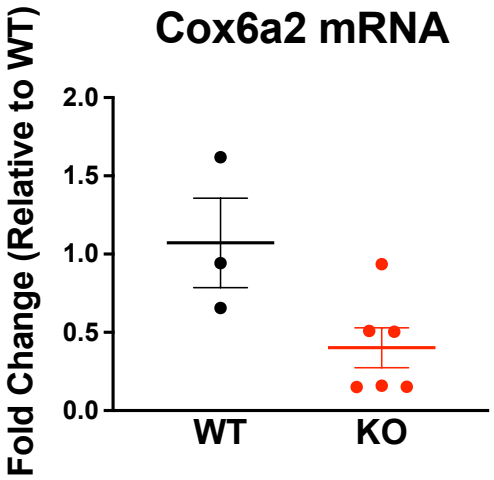

Supplemental Figure 1: Cox6a2 mRNA following one round of tamoxifen

Cox6a2 mRNA was reduced in KO animals by an average of 60% following one 5-day round of tamoxifen.